GNSS Remote Sensing

Chen Wu

Department of Land Surveying and Geoinformatics

Hong Kong Polytechnic University

Global Navigation Satellite Systems (GNSS)

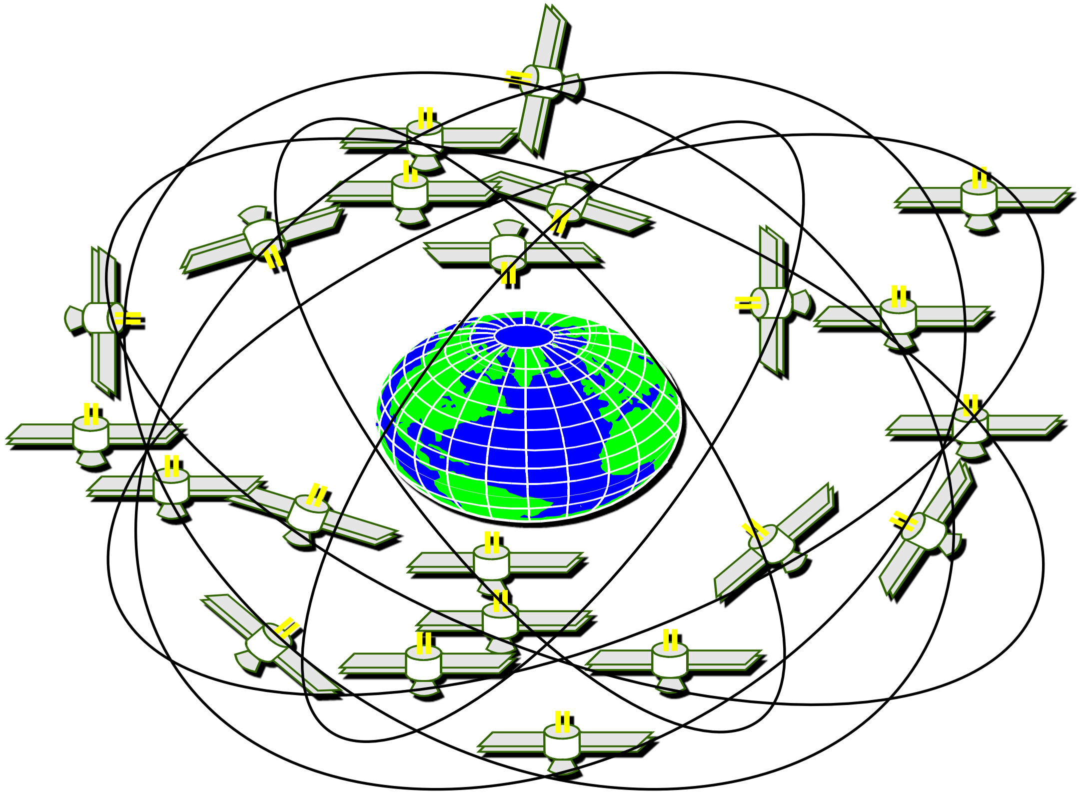

- GNSS
  - GPS, Beidou, GLONASS, Galileo, and Augmentation Systems
- Many Applications
  - Timing and Positioning
  - Navigation
  - Farming
  - Transport
  - Military
  - Atmosphere remote sensing
  - …………………..

GNSS Error Sources

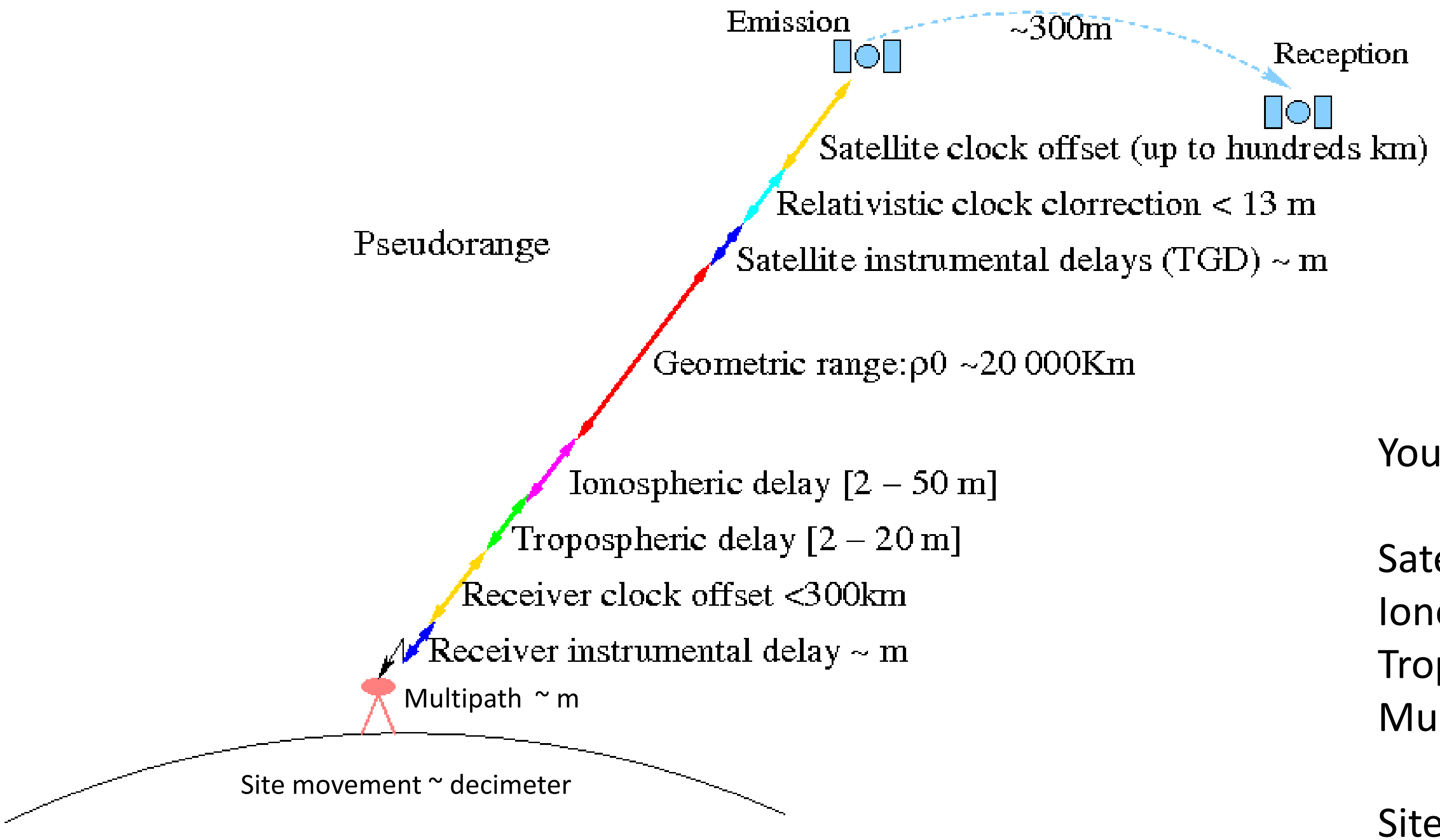

https://galileoic-brazil.com/wp-content/uploads/2021/07/Day-4-L1.-Overview-of-GNSS-positioniong-techniques.pdf

Your rubbish is my data!

Satellite clock: relativity effects
Ionosphere delay: TEC and changes
Tropospheric delay: Water vapour
Multipath: L-band remote sensing and Passive Radar
Site movement: tide, groundwater, ….

GNSS observation

- From Ground
- Space to Space
- From Space

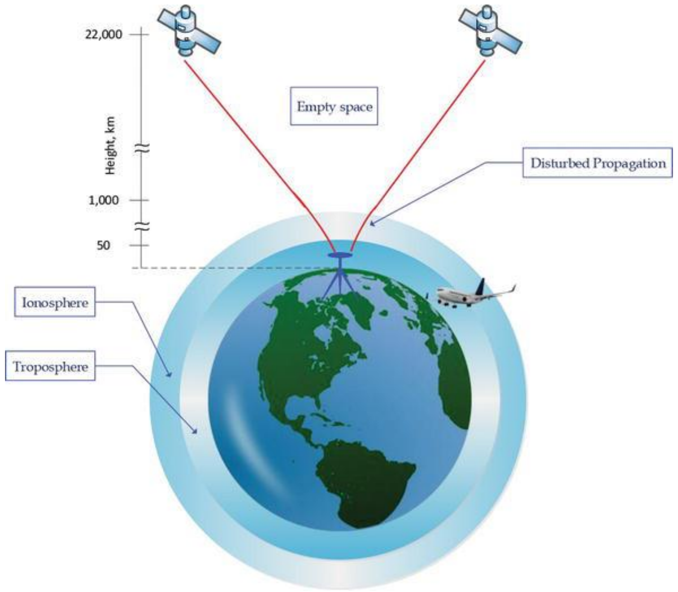

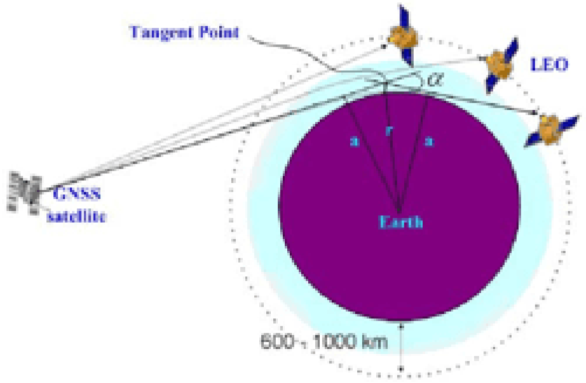

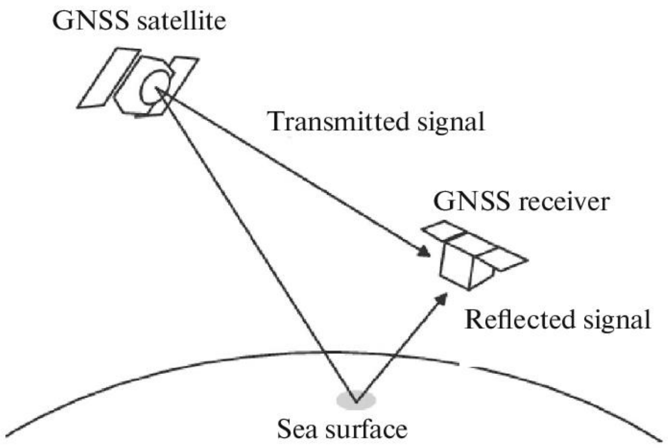

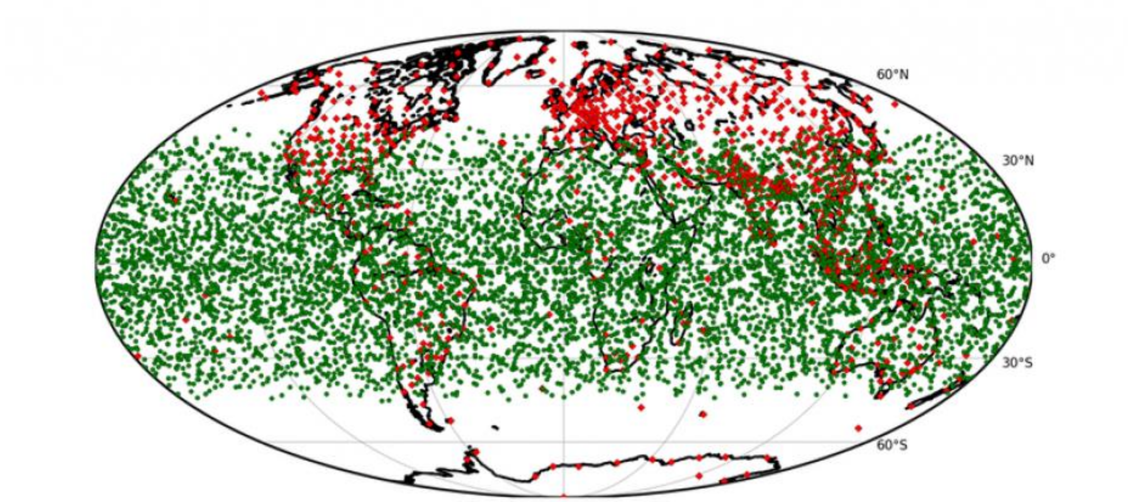

https://www.cosmic.ucar.edu/what-we-do/gnss-radio-occultation

GNSS occultation

- Provide vertical profile of atmosphere
- Ionosphere: TEC along path
- Troposphere: based on Abel Transformation
    - Covert the bend angle to refractivity
    - Different parameters:
        - dry density, dry pressure, dry temperature, density, pressure, temperature, specific etc. humidity
- Advantage:
    - High vertical resolution: 100 m
    - All-weather operation
    - Global coverage
- Applications:
    - Weather forecasting and atmospheric processes
    - Climate monitoring and model verification
    - Space weather and ionospheric research

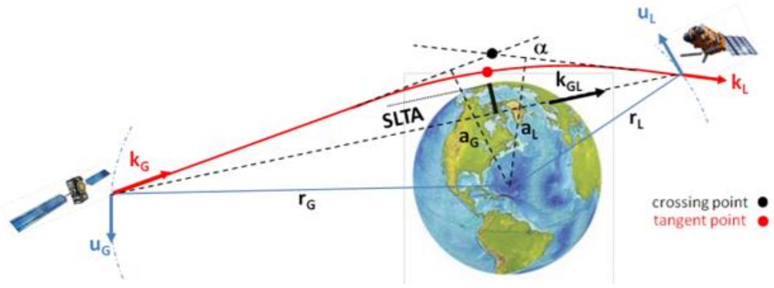

Space borne GNSS Reflectometry

- Applications:
  - Sea Surface and Land Topography (as a altimeter)
  - Sea-Surface Wind Speed and Wave Height
  - Rainfall Detection and Rainfall Intensity Retrieval
  - Soil Moisture and Vegetation Parameters
  - Sea Ice Detection and Sea Ice Thickness Estimation
  - Flood and Tsunami Detection
  - Land Classification
  - ....

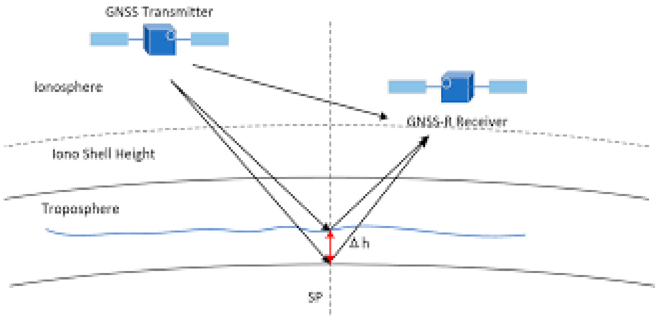

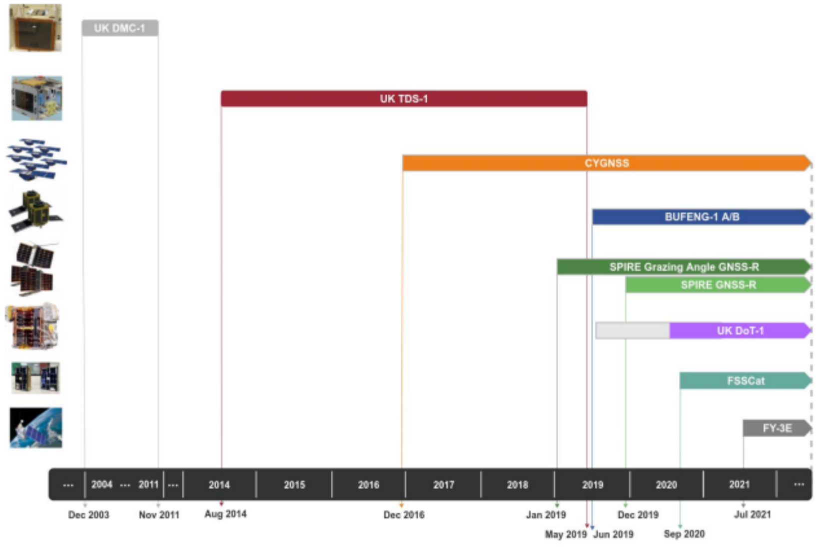

https://www.mdpi.com/2072-4292/14/7/1605

Effects on Radio Signals

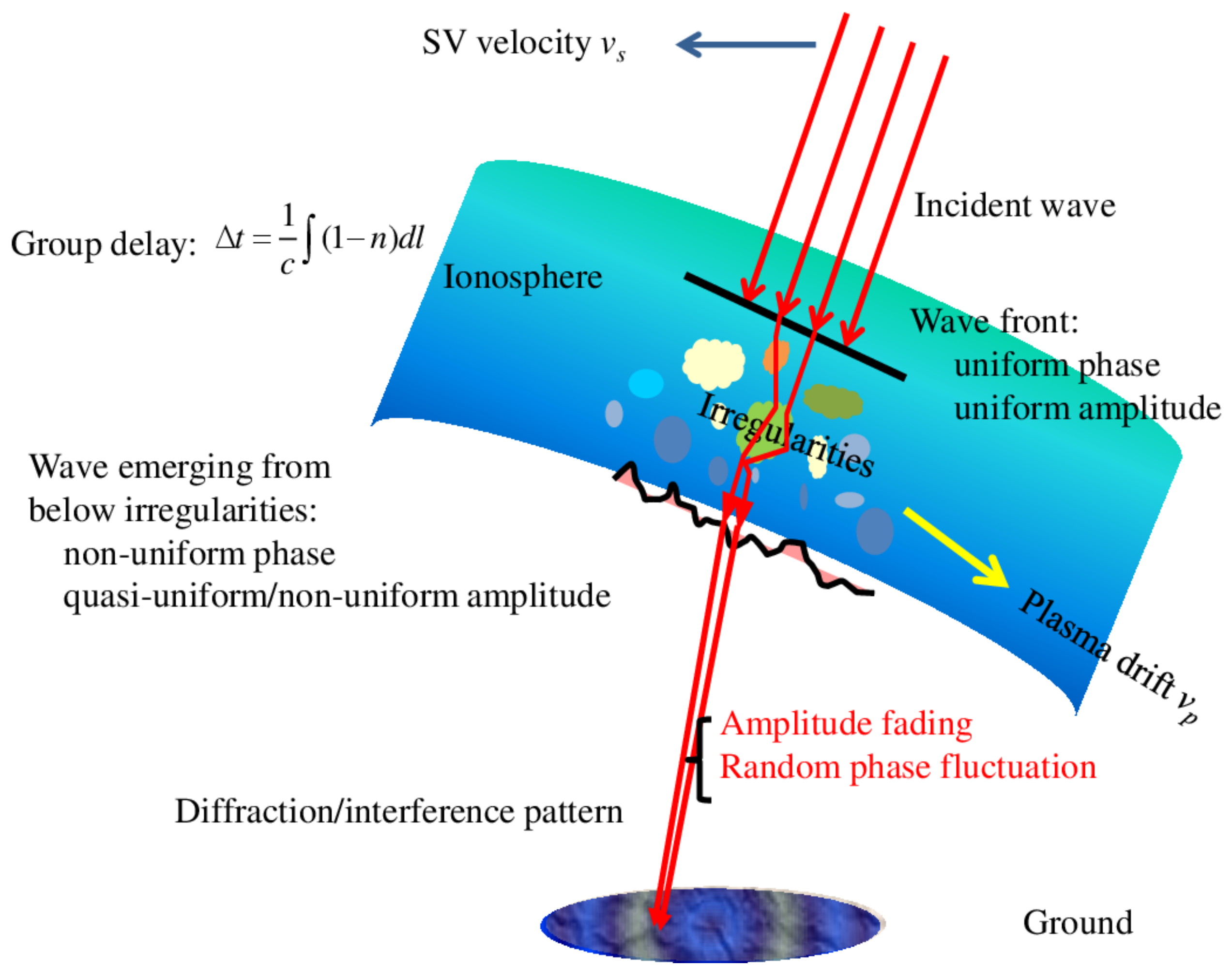

GNSS measurements

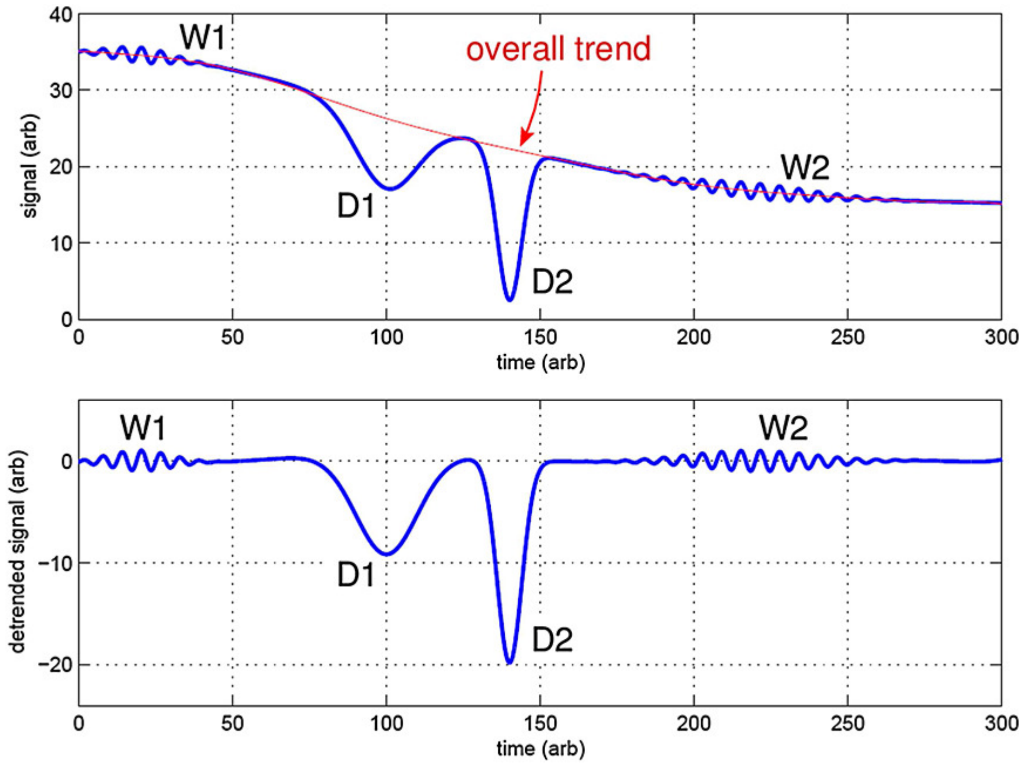

GNSS for ionosphere study

- Total electron Count (TEC): P1-P2 (geometry –free)

$$L_4 = \alpha \cdot TEC + C_L \qquad TEC = map(\theta) \cdot VTEC$$
$$P_4 = \alpha \cdot TEC + C_P \qquad VTEC = f(B, L, H)$$

- Tomography: 3D electron density
- Irregularities: un-uniformed distributions of electrons
- Ionospheric delay model

Hong Kong (Low latitude) TEC

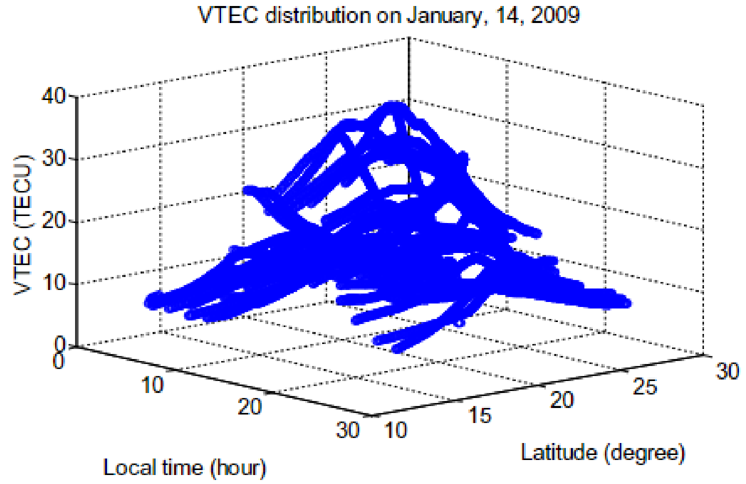

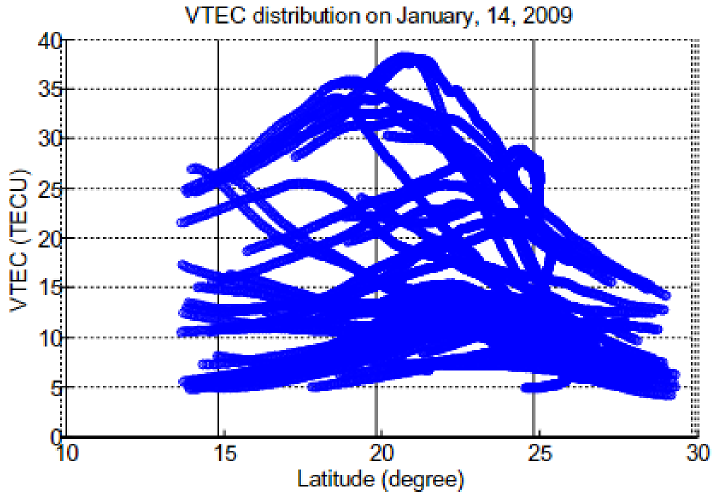

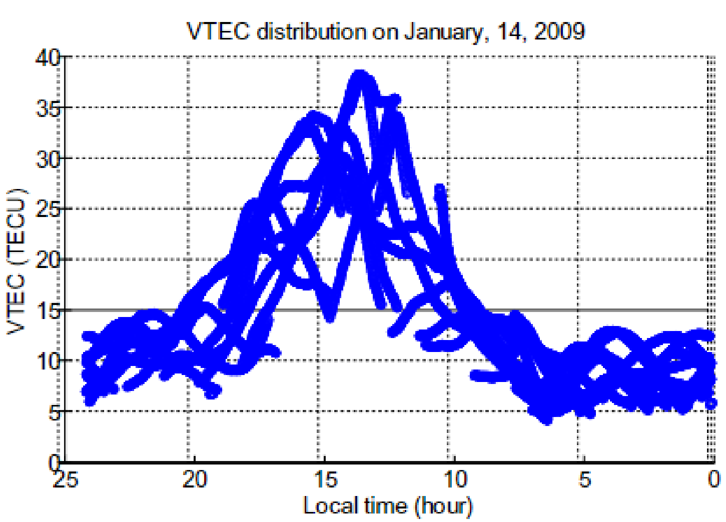

Tomography

- Accuracy depends on:
  - Station density
- Integration of ground and occultation data provide density distributions of different layers

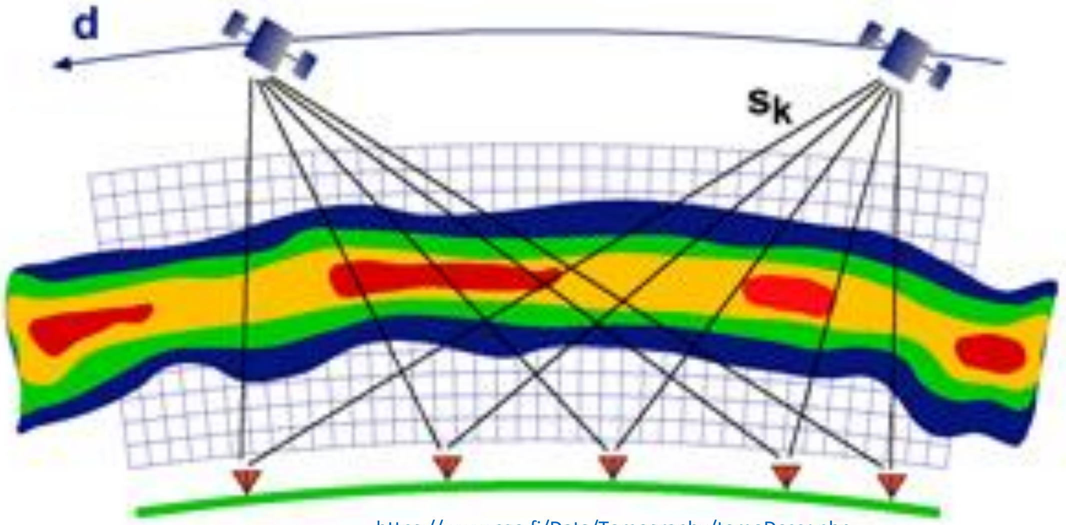

https://www.sgo.fi/Data/Tomography/tomoDescr.php

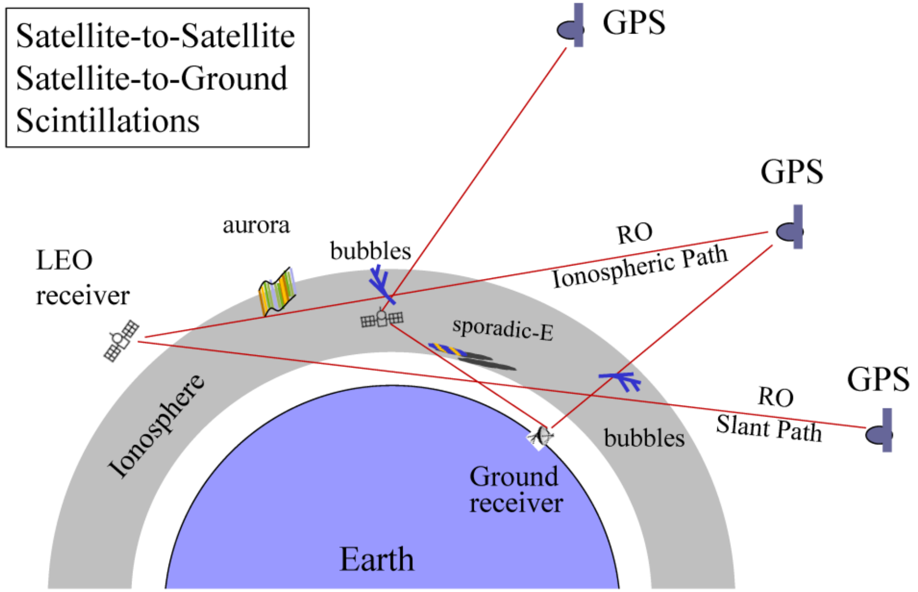

Ionosphere response to earthquakes

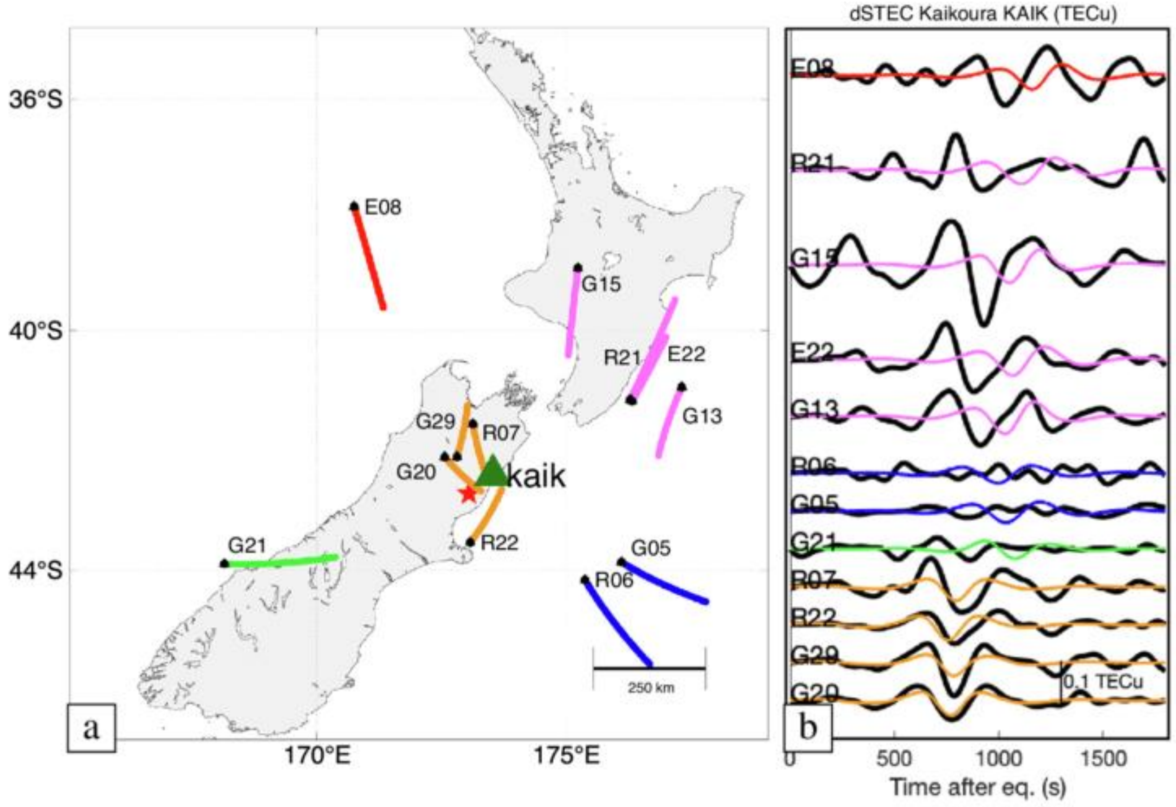

https://reader.elsevier.com/reader/sd/pii/S027311772100466X?token=F318FD58E7FD70105F292FEB68443F1B8B5EA23AE4F039BBDC2B55AE1CF7381FF2D20EA1A9B72A010B997EF7022AAF91&originRegion=us-east-1&originCreation=20221214083622

GNSS tropospheric delay

- The Refractivity

$$N = 77.6 \frac{P}{T} + 3.73 \times 10^5 \frac{e}{T^2}$$

Where P = Total Pressure,
T = Absolute Temperature and,
e = Partial Water Vapour Pressure.

- Delay in GNSS measurement

$$\text{Total delay} = \text{VDry}*M_d(\alpha)+\text{VWet}*M_w(\alpha)$$

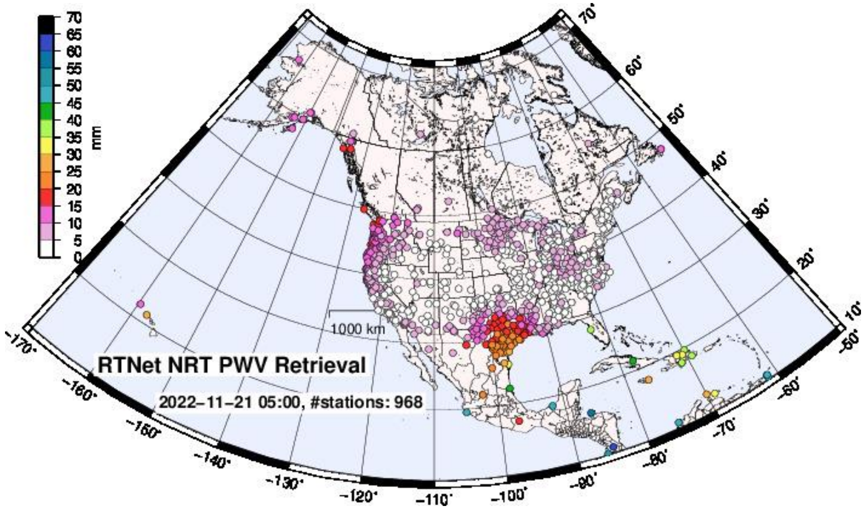

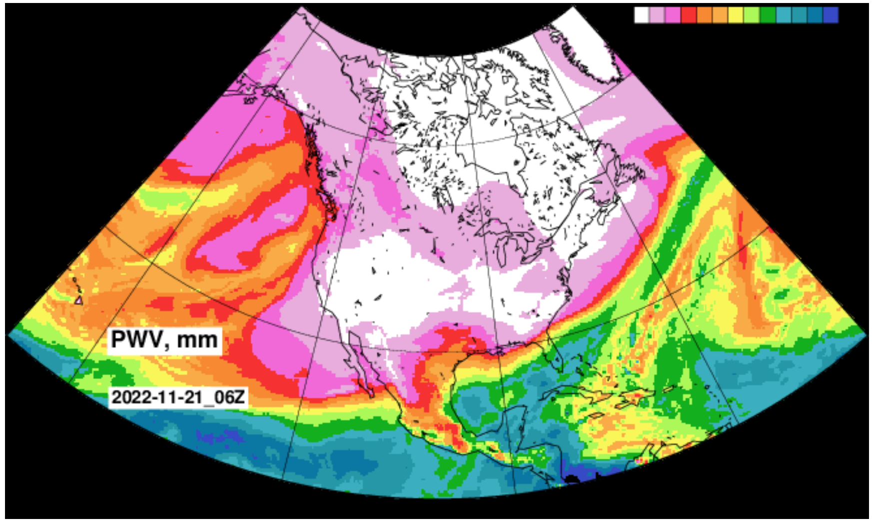

https://gps-solutions.com/

GNSS PWV and Rainfall

- Significant drop on PWV
- Followed by heavy rains

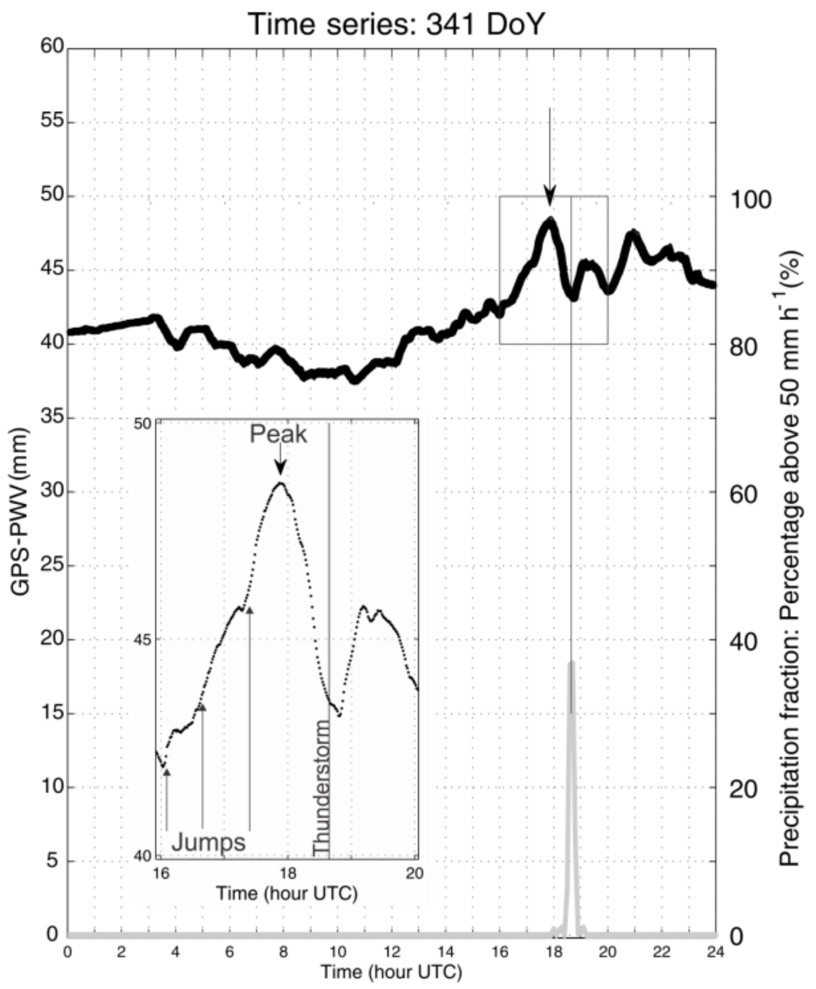

https://rmets.onlinelibrary.wiley.com/doi/epdf/10.1002/met.1735

Site movement

- The fundamental function of GNSS
- What are the reasons?
- Earth Tide
  - GNSS has been used to estimate tidal information
- Earthquakes
  - Type of the earthquakes
- Ground water changes
- Glacier rebounding

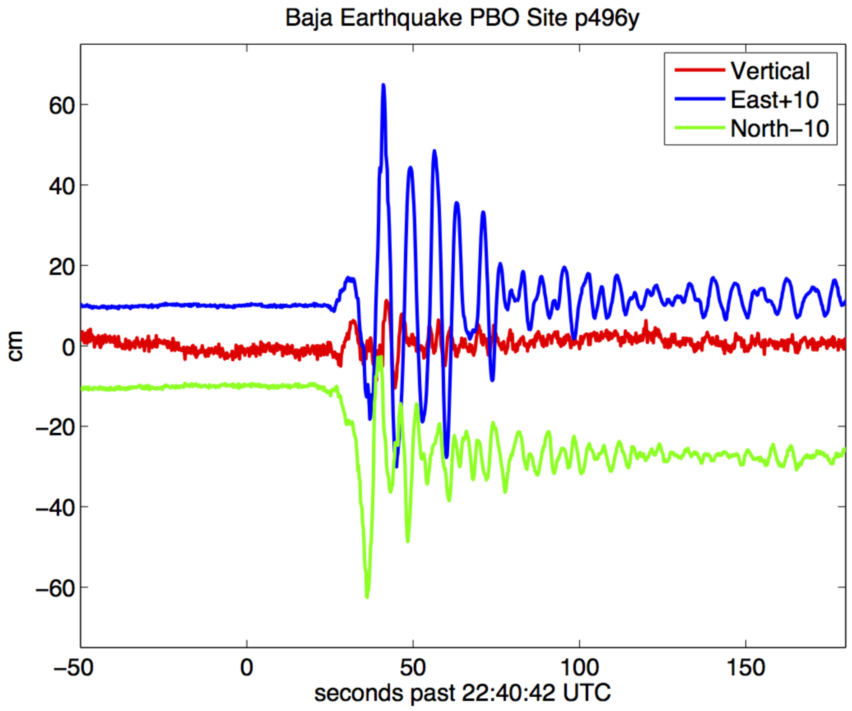

https://agupubs.onlinelibrary.wiley.com/doi/epdf/10.1029/2011EO150001

GNSS reflectometry

Concept of GNSS reflectometry

- In conventional GNSS applications, the multipath of GNSS signal influence the position accuracy, and need to be eliminated
  - Antenna Design
  - Receiver Design
  - Data filtering

- On the other hand, GNSS signal reflected from the ground carries information of the reflect surface
- GNSS Reflectometry
  - To study the reflected signals
  - To some extend: L-band remote sensing with constant signal sources

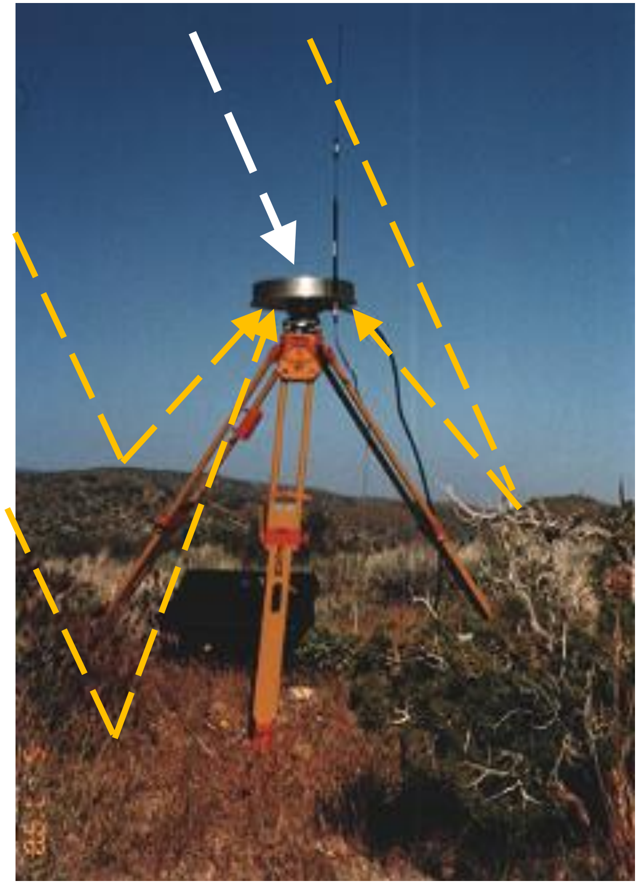

Concept of GNSS reflectometry

- What can the reflected signals tell us?

- Data source: (from Aug. 1st to Aug 27th , 2013)
  - GPS observation data from HKKT GPS reference station (red pot) with normal GPS receiver.
  - Weather data from Shek Kong weather station (pink pot).
  - The distance between two stations is about 2 km.

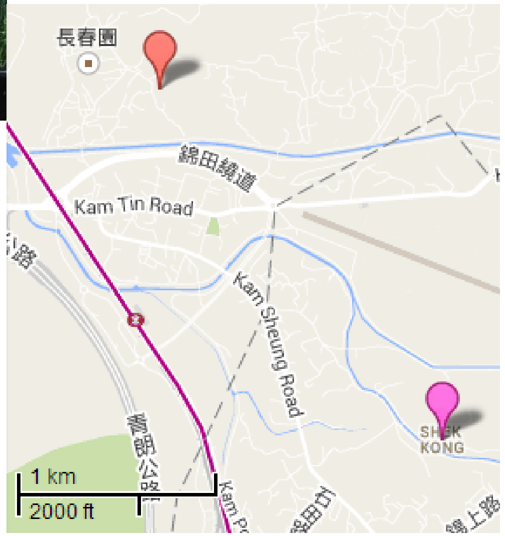

Concept of GNSS reflectometry

Data Processing:

- Calculate C/A code multipath data from GPS observation:

$$MP_{P_1} = P_1 - \frac{9529}{2329}\emptyset_1 + \frac{7200}{2329}\emptyset_2 + K_1$$

$$MP_{P_2} = P_2 - \frac{11858}{2329}\emptyset_1 + \frac{9529}{2329}\emptyset_2 + K_2$$

- Where:

MP_{P_1}, MP_{P_2} are C/A code multipath on L1 and L2 band respectively, with noise in it.

P and Ø are the observation of code and carry phase.

K is constant while no circle slip occurs and includes ambiguity, Doppler affection and noise etc.

The output MP_{P_1} and MP_{P_2} contain random system noise which depends on the GPS receiver.

Concept of GNSS reflectometry

- The Least Mean Square (LMS) adaptive filter was used to separate the Multipath and Noise:

$$y(n) = \boldsymbol{w}^T(n-1)\,\boldsymbol{u}(n)$$

Where: $u(n)$ is input data which is the day 1 multipath time series; $d(n)$ is the expected data which is the day 2 multipath time series; $y(n)$ is output data; $\boldsymbol{w}(n)$ is the weight Matrix:

$$\boldsymbol{w}(n) = \boldsymbol{w}(n-1) + \mu e(n)\frac{\boldsymbol{u}^*(n)}{\boldsymbol{u}^H(n)\,\boldsymbol{u}(n)}$$

$$e(n) = d(n) - y(n)$$

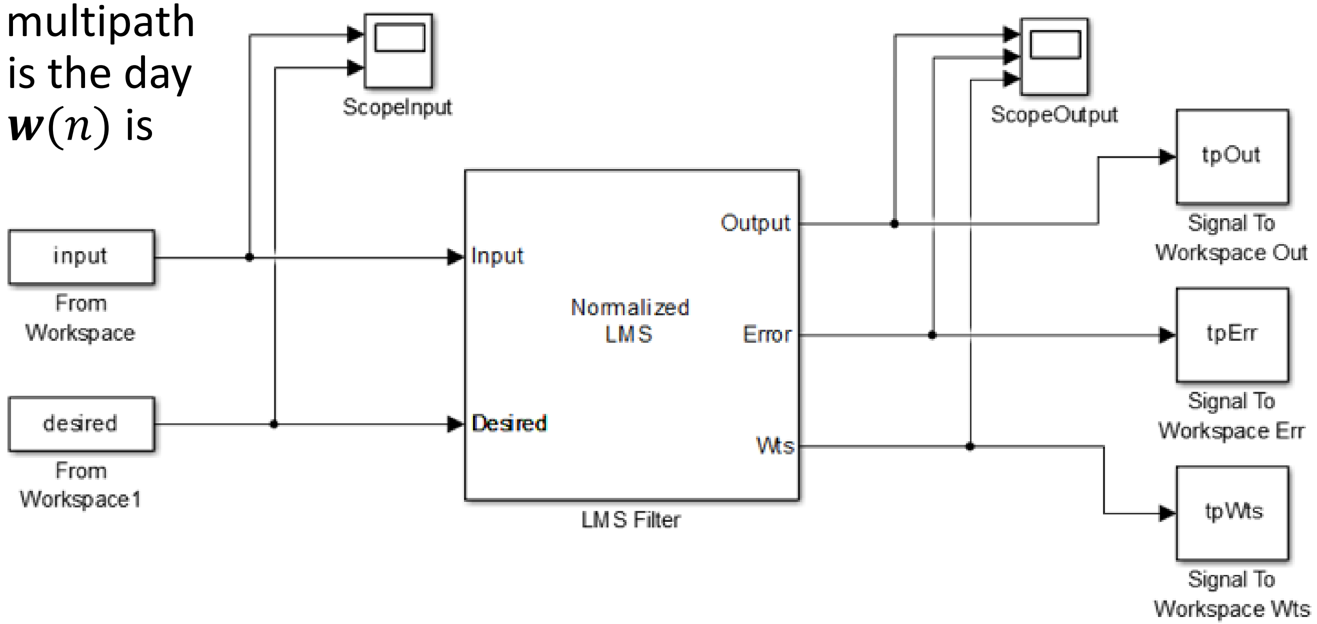

Concept of GNSS reflectometry

- LMS filter results analysis:
  - The Multipath show great correlation between two continues days.
  - The fluctuations of multipath are different especially the peak value.

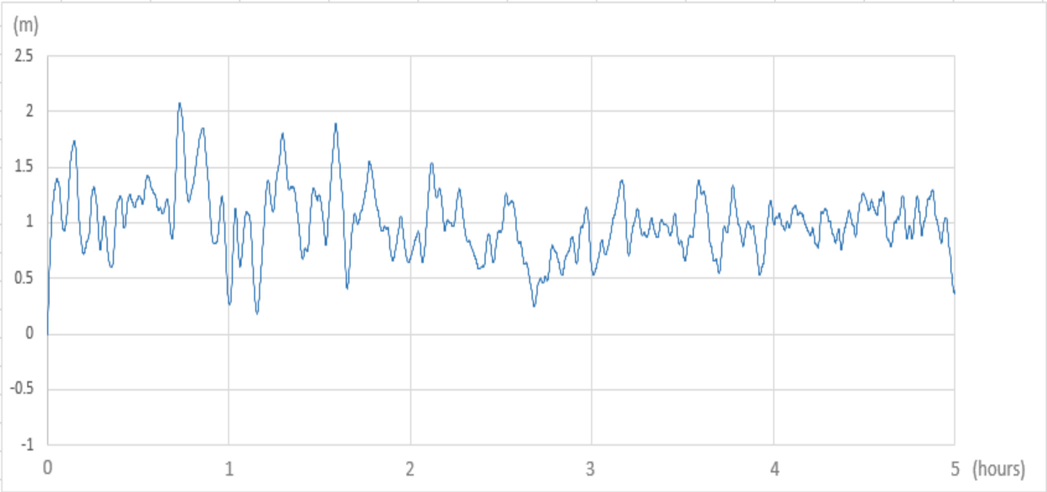

Fig. Multipath of Aug. 1st

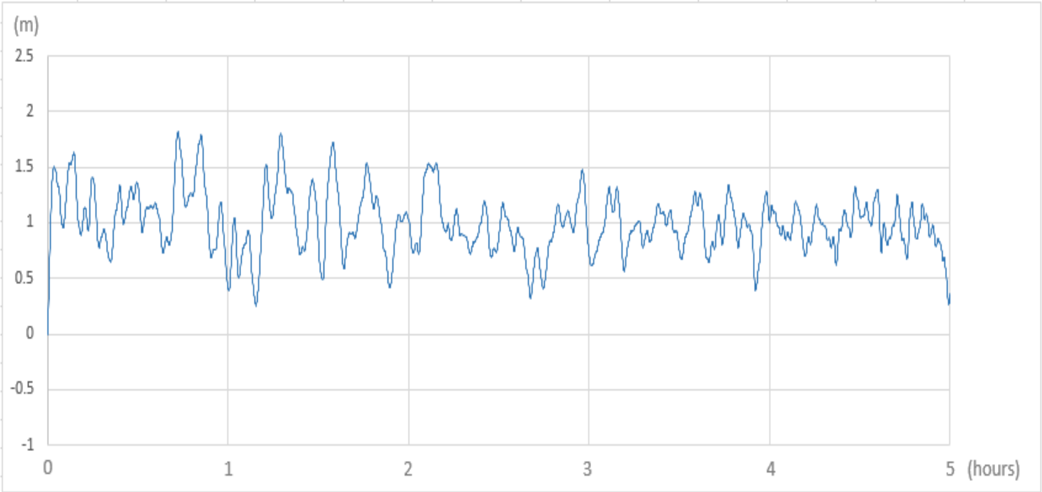

Fig. Multipath of Aug. 2nd

Concept of GNSS reflectometry

- The comparison of Std. of multipath and rain penetration:

The Std. of multipath has strong relationship with the penetration data: the Std. goes up when it rains;

The Std. slowly decrease and tends to stability after the rain day;

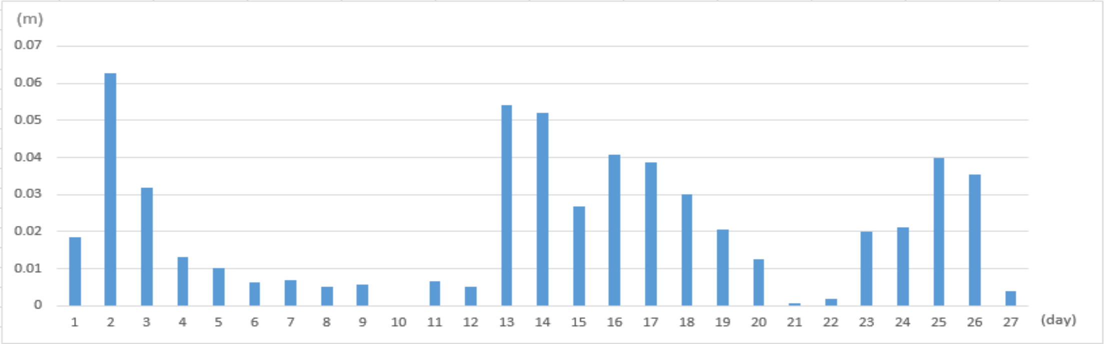

Std. of filtered multipath (Aug. 1st to Aug. 26th)

The Dielectric Constant can be strongly influenced by soil moisture.

And the strength of multipath signal can also be influenced.

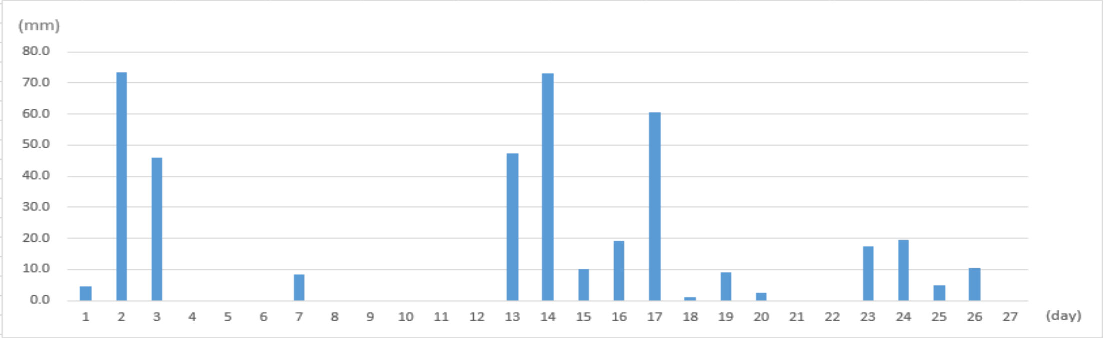

Penetration data (Aug. 1st to Aug. 26th)

Geometry of GNSS-R

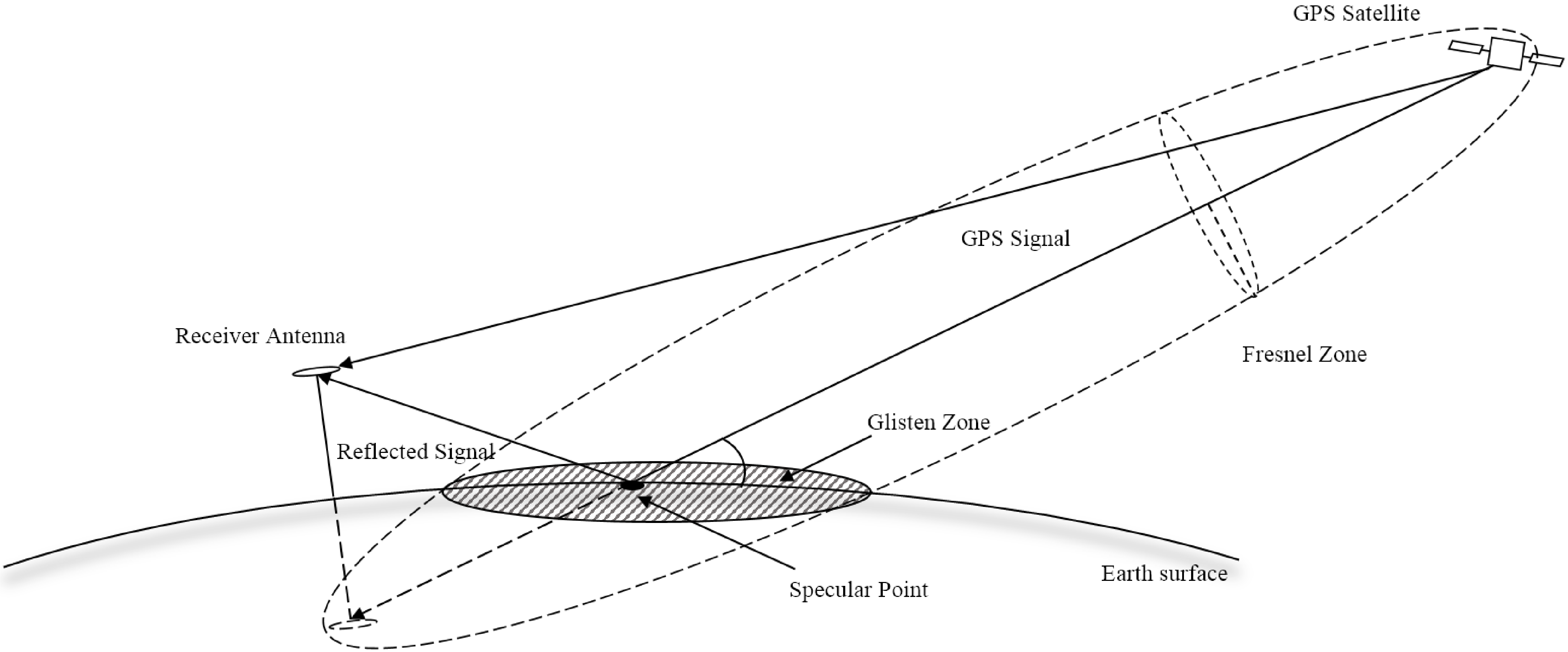

Basic Properties of the reflected signals

- In the glisten zone, the reflected signal from multiple reflect points have difference delay and Doppler frequency

- The delay and Doppler frequency depends on the receiver height from the reflect surface, and the relative speed between GPS satellite and the receiver

- The signal strength is related to the properties of the reflected points

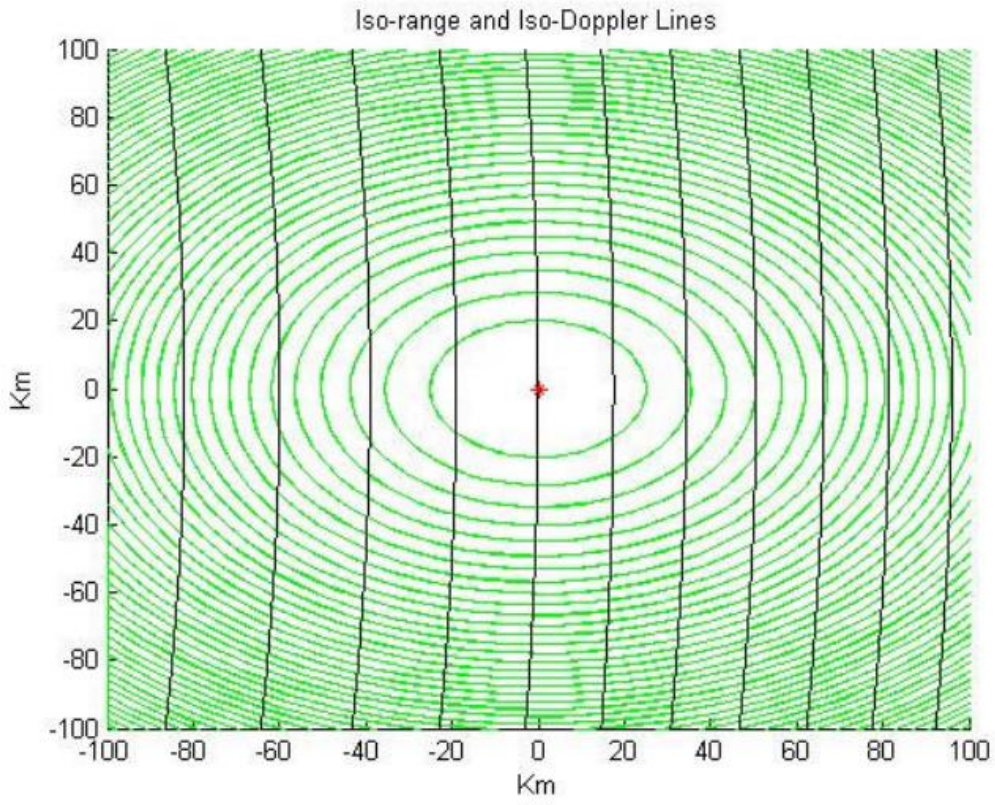

Green circles: The iso-range lines
Black trip: iso-frequency lines

https://www.intechopen.com/chapters/59160

Basic theory

- Direct signal (RHCP):

$$R_d(t) = A \cdot exp[i(\omega t + \emptyset)] \cdot y(t) \cdot d(t)$$

- Reflected signal (LHCP):

$$R_r(t) = \sum_{k=1}^{n} A_k \cdot exp[i(\omega(t - \tau_k) + \emptyset_k)] \cdot y(t - \tau_k) \cdot d(t - \tau_k)$$

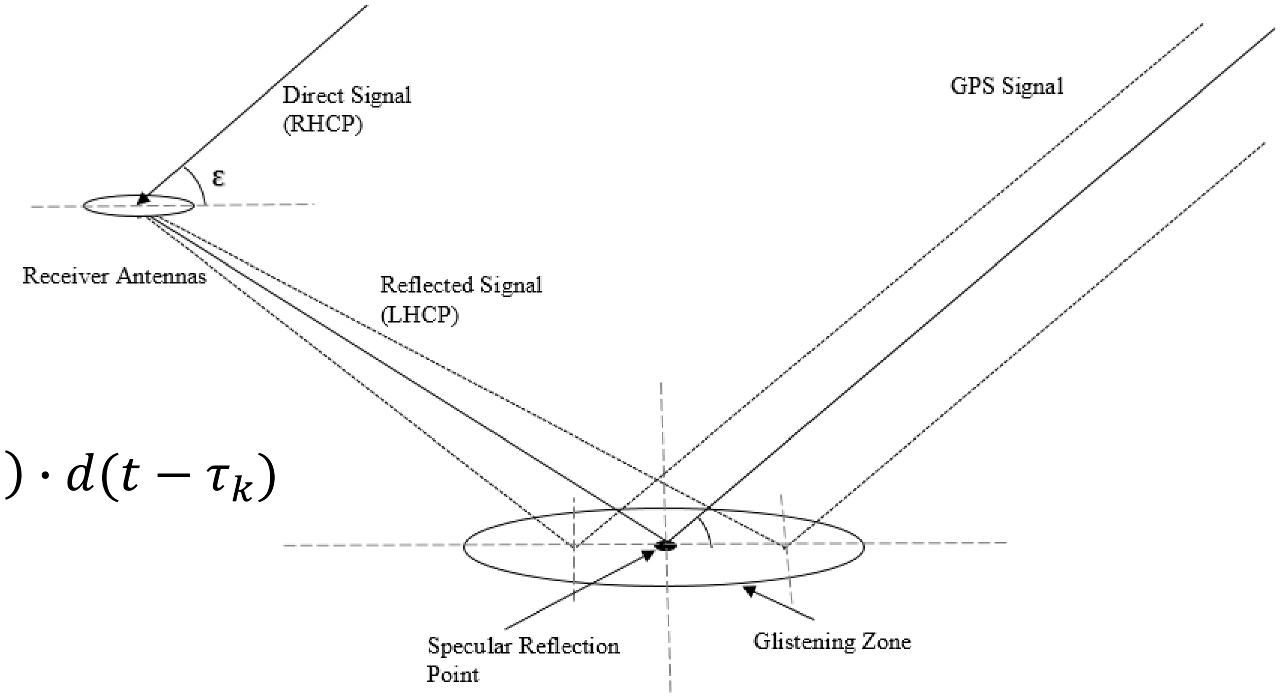

Basic theory

- The difference between the direct and reflected signal:
  - A: the amplitude (SNR);
  - τ: signal delay;
  - $\emptyset$: carrier phase;
  - $\omega = 2\pi f$: signal frequency (Doppler frequency);
  - The interference between multiple reflected signals;

- The difference of signal parameters reflect the physical properties of the reflect surface. The relationship can be modeled by Isolating and analyzing the reflected signal.

Front-end and software receiver

- Japan IRX front-end
  - Channel: 2
  - IF: 4.092MHz
  - Sampling Frequency: 16.368MHz

- Beihang University front-end
  - Channel: 4 (GPS and Beidou)
  - IF: 3.996MHz
  - Sampling Frequency: 16.369MHz

Front-ends and software receiver

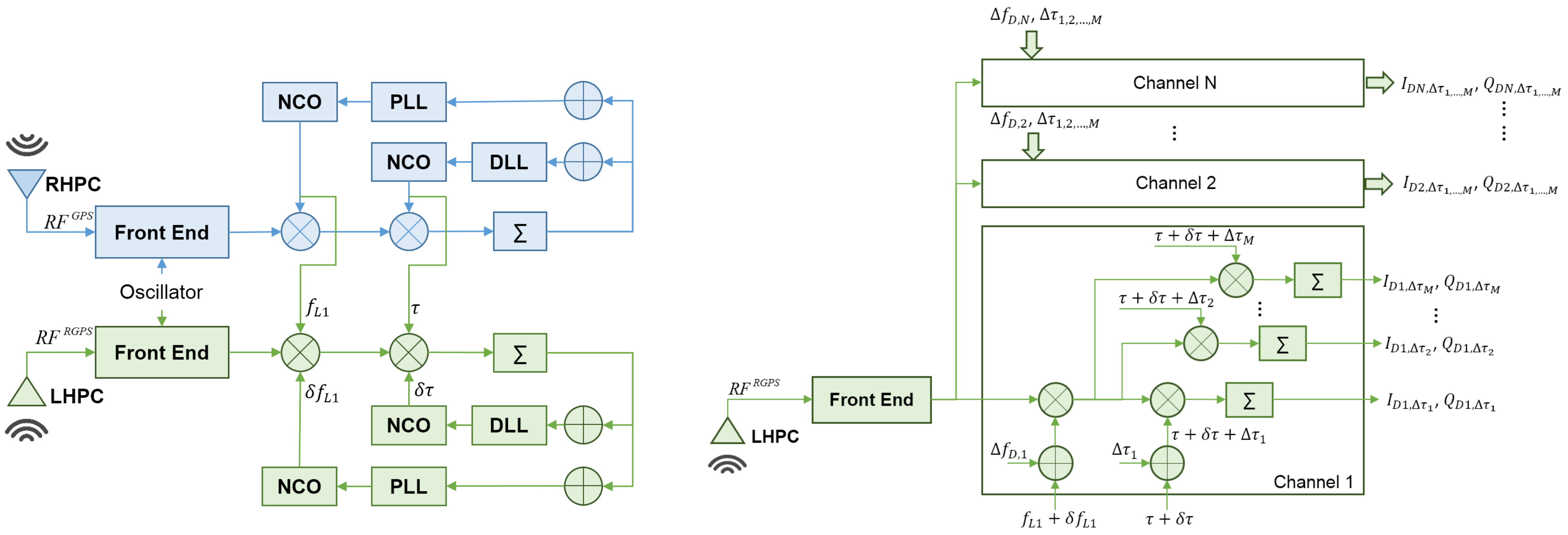

Software receiver: tracking loop and multi-channel Doppler delay correlator

Applications and approaches: some examples

- Surface monitoring
  - Sea wave height;(Clarizia, M. P., 2012)
  - Soil moisture; (Botteron, C., 2013)
  - Forest biomass; (Ferrazzoli, P., 2011)
  - Vegetation water content; (Wan, W., 2015)
  - Floating ice; (Gleason, S., 2006)
  - Oil slick; (Li, C., 2013)
  - etc.

- Altimetry
  - Sea level height; (Larson, M.K., 2013)
  - Vegetation height; (Small, E. E., 2010)
  - Topography retrieval; (Rodriguez-Alvarez, N., 2011)
  - Snow depth; (Gutmann, E., 2012)
  - etc.

- Reflect surface image
  - GNSS-SAR; (M Antoniou et al, 2018)

Some results in the following slides come from these references

Applications and approaches

- Based on the signal parameters, different approaches for monitoring the surface has been developed.
  - S/N ratio
  - Doppler Delay Map simulation
  - The Interferometric Complex Field method
  - The Interference-pattern Technology

- For altimetry applications, the delay lags between the direct and reflected signal need to be precise measured.

SNR Oscillation

- The SNR oscillation method use single normal GPS antenna (RHCP) and receiver.
- When satellite moves, the SNR at any instant is described by:

$$SNR = Acos\left(\frac{4\pi h}{\lambda} sin\varepsilon + \phi\right)$$

Where:
A: amplitude of the SNR.
h: antenna height above the reflect surface;
ε: elevation angle;
ϕ: phase offset;

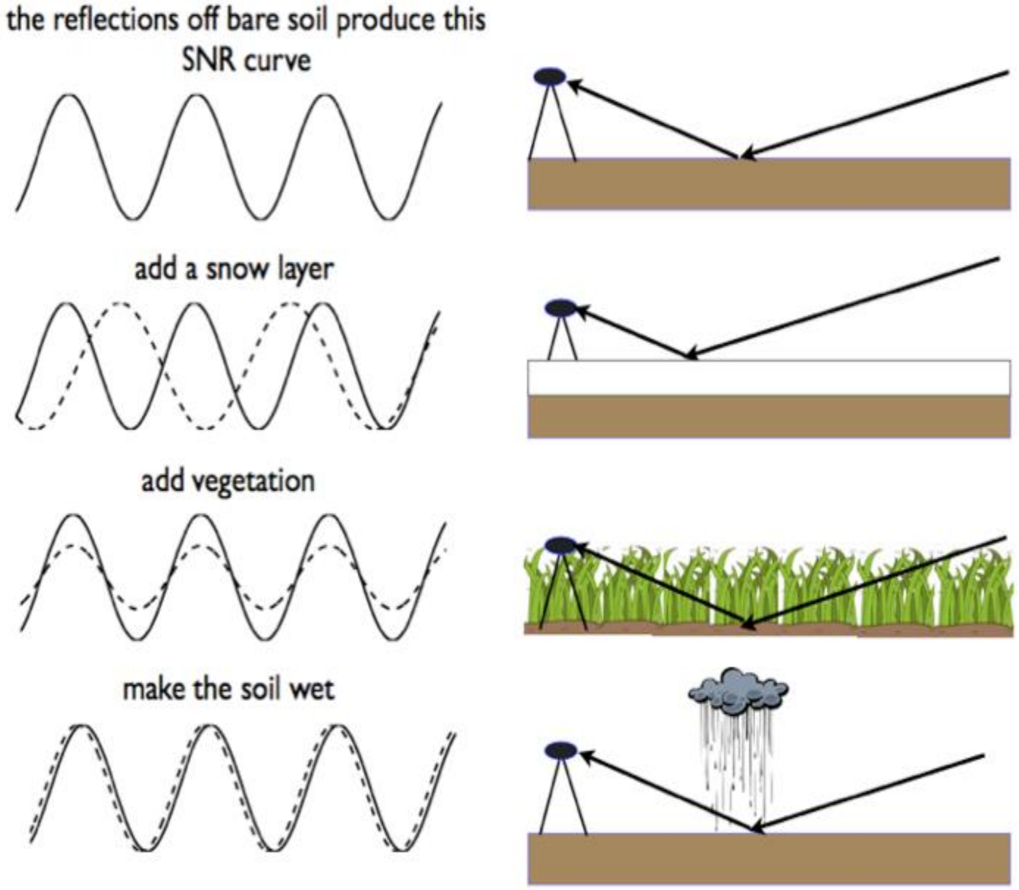

SNR Oscillation

SNR oscillation approach for soil moisture measurement

$$SNR = A cos\left(\frac{4\pi h}{\lambda} sin\varepsilon + \phi\right)$$

ϕ: Phase offset, which is closely related to the reflector depth.

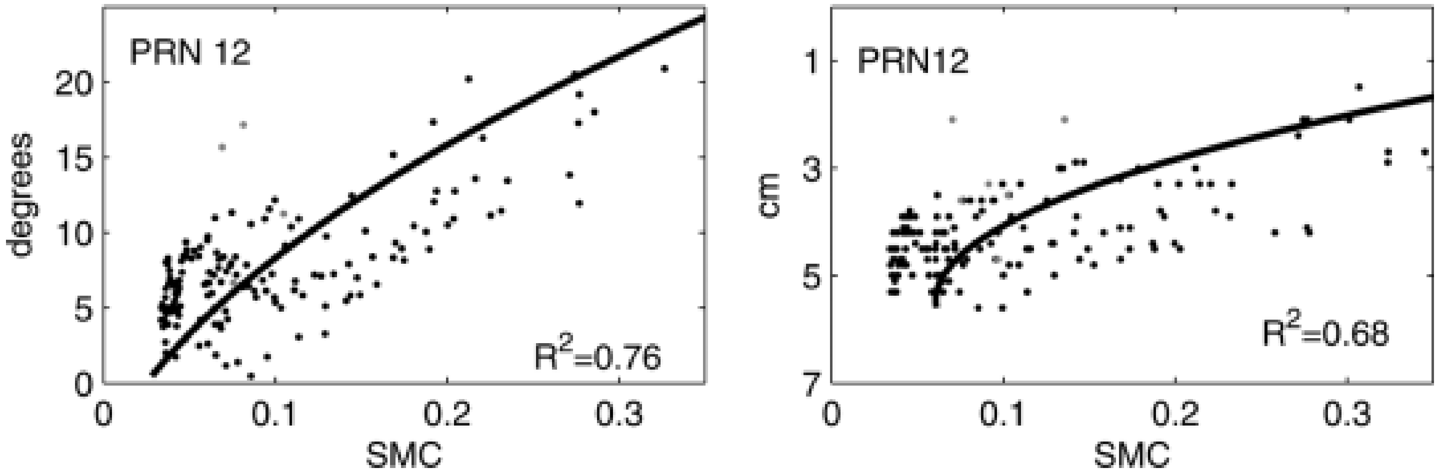

Comparison of soil moisture content (SMC) measured at 2.5 cm and estimated ϕ (left column) and h (right column).

SNR Oscillation

Soil Moisture Measurement

- The relationship between the reflector depth and the soil moisture

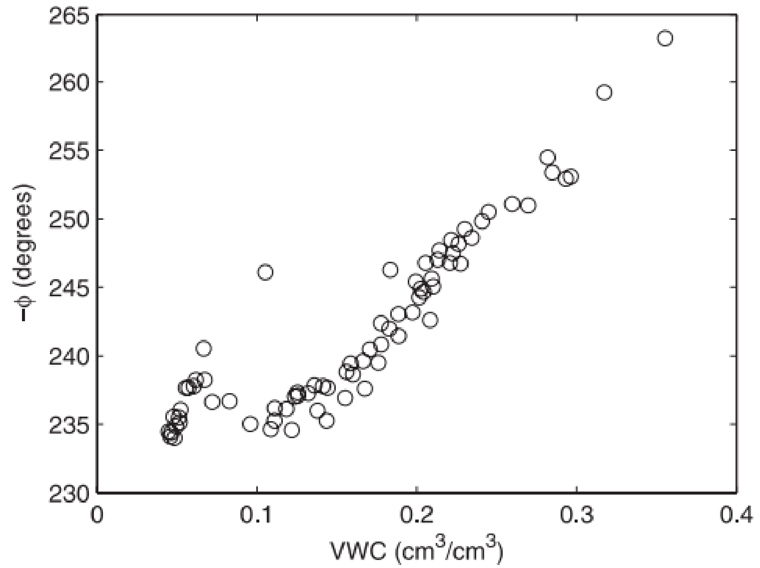

Estimated ϕ compared with Volumetric Water Content (VWC)

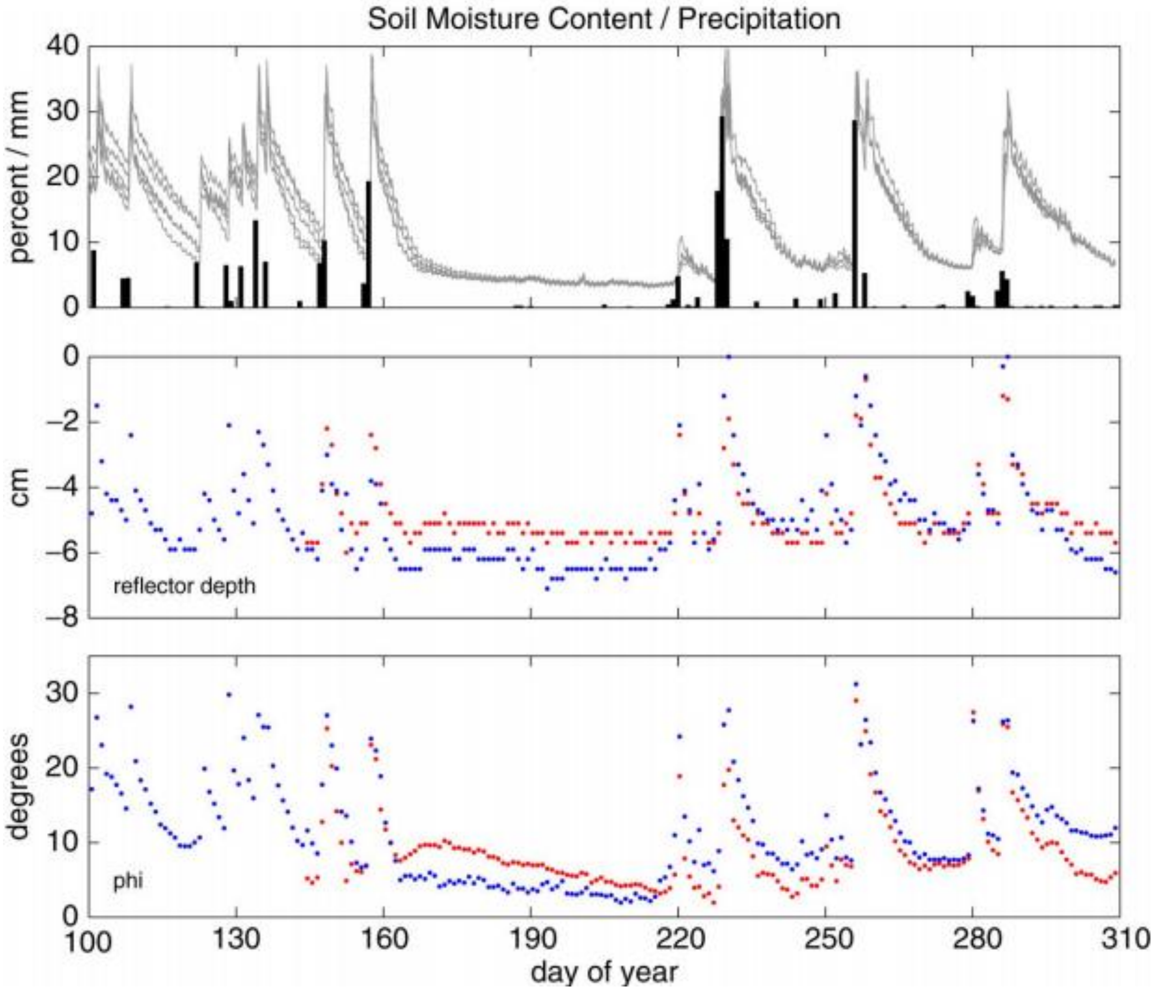

SNR Oscillation

soil moisture measurement

- Inversion through the modeled relationship between the phase offset and the soil moisture

The phase offset ϕ

↓

The penetration depth

↓

The soil moisture

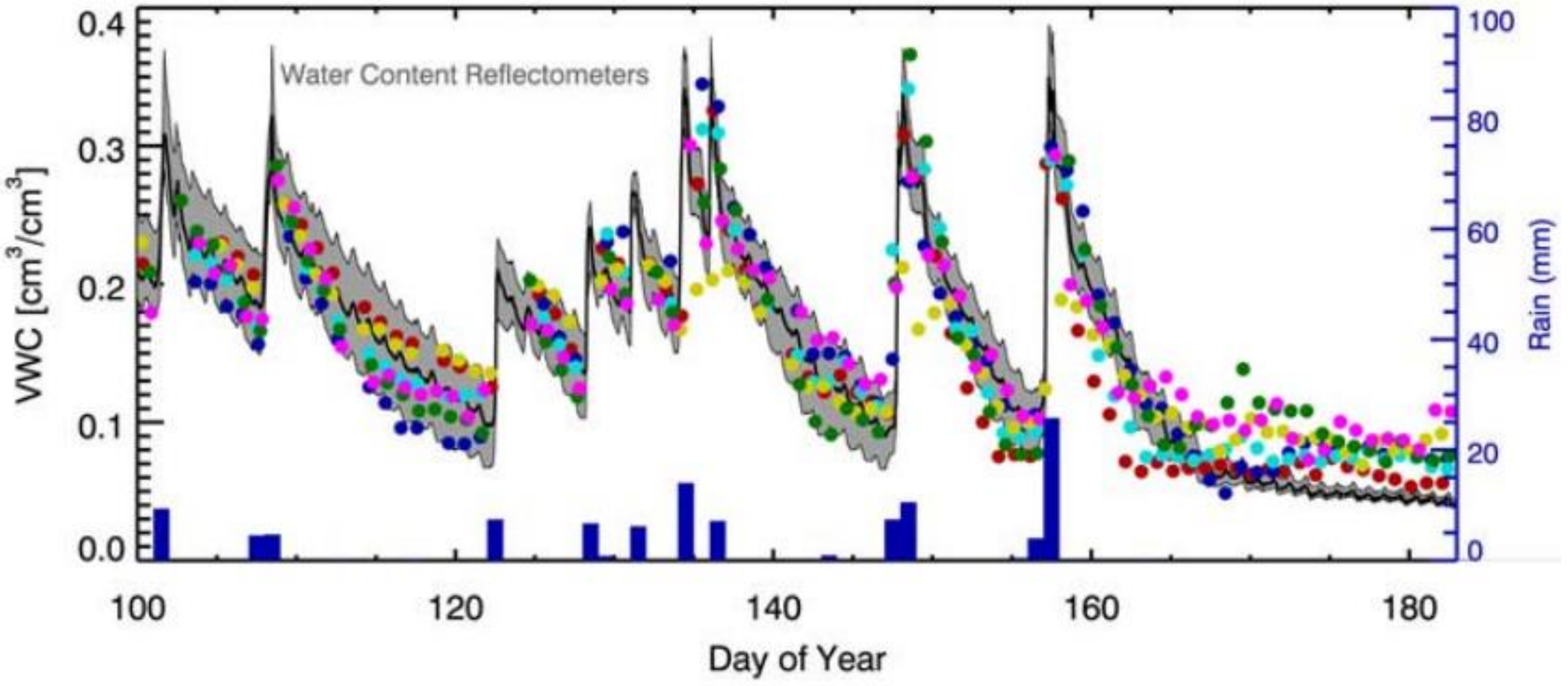

Variation in (Volumetric Water Content) VWC from multiple GPS satellites (different color dots).

SNR Oscillation

- The SNR oscillation method also can be used for snow depth measurement.

- The reflected signal will have interference with the direct signal and the signal strength will vary with the phase difference.

$$SNR = A\cos\left(\frac{4\pi h}{\lambda}\sin\varepsilon + \phi\right)$$

ϕ: Phase offset, which is closely related to the reflector depth.

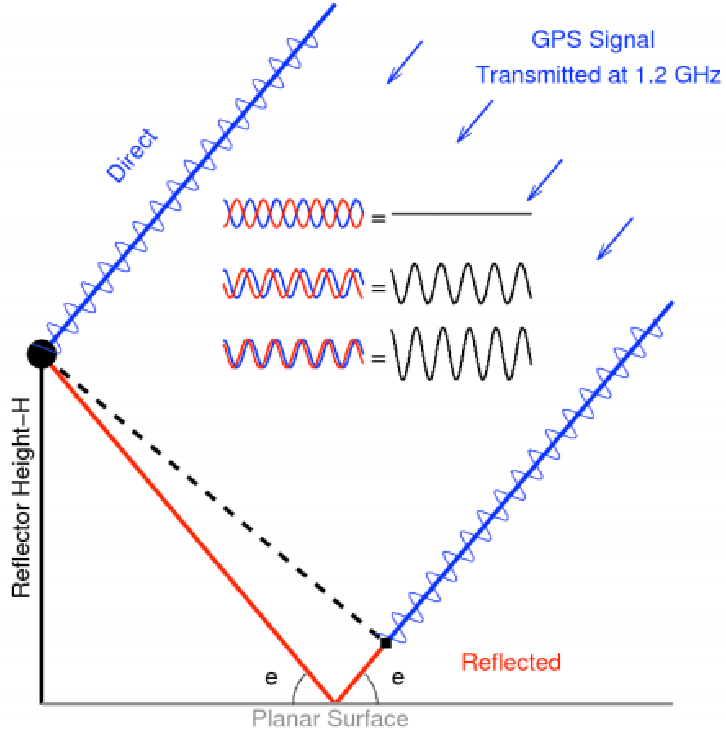

SNR Oscillation

snow depth measurement

- The Plate Boundary Observatory operates lots of GPS stations and provide data for analysis.

- The PBO sites in Alaska, USA are chosen.

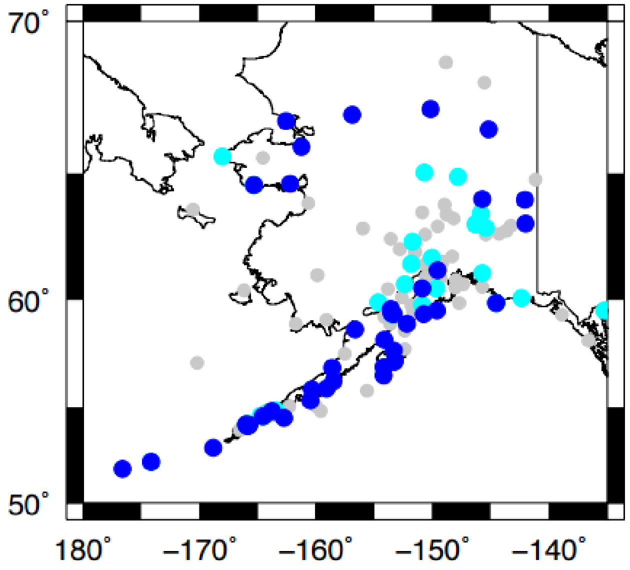

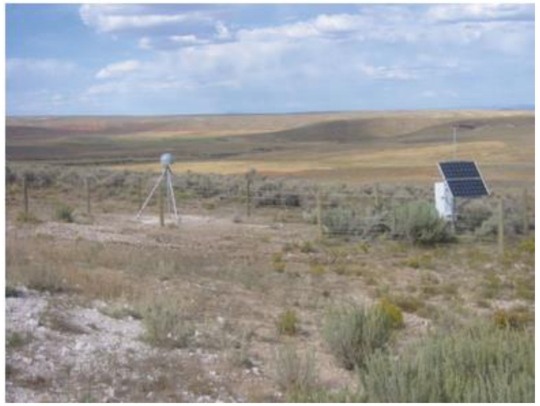

SNR Oscillation

snow depth measurement

- GPS snow depth retrievals from PBO sites p360 and p101.
- Standard deviations represent the standard deviation of the individual satellite tracks and a formal error of 2.5 cm, added in quadrature. SNOTEL data are also shown as reference data.

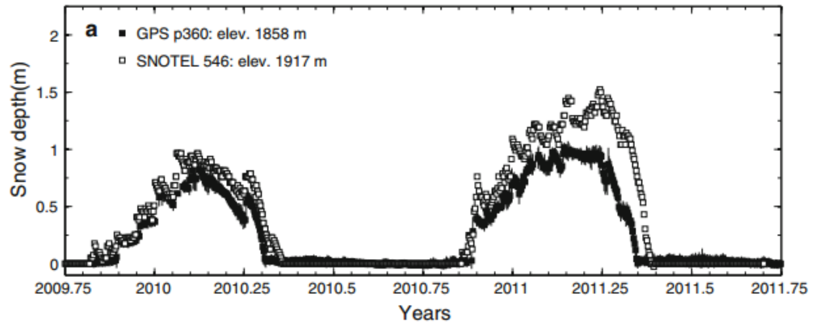

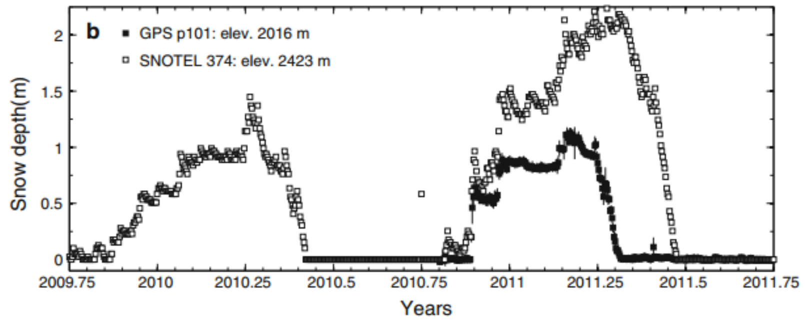

- Snow depth measured at GPS site near Galena, Idaho for three years. The average of error are 4 cm.

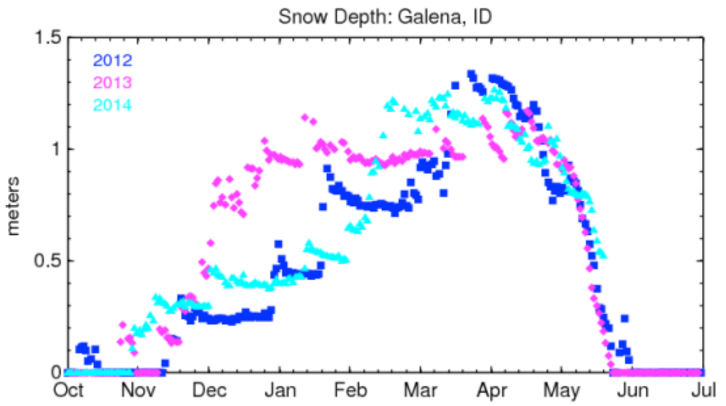

DDM simulation

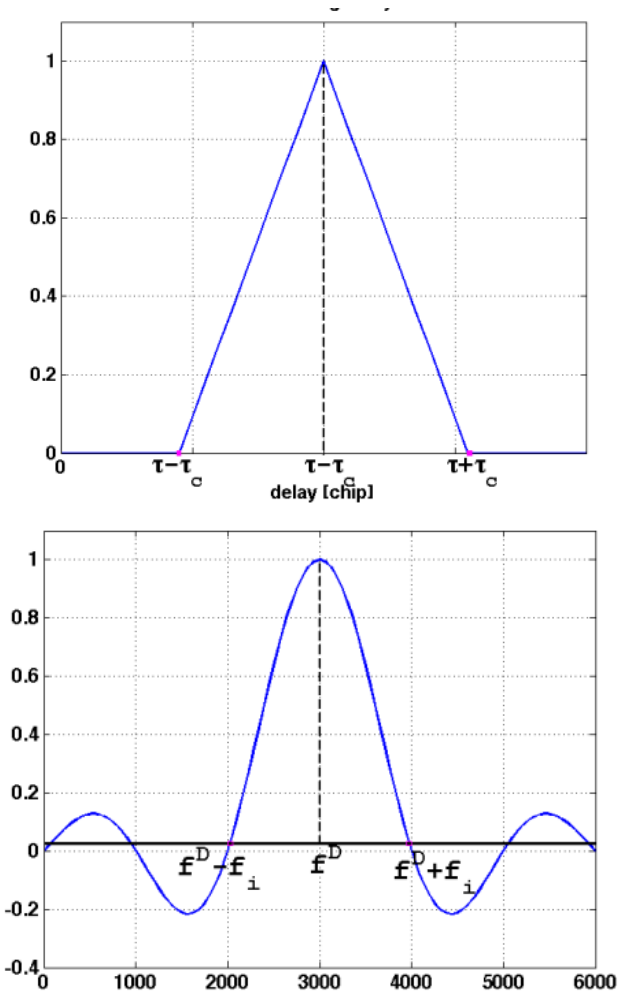

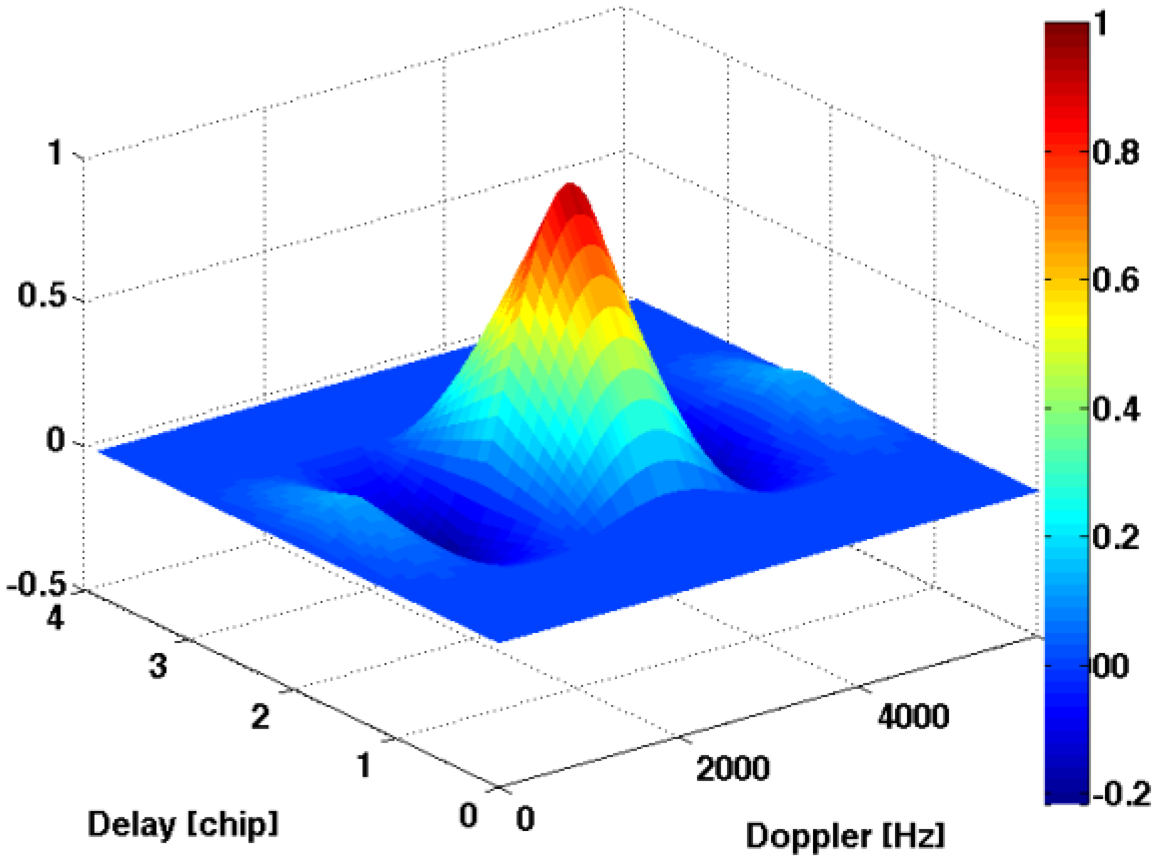

DDM simulation

Doppler-Delay Map for dynamic GNSS-R receiver (LEO satellite)

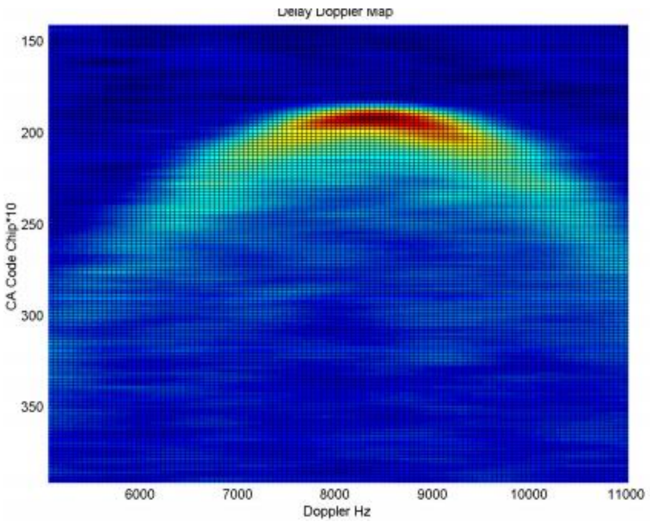

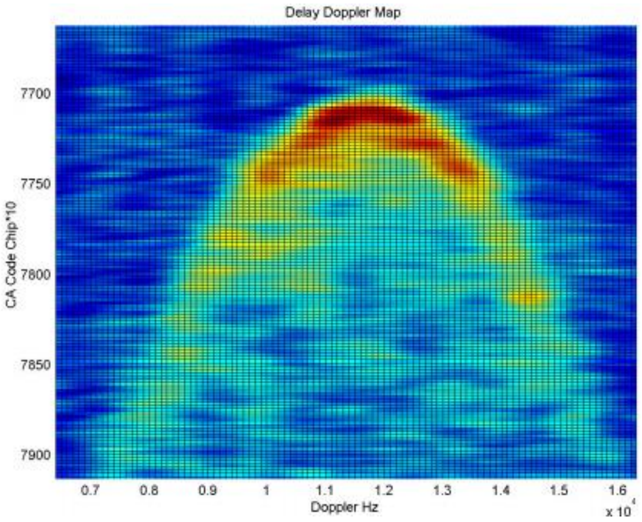

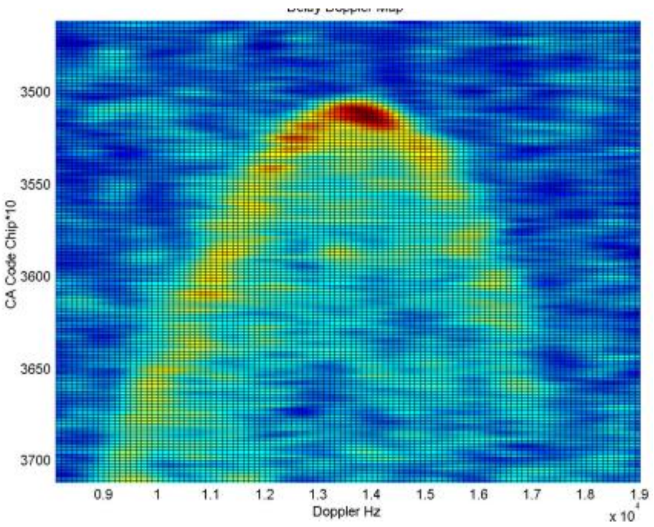

Date d/m/y	23/03/04 a	04/03/05 b	03/10/04 c
Wind	~2.0 m/s	7.0 m/s	10.3 m/s
Wave Height	-	2.6 m	2.8 m

DDM simulation

- The Z-V model simulator requires some input parameters which can be grouped into:
- 1. Geometry parameters: positions and velocities of the transmitter and receiver;
- 2. Dimension and resolution of the Glistening Zone;
- 3. Antenna parameters;
- 4. Sea state parameters: the Directional Mean Square Slopes (DMSS) and the Principal Wave Slope Direction (PWSD), also the Probability Density Function (PDF) of the sea surface wave slopes;
- 5. Delay-Doppler parameters: the delay range the Doppler range.

- Reason of difference:
- 1. Residual speckle noise; 2. Thermal noise; 3. limitations of modeling or simple PDF (Gaussion distribution)

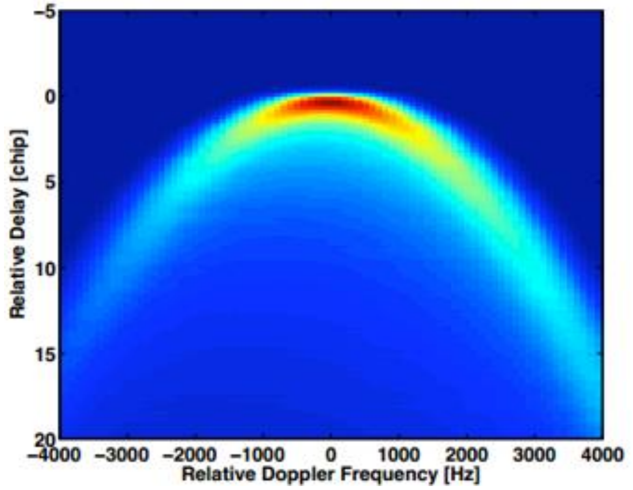

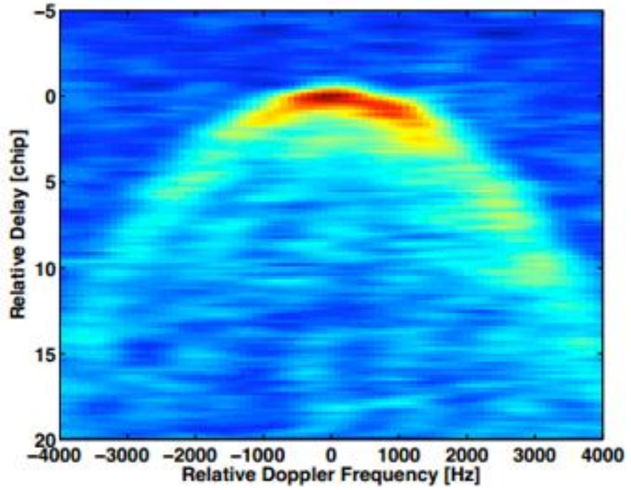

DDM simulation

- Experiment parameters at Shenzhen

Equipment specification		
Antennas	Direct antenna	Right hand circular polarization (RHCP)
		45 degree from zenith
	Reflect antenna	Left hand circular polarization (LHCP)
		135 degree from zenith
Satellite acquisition	GPS and Chinese BeiDou system	
Channels	4 channels direct and reflected signal	
Intermedia Frequency	3.996 MHz	
Sample rate	16.369 MHz	
Data output	Sampled IF data in binary	
Experiment		
Data collection duration	106 hours	
Data size	6.3 TB	
File number	3289 (each file includes 2 minutes data of about 2 GB)	

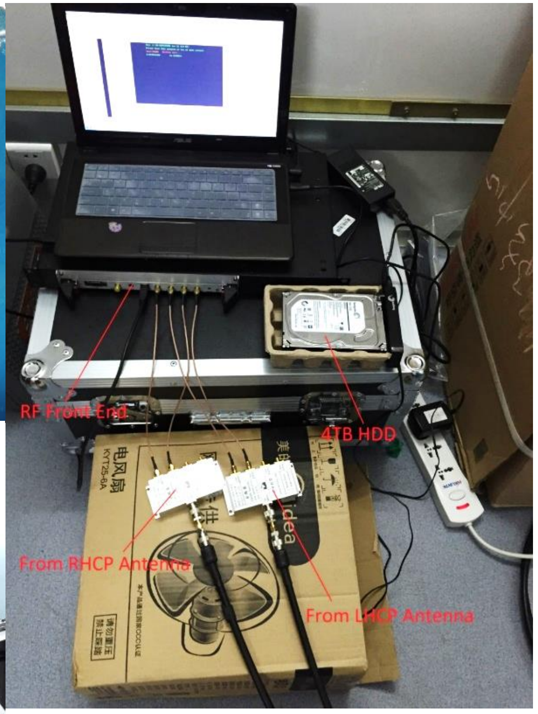

Satellite view

Antenna platform

Radio Front End

DDM simulation

- The delay waveform can be obtained from multiple delay lags correlation of direct and reflected signal;
- Doppler Delay Map (DDM) can be calculated base on each delay lags by applying multiple Doppler shift correlators.

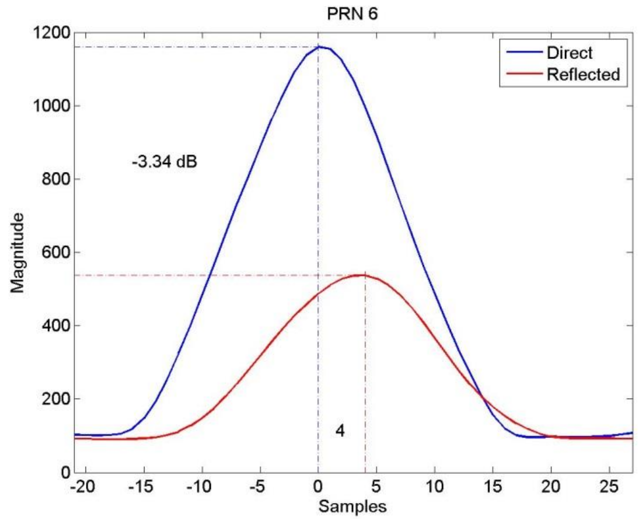

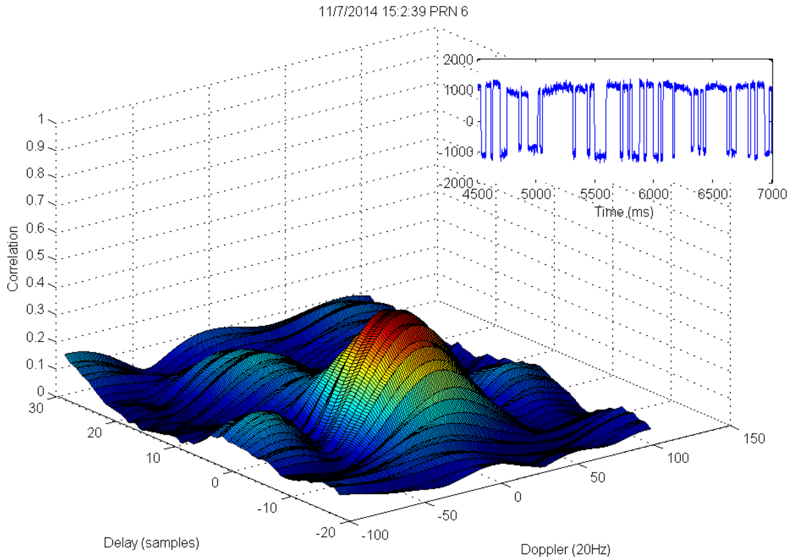

Delay waveforms and DDM of Nov 7th, 2014.

DDM simulation

- The Relationship between correlation value and wind speed.

- The relationship between the average DDM correlation peak and the average wind speed.

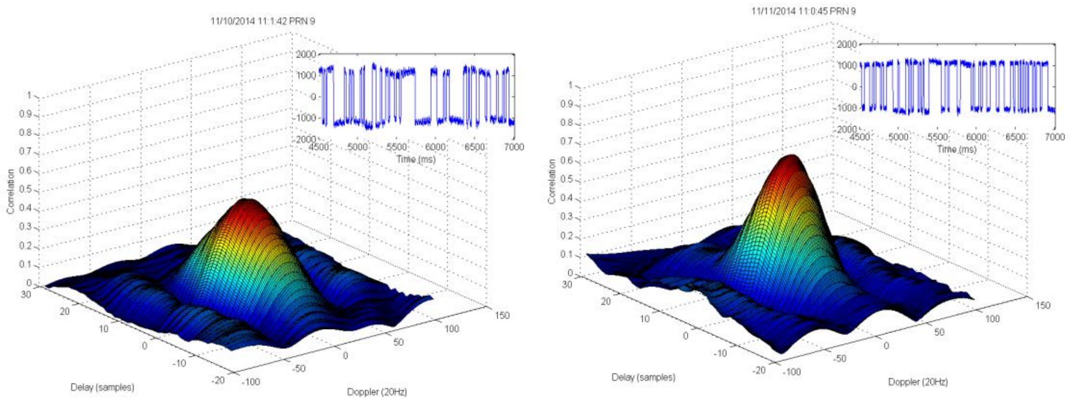

Wind speed: 11.4 m/s

wind speed: 7.4 m/s

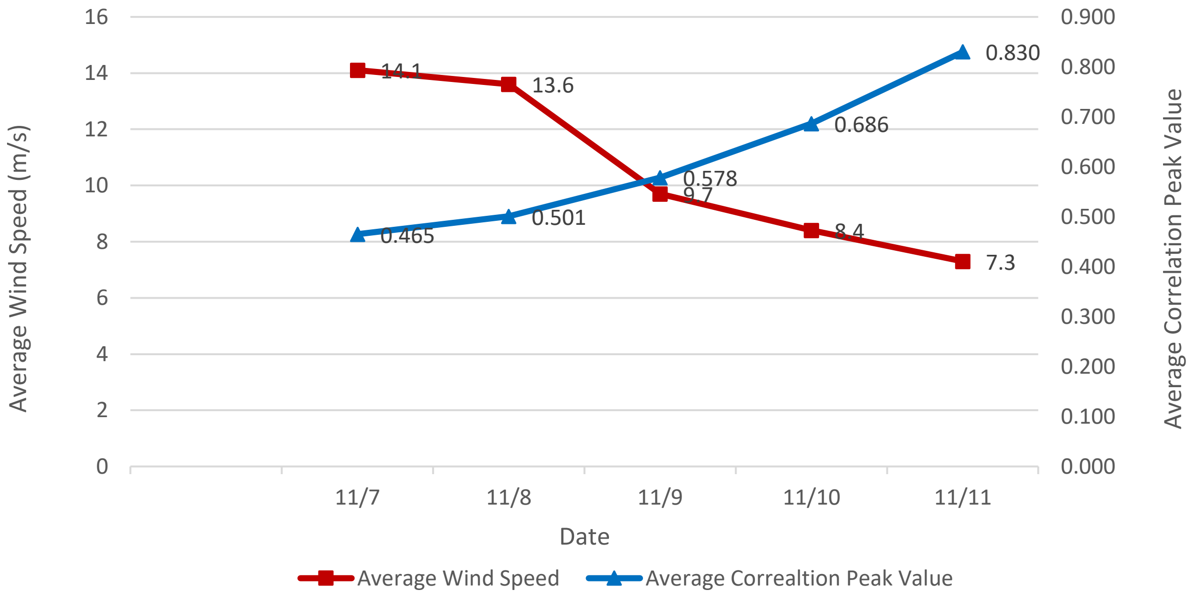

DDM simulation

- DDM can be simulated with input parameter of Mean square slop (MSS).
- Matching the obtained DDM and simulated DDM to inversely calculate the sea surface status.
- Also, by applying wind-driven sea surface model, the wind speed above the sea can be obtained.

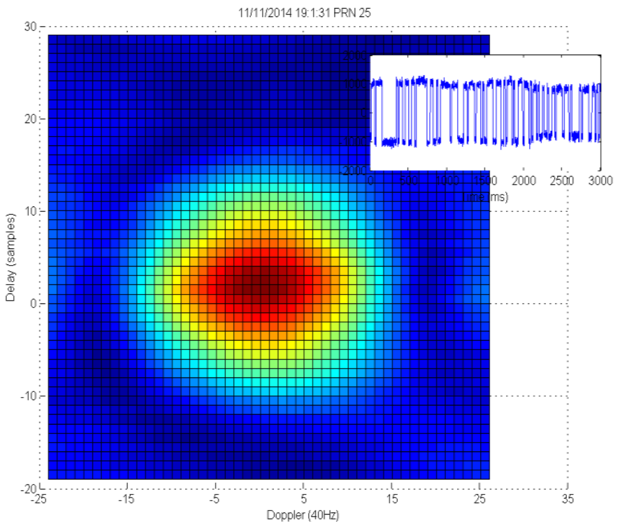

Obtained DDM

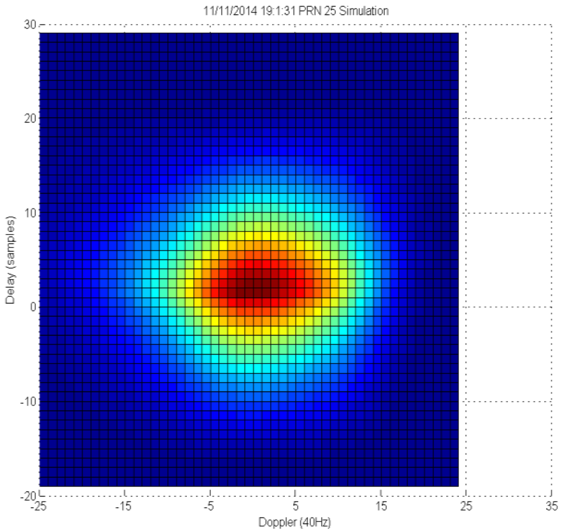

Simulated DDM

DDM simulation

- Other applications:
  - Oil slick

    The oil covered area has difference reflectivity compared with sea surface.

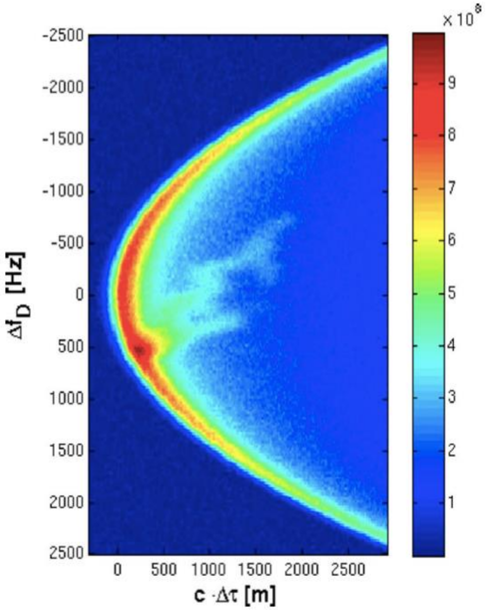

DDM

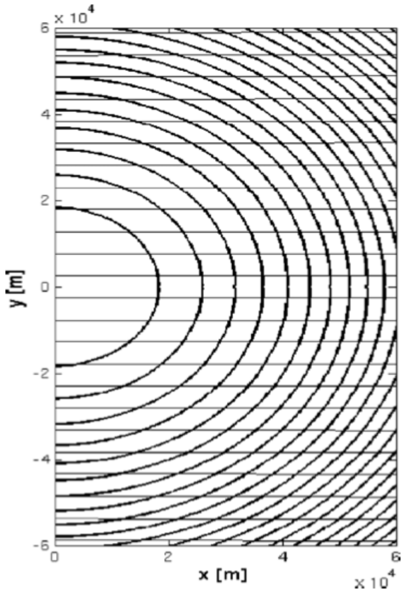

Grid glistening zone (half)

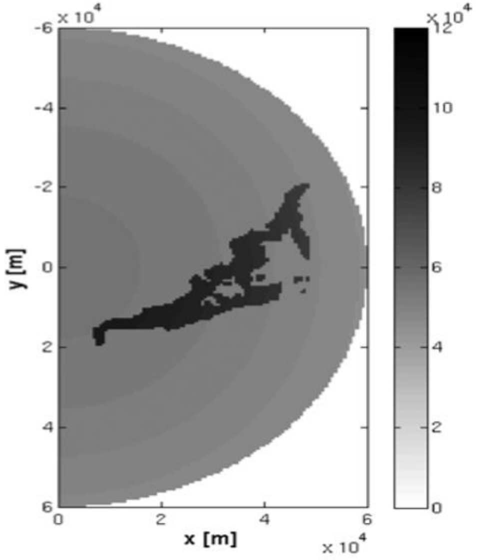

Estimated result

The satellite image

Interferometric Complex Field method

Oceanpal® Instrument architecture

The Interferometric Complex Field (ICF) is defined as:

$$ICF(t) = \frac{P_R(t)}{P_D(t)}$$

Where: P_R and P_D represent the time series of waveform peaks for the reflected and direct signals, respectively.

Data Processing and storage:

L0 : Interferometric Complex Field (ICF)

L1 : field coherence time, direct/reflected lapses

L2 : geophysical products (SWH and H)

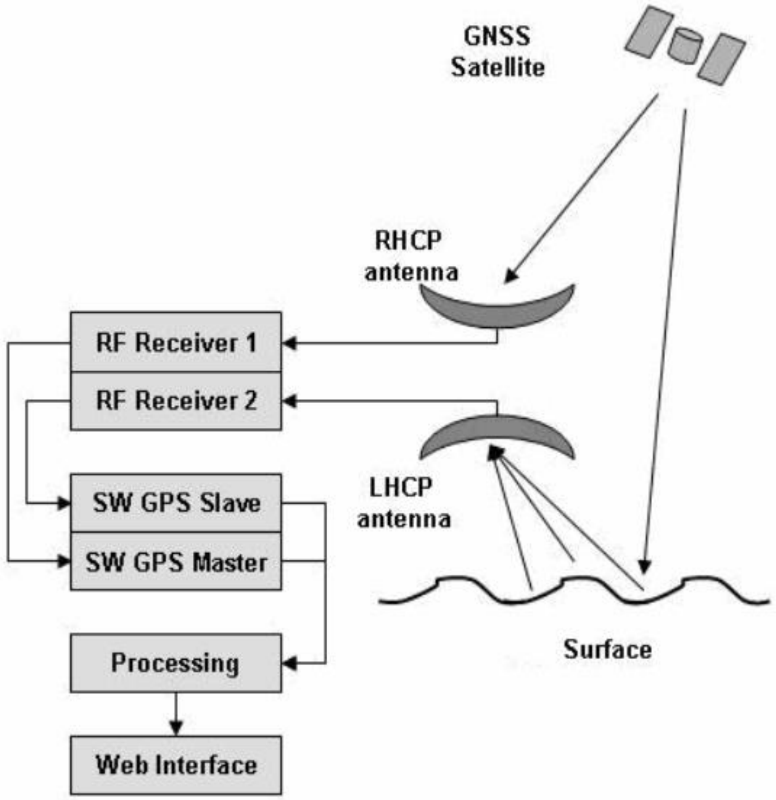

Interferometric Complex Field method

- **Sea state retrieval**
- Sea roughness is related to the coherent of the signal.
- For a time interval Δt, the autocorrelation function can be described as:

$$\Gamma(\Delta t) \approx A(\sigma_Z, l_Z, \varepsilon, G_r) \cdot e^{-4k^2 {\sigma_Z}^2 \frac{\Delta t^2}{2\tau_Z^2} \sin^2 \varepsilon}$$

- Where:

  σ_Z is the standard deviation of the sea surface elevation;

  l_Z is the autocorrelation length sea surface;

  τ_Z is the correlation time of the sea surface (incoherent time);

  G_r is the gain pattern of antenna;

  ε is the elevation angle.

Front end and data management unit

Antennas

Mask

Interferometric Complex Field method

- The coherence time of the interferometric field can be written as:

$$\tau_I = \frac{\tau_Z}{2k\sigma_Z sin\varepsilon} = \frac{\lambda}{\pi sin\varepsilon}\frac{\tau_Z}{SWH}$$

Where τ_I is the coherence time of the interferometric field, defined as the width of the autocorrelation function $\Gamma(\Delta t)$ of the interferometric field.

- τ_Z and SWH are not independent parameters and very difficult to derive theoretically. So the semi-empirical approach is preferred through extensive Monte-Carlo simulation:

$$SWH = SWH_0 + \frac{\alpha}{k\tau_I sin\varepsilon - \beta}$$

Where:

SWH_0, α and β are calibration parameters. Then it is possible to derive the SWH value from the measured value of τ_I.

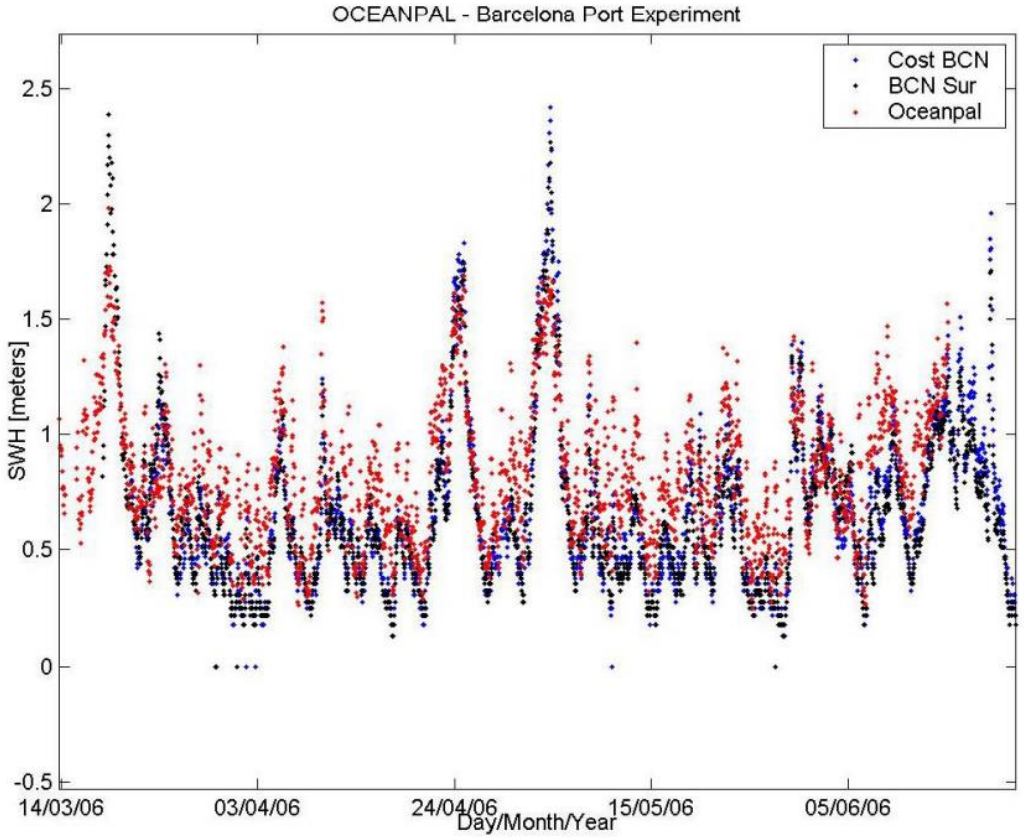

SWH Buoys data and Oceanpal data comparison during 3 months. Red dots: Oceanpal data; Blue dots: Buoy data at Cost BCN; Black dots: Buoy data at BCN Sur;

Interferometric Complex Field method

- **Soil moisture measurement**

The *ICF* squared is related to the soil moisture volumetric content.

$$\Gamma_{av} = \frac{1}{N}\sum_{i=1}^{N} |ICF(t)|^2$$

Where : *N*: the number of waveforms computed during one data acquisition.

Γ_{av}: the averaged value of the soil's reflectivity.

- Fresnel equation: $\Gamma_v = \frac{\varepsilon_r . sin\gamma - \sqrt{\varepsilon_r - cos^2\gamma}}{\varepsilon_r . sin\gamma + \sqrt{\varepsilon_r - cos^2\gamma}}$ $\Gamma_h = \frac{sin\gamma - \sqrt{\varepsilon_r - cos^2\gamma}}{sin\gamma + \sqrt{\varepsilon_r - cos^2\gamma}}$

$$\Gamma_{av} = \begin{cases} \frac{\Gamma_v + \Gamma_h}{2} & if\ co - polarization \\ \frac{\Gamma_v - \Gamma_h}{2} & if\ cross - polarization \end{cases}$$

Where: ε_r is the permittivity of the reflect surface.

Interferometric Complex Field method

- **Soil moisture measurement**
- The ε_r can be solved based on the previous equation as following:

$$\varepsilon_r = \frac{1 \pm \sqrt{1 - 4sin^2\gamma \cdot cos^2\gamma \cdot \left(\frac{1-\Gamma}{1+\Gamma}\right)^2}}{2sin^2\gamma \cdot \left(\frac{1-\Gamma}{1+\Gamma}\right)^2}$$

- The permittivity (dielectric constant) has close relationship with the soil moisture, but differs at different soil components.
- The empirical equation of the dielectric constant and the soil moisture:

$$\varepsilon_r = 2.862 - 0.012s + 0.001c + (3.803 + 0.462c - 0.341s)m_v + (119.003 - 0.500s + 0.633c)m_v^2$$

Where: *s* and *c* are the sand and clay textual compositions of a soil in percent by weight;

m_v is the volumetric soil moisture.

The Interference-pattern Technology

Soil **M**oisture **I**nterference-pattern **G**NSS **O**bservations at **L**-band Reflectometer (SMIGOL)

which is a ground-based instrument that measures the instantaneous power of the interference of the direct and reflected GPS signals from the Earth's surface.

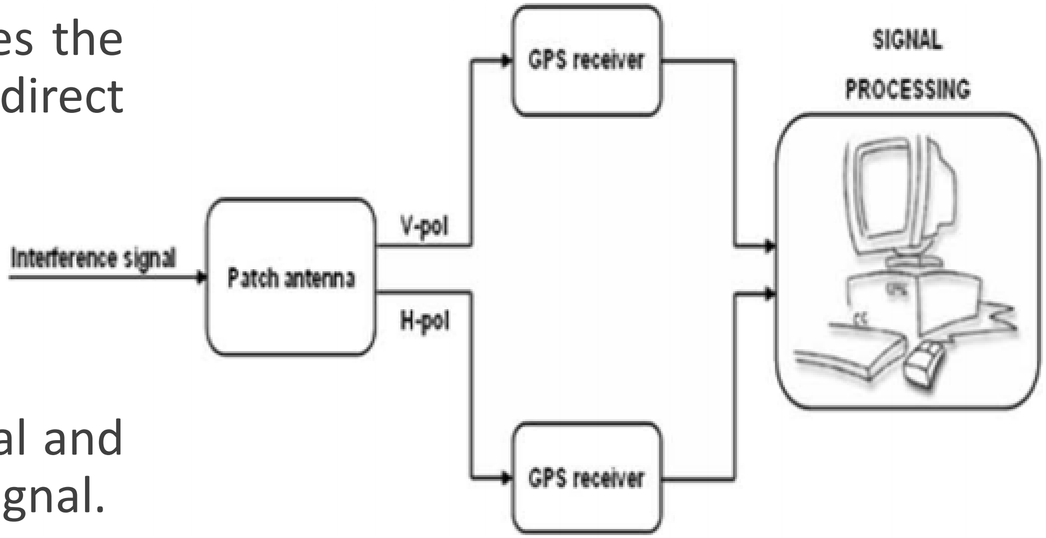

Two linear polarization antenna received horizontal and vertical polarization for both direct and reflected signal.

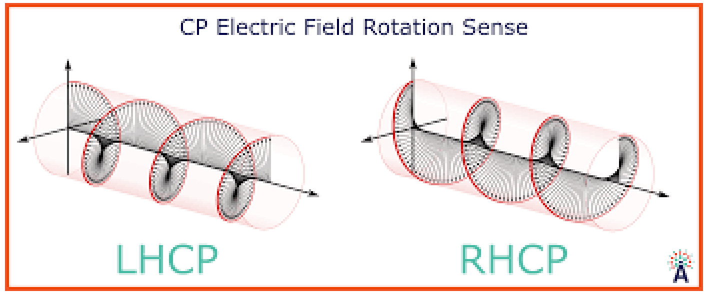

The SMIGOL instrument provide the interference power with respecting to the elevation angle.

The Interference-pattern Technology

- The total power received (P) can then be derived from:

$$P \propto |E_i + E_r|^2 \equiv |F_n(\theta) \cdot |1 + R \cdot e^{j\phi}|^2$$

Where:

$F_n(\theta)$: The antenna pattern;

E_i and E_r: direct and reflected signal strength, respectively;

R: The reflection coefficients;

$$\phi = \frac{4\pi}{\lambda} \cdot h_1 \cdot \cos(\theta_{\text{inc}})$$

- The total received power will vary as a function of the incidence angle, which is different at horizontal and vertical polarizations, and depends on the geophysical parameters that characterize the soil.

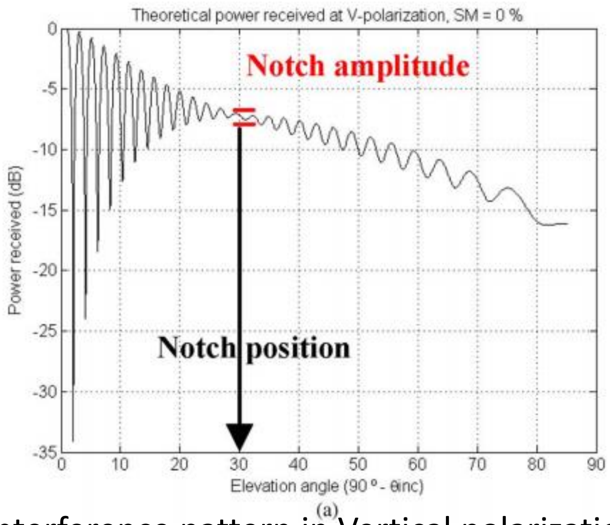

Interference pattern in Vertical polarization

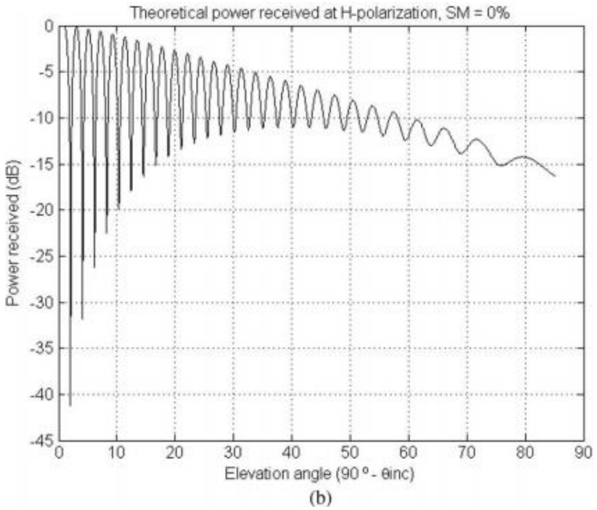

Interference pattern in Horizontal polarization

The Interference-pattern Technology

- **Soil Moisture measurement**
- For the vertical polarization interference power, a minimum amplitude shows at the Brewster's angle (the first notch point).
- The Brewster's angle:

$$\theta_B = arctan\left(\frac{n_2}{n_1}\right) = arctan\left(\sqrt{\frac{\mu_{r2}\cdot\varepsilon_{r2}}{\mu_{r1}\cdot\varepsilon_{r1}}}\right) = arctan\left(\sqrt{\frac{\varepsilon_{r2}}{\varepsilon_{r1}}}\right)$$

Interference power at bare soil surface of different moisture.

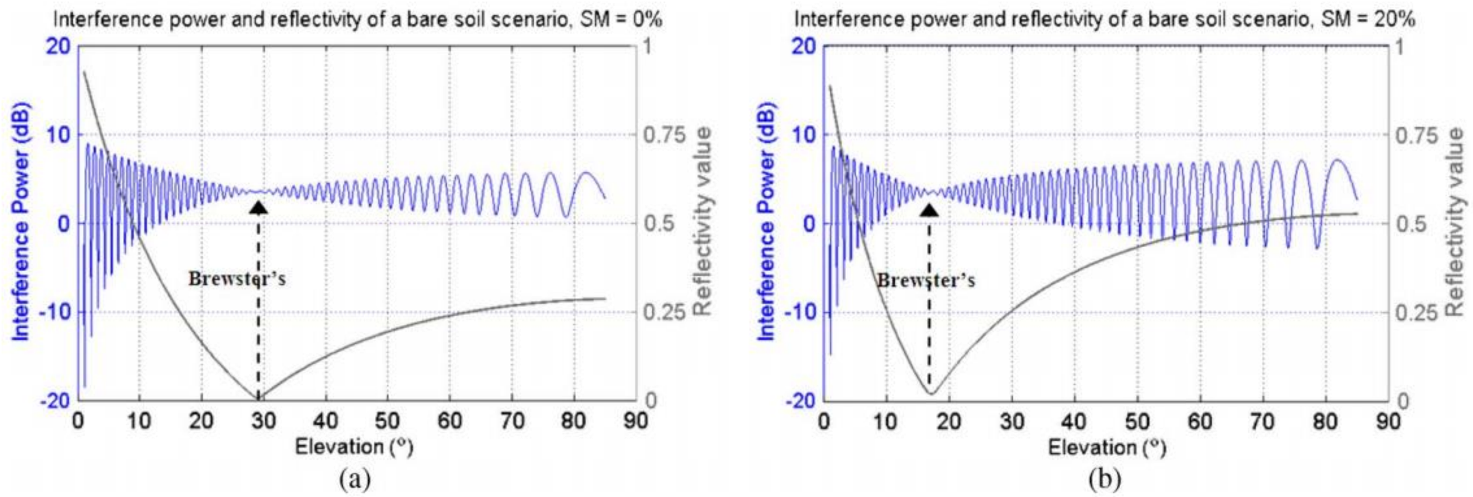

GNSS L-Band Radar

Inherited advantages

- **Low cost**
- **Small size**
- **License-free**
- **Security**
- **No electromagnetic pollution**

… …

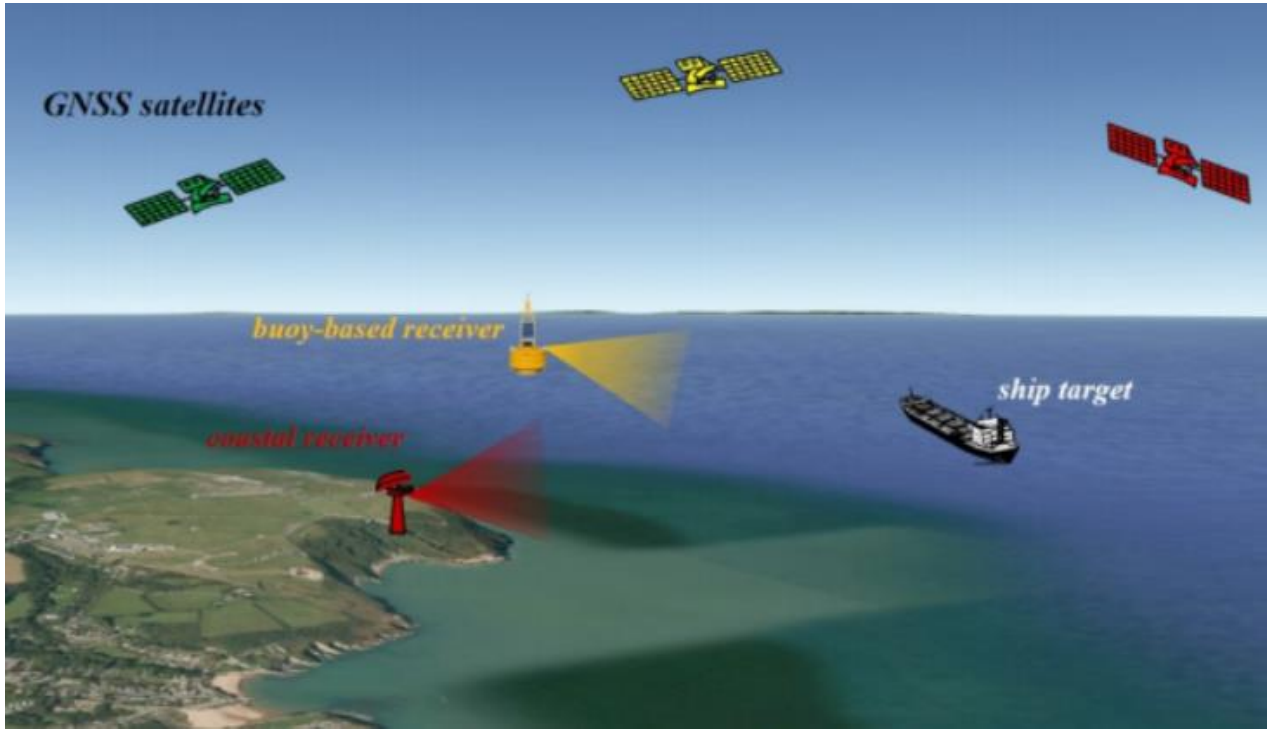

A promising alternative to the active radar systems with heavy transmitters

GNSS Radar

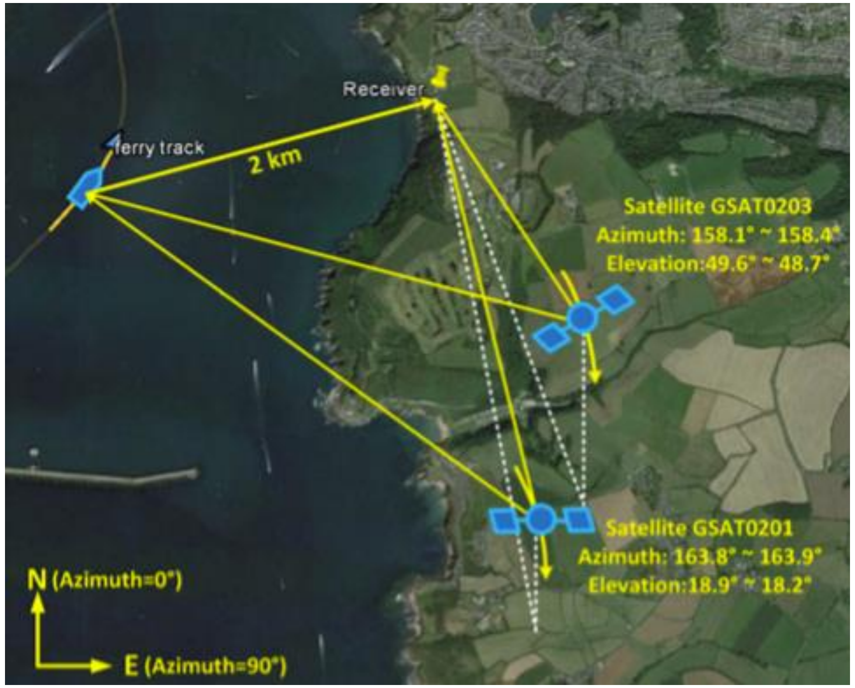

- GNSS signals not originally designed for radar applications
- Signal waveform cannot be changed

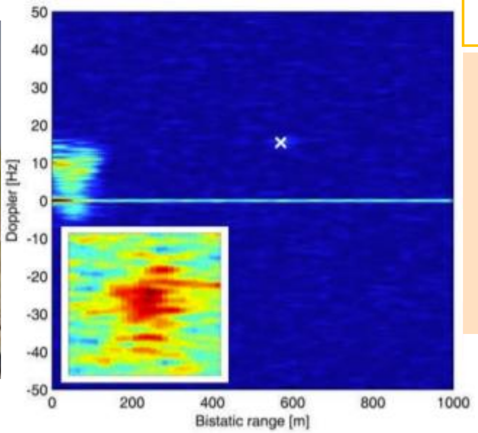

Main drawbacks

- Restricted signal power → -135 dBW/m^2
- Coarse range resolution → > 150 m for GPS L1

GNSS-based passive radar system

System acquisition geometry

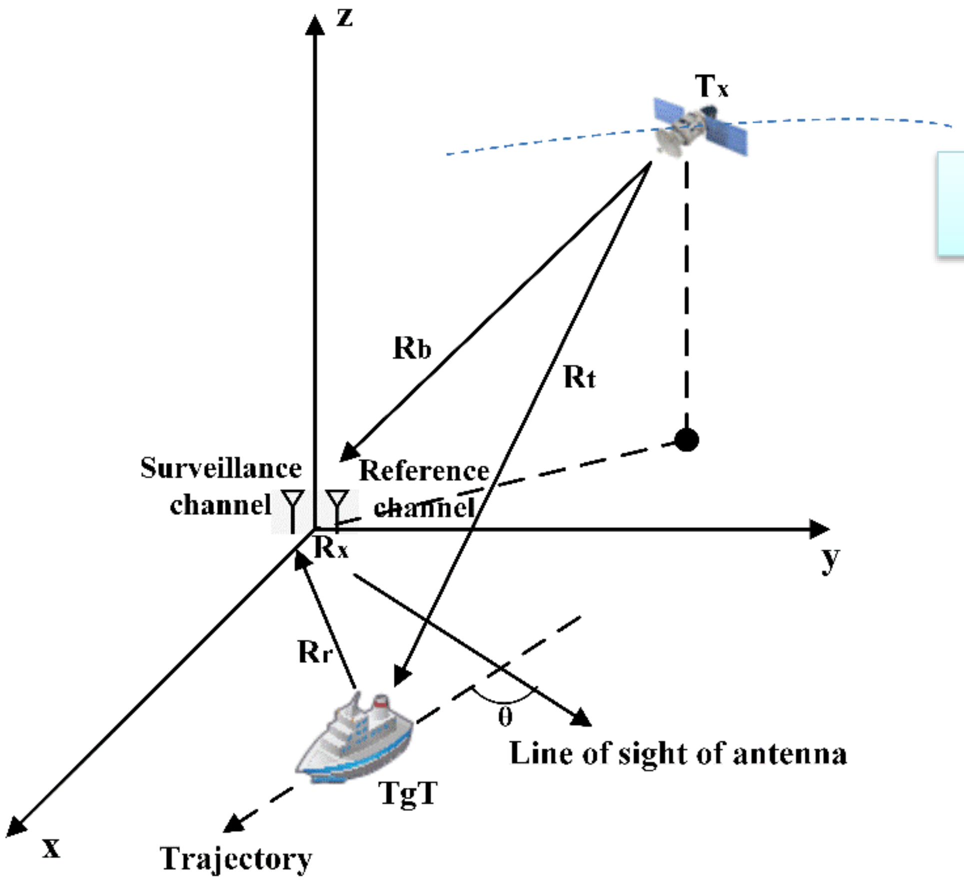

The definition of bistatic range history

$$R_{bi}(t_m) = R_t(t_m) + R_r(t_m) - R_b(t_m)$$

T_x-TgT range   TgT-R_x range T_x-R_x range

GNSS-based passive radar system

Receiver front-end

Typical structure of GNSS L1 front-end

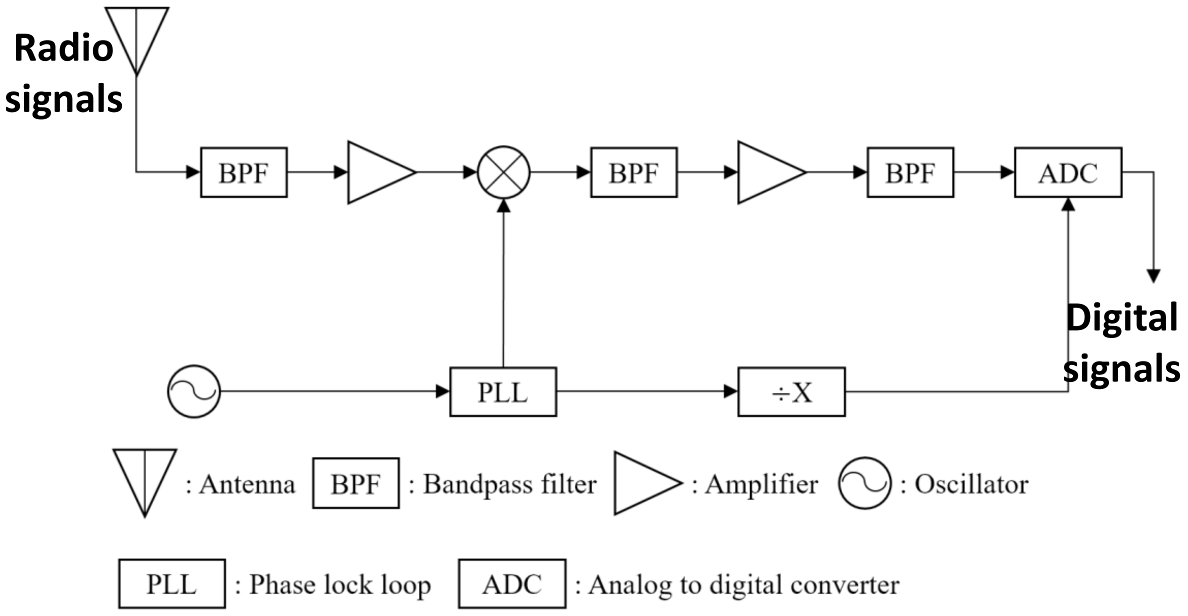

Dual-channel receiver front-end

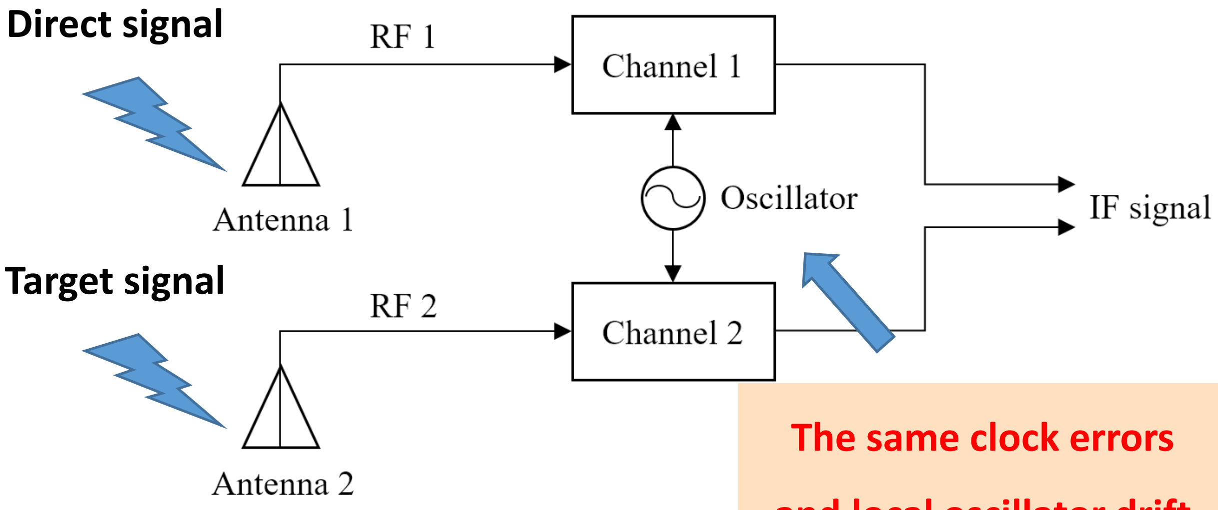

The same clock errors and local oscillator drift

GNSS-based passive radar system

Signal model description

Noise-free replica of the direct signal

$$S_d(t, t_m) = C\big(t - \tau_d(t_m)\big) \times D\big(t - \tau_d(t_m)\big) \times e^{j(2\pi f_d(t_m)t + \varphi_d(t_m))}$$

fast-time ∈ [0, 1ms]

slow-time ∈ [-T/2, T/2]

code phase delay

carrier frequency

carrier phase term

propagation delay term + error terms (atmospheric delays and receiver errors)

The target signal

$$S_e(t, t_m) = C\big(t - \tau_e(t_m)\big) \times D\big(t - \tau_e(t_m)\big) \times e^{j(2\pi f_e(t_m)t + \varphi_e(t_m))} + n(t, t_m)$$

Noise term

Conventional Moving Target Detection Technique

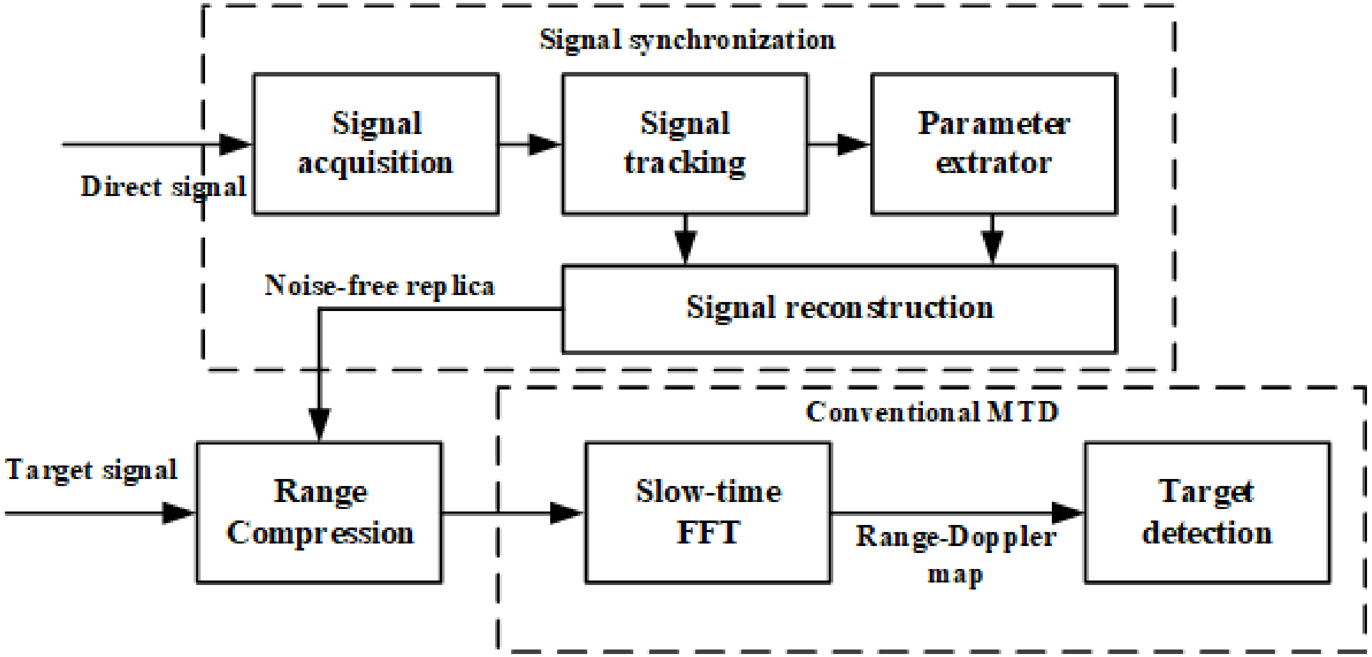

- Providing coherent integration gain
- Distinguishing different radar signals

Long-time integration techniques for moving target detection

Conventional MTD

fast Fourier transform (FFT)

$rd(r, f_m$

$r = c \times \tau$

$n)$

Drawbacks

Ignoring range and Doppler migrations

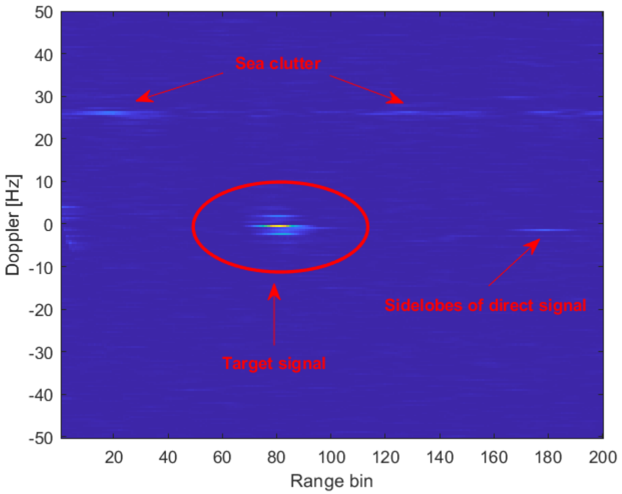

Limited
tegration gain

Suitable

r cross section (RCS) and/or
t-range target detection

Long-time integration techniques for moving target detection

Low-RCS and/or long-range target detection

Solution: long integration time (tens of seconds)

→ **range/Doppler migration correction**

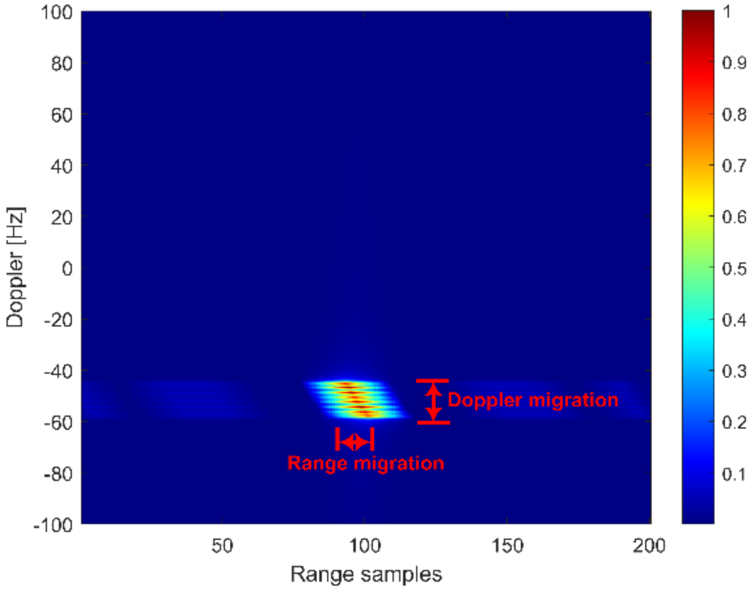

$$R_{bi}(t_m) = R_t(t_m) + R_r(t_m) - R_b(t_m)$$

Constant velocity assumption

Taylor Series Expansion

Cruising speed

$$R_{bi}(t_m) = R_0 + at_m + \frac{b}{2}t_m^2 + \frac{c}{6}t_m^3 + \frac{d}{24}t_m^4 + \cdots$$

Super-resolution Techniques for Range Resolution Enhancement

Problem: Poor range resolution

Convolut

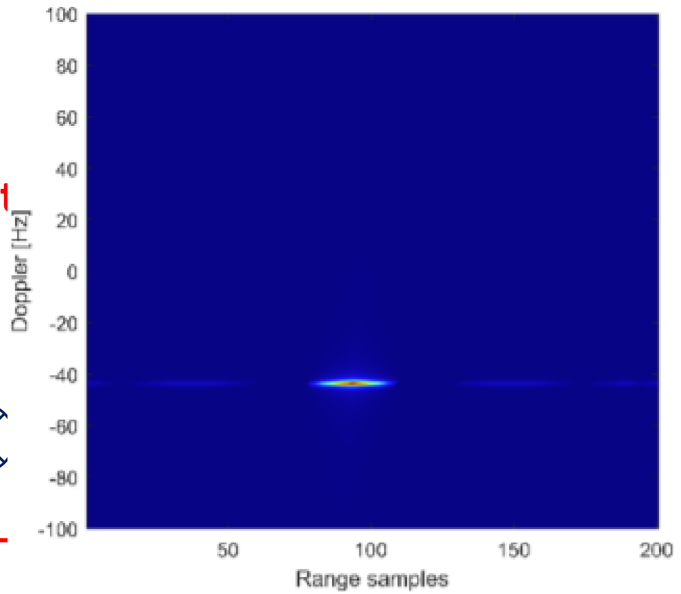

Rough range resolution = High-resolution scattering coefficient $\otimes$

Deconvolution

Target signal in the RD map:

$$y(r) = h(r - R_c) + n(r)$$

Convolution model form:

$$y(r) = h(r) \otimes \delta(r - R_c) + n(r)$$

PSF

Scattering coefficient

Normalized auto-correlation function of the ranging code

Discrete expression:

$$\boldsymbol{y} = \boldsymbol{h} \otimes \boldsymbol{x} + \boldsymbol{n}$$

$\boldsymbol{h} = [h_1, h_2, \cdots, h_L]^T$

$\boldsymbol{n} = [n_1, n_2, \cdots, n_L]^T$

$\boldsymbol{y} = [y_1, y_2, \cdots, y_L]^T$

$\boldsymbol{x} = [\delta_1, \delta_2, \cdots, \delta_L]^T$

Number of range sampling points

Matrix-vector form:

$$\boldsymbol{y} = \mathbf{A}\boldsymbol{x} + \boldsymbol{n}$$

Obtained by

$$\mathbf{A} = \begin{bmatrix} h_1 & h_2 & \cdots & h_L \\ h_L & h_1 & \cdots & h_{L-1} \\ \vdots & \vdots & \ddots & \vdots \\ h_2 & h_3 & \cdots & h_1 \end{bmatrix}$$

Super-resolution Techniques for Range Resolution Enhancement

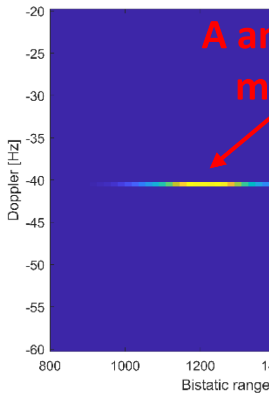

(a) Ori

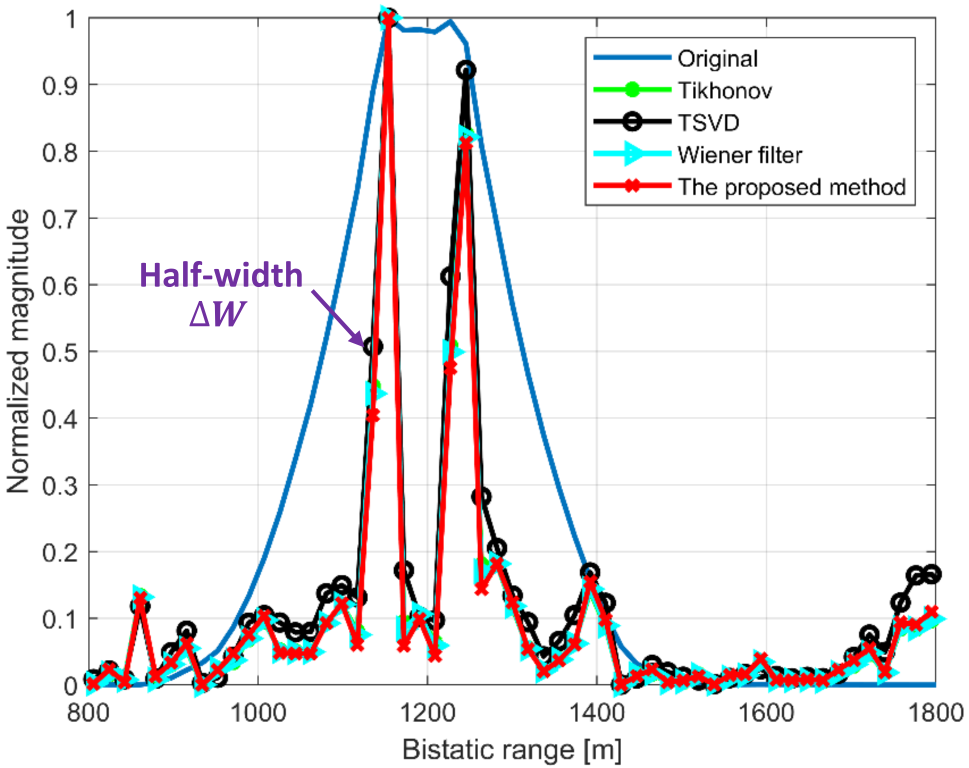

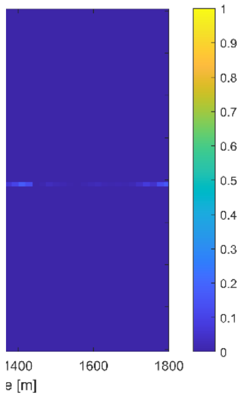

SVD

Method	ΔW	ΔP
Tikhonov	26.7 m	16.25 dB
TSVD	29.7 m	14.47 dB
Wiener filter	26.3 m	16.12 dB
The proposed method	25.1 m	15.64 dB

System integration of GNSS-based passive radar

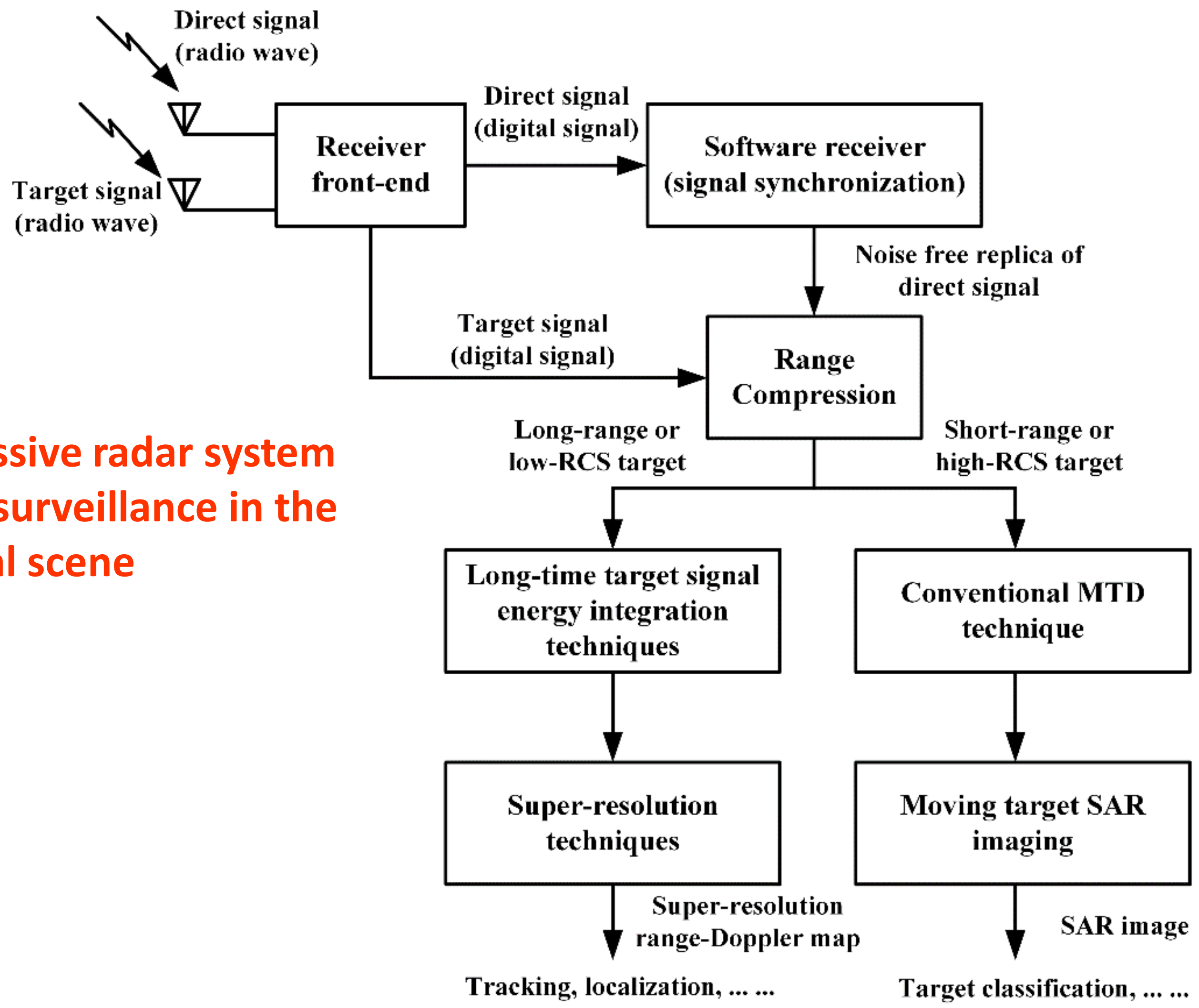

Apply this passive radar system for maritime surveillance in the real scene

System integration of GNSS-based passive radar

Mari

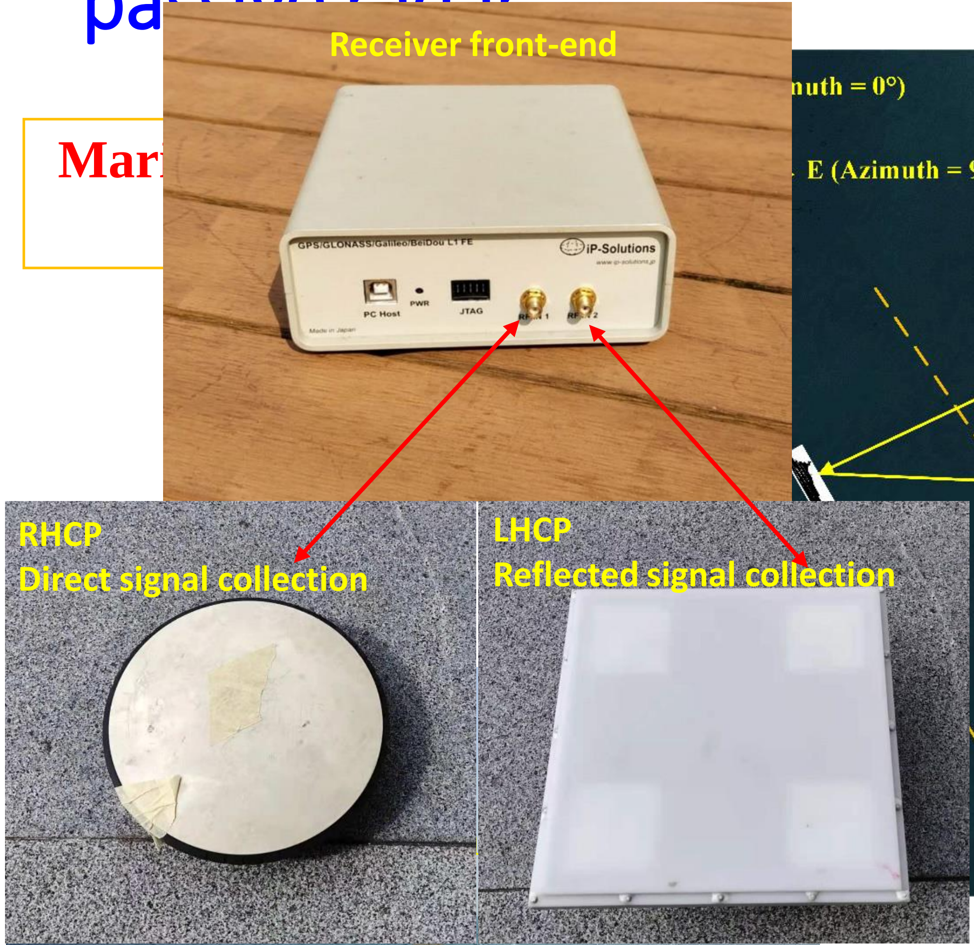

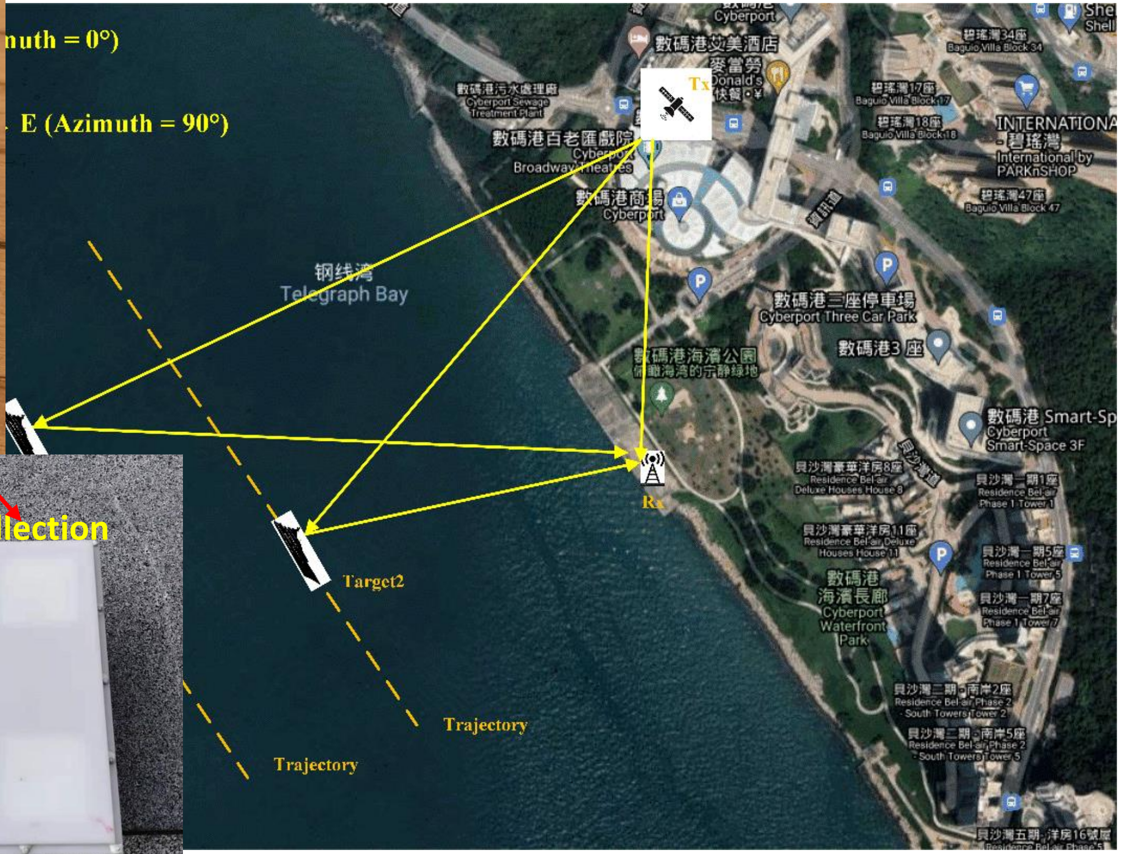

Geometry of the experimental site

Receiving hardware on the shore

System integration of GNSS-based passive radar

Long-time integration and super-resolution results

SITC DALIAN

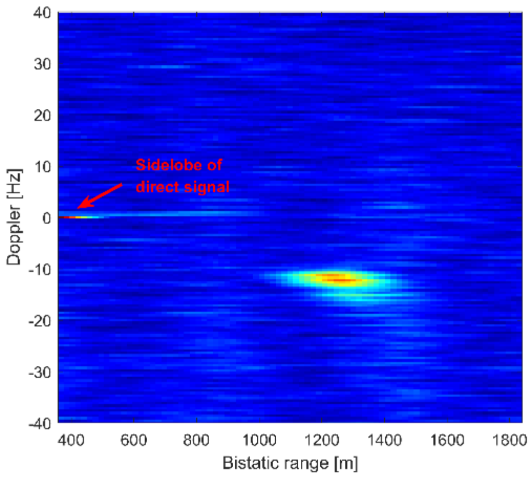

Conventional MTD

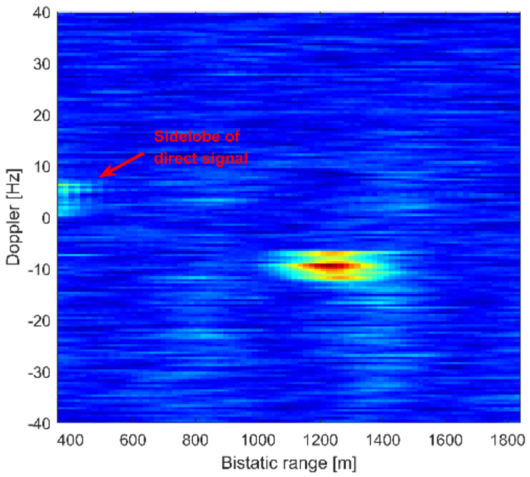

MTD+TMC

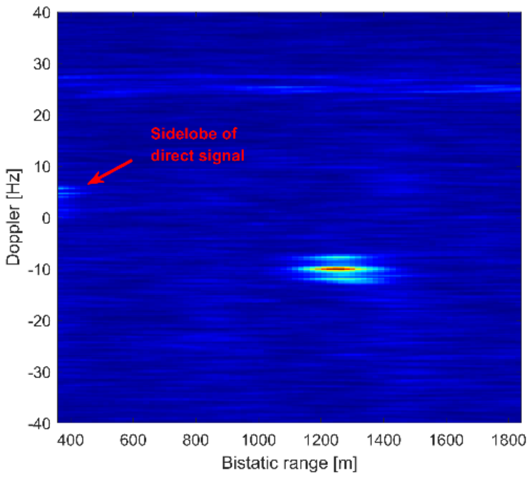

The proposed KT+LVD

	Estimated bistatic range	Estimated Doppler	Peak of moving target	Peak of sidelobes	Normalized difference
Conventional MTD	1245 m	-12.2 Hz	0.65	1	-0.35
MTD+TMC	1227 m	-9.3 Hz	1	0.32	0.68
KT+LVD	1264 m	-10 Hz	1	0.1	0.9

System integration of GNSS-based passive radar

Long-time integration and super-resolution results

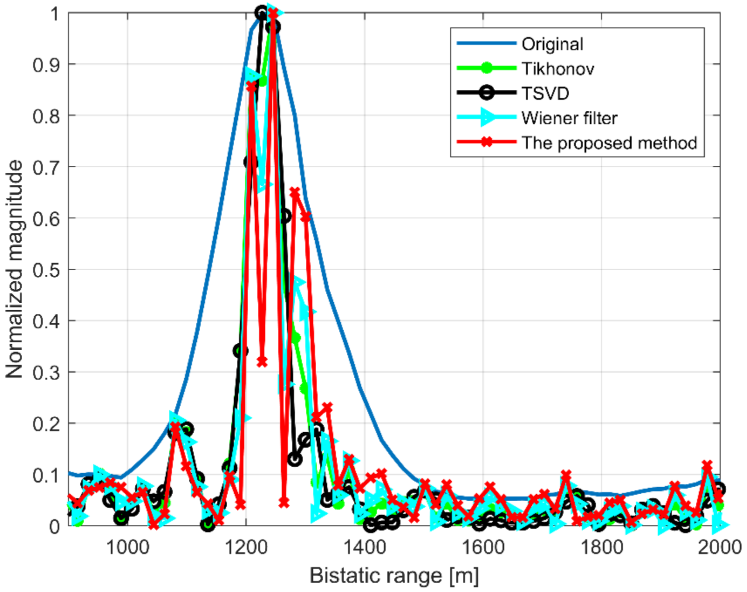

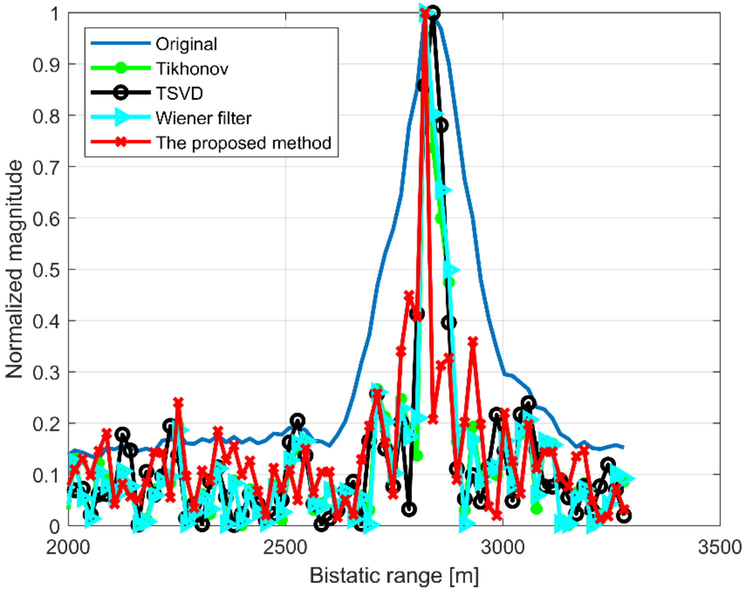

Ship length	Ship name	Original ΔW	Method	ΔW	ΔP
143 m =	SITC DALIAN	191.9 m	Tikhonov	66.8 m	28.66 dB
			TSVD	69.4 m	29.57 dB
			Wiener filter	59.6 m	26.83 dB
			The proposed method	23.0 m	24.22 dB
260 m =	NAVIOS AMARILLO	225.6 m	Tikhonov	61.8 m	23.28 dB
			TSVD	64.7 m	22.36 dB
			Wiener filter	66.4 m	23.50 dB
			The proposed method	27.0 m	20.03 dB

System integration of GNSS-based passive radar

Target imagery results

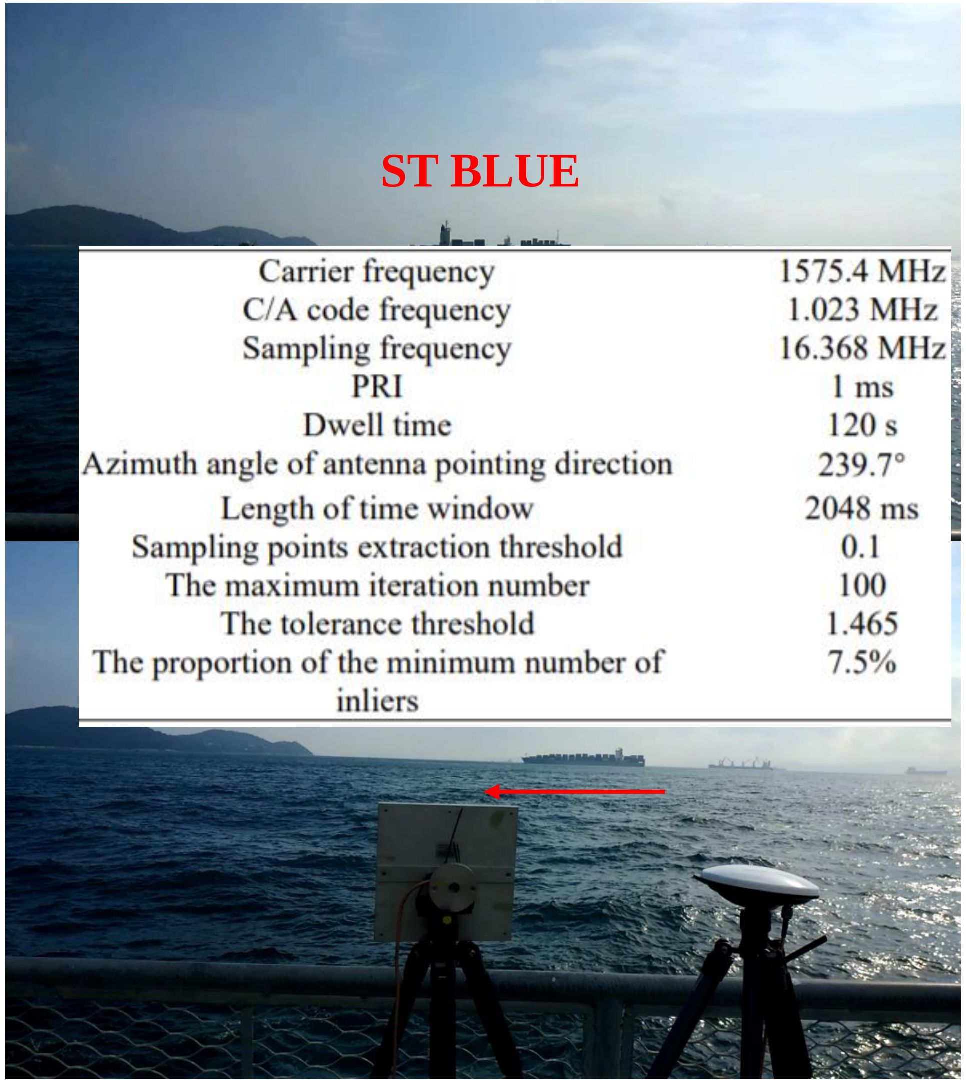

Carrier frequency	1575.4 MHz
C/A code frequency	1.023 MHz
Sampling frequency	16.368 MHz
PRI	1 ms
Dwell time	120 s
Azimuth angle of antenna pointing direction	239.7°
Length of time window	2048 ms
Sampling points extraction threshold	0.1
The maximum iteration number	100
The tolerance threshold	1.465
The proportion of the minimum number of inliers	7.5%

ST BLUE	Ship length	199 m
	Average speed	6.54 m/s
	The closest range to the shore	845 m
	GPS name	GPS BIIR-10
	Ranging code	PRN22
	Elevation angle	32°
	Azimuth angle	68°
KUO LIN	Ship length	170 m
	Average speed	7.52 m/s
	The closest range to the shore	785 m
	GPS name	GPS BIIR-10
	Ranging code	PRN22
	Elevation angle	25°
	Azimuth angle	53°
WAN HAI 506	Ship length	269 m
	Average speed	4.94 m/s
	The closest range to the shore	1664 m
	GPS name	GPS BIIF-8
	Ranging code	PRN3
	Elevation angle	40°
	Azimuth angle	68°
WAN HAI 313	Ship length	213 m
	Average speed	7.21 m/s
	The closest range to the shore	939 m
	GPS name	GPS BIIR-10
	Ranging code	PRN22
	Elevation angle	19°
	Azimuth angle	46°

System integration of GNSS-based passive radar

Target imagery results

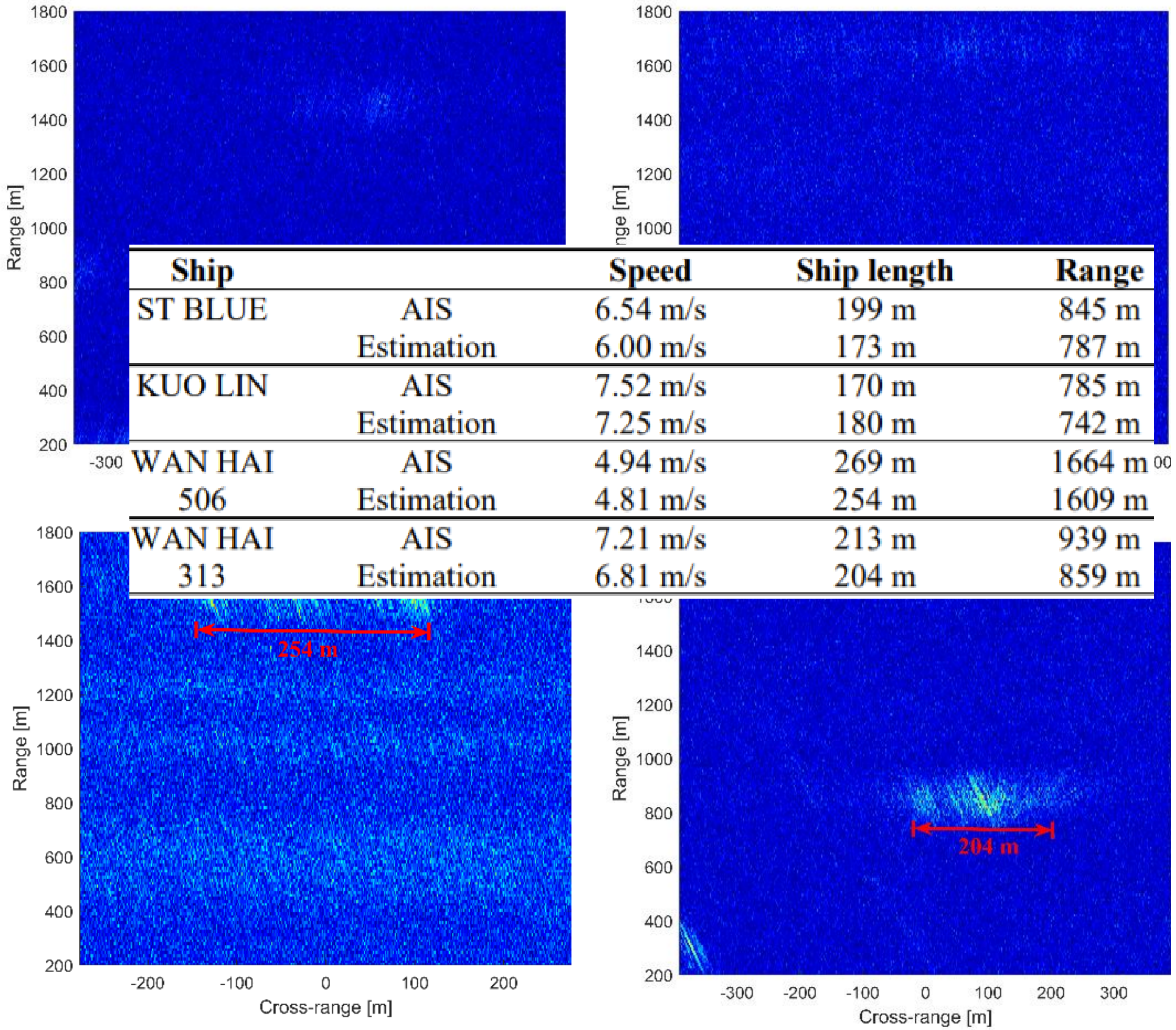

Ship		Speed	Ship length	Range
ST BLUE	AIS	6.54 m/s	199 m	845 m
	Estimation	6.00 m/s	173 m	787 m
KUO LIN	AIS	7.52 m/s	170 m	785 m
	Estimation	7.25 m/s	180 m	742 m
WAN HAI 506	AIS	4.94 m/s	269 m	1664 m
	Estimation	4.81 m/s	254 m	1609 m
WAN HAI 313	AIS	7.21 m/s	213 m	939 m
	Estimation	6.81 m/s	204 m	859 m

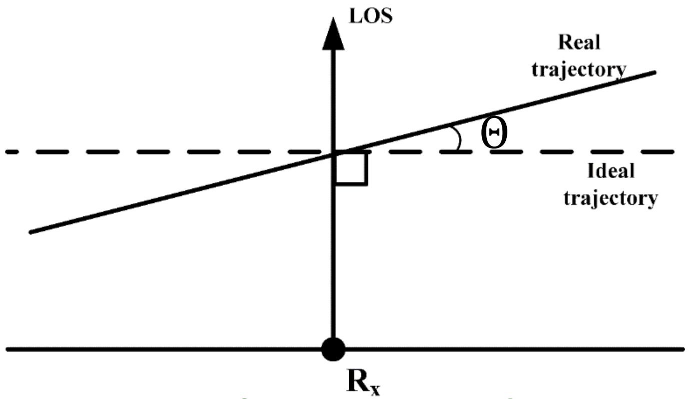

Bistatic angle is corrected:

$$\cos\theta_{bi} = \cos\alpha \times \cos(\varphi + az + \Theta)$$

Small intersection angle

TgT-R_x vertical range

$$R_s^{tru}(\tau) = \frac{c \times \tau}{1 + \cos\alpha\cos(az + \Theta)}$$

$$R_s^{tru} \geq R_s^{est}$$

$$\gamma = -\frac{v^2}{\lambda R_s}$$

Slope deformation Monitoring

- Most slope deformation monitoring equipment is installed on site
- Difficult for active slopes
- GNSS-R provides a possibility to monitoring deformation remotely (i.e. drones, or off-site GNSS receivers)
- How accurate can it achieve?
  - mm level required

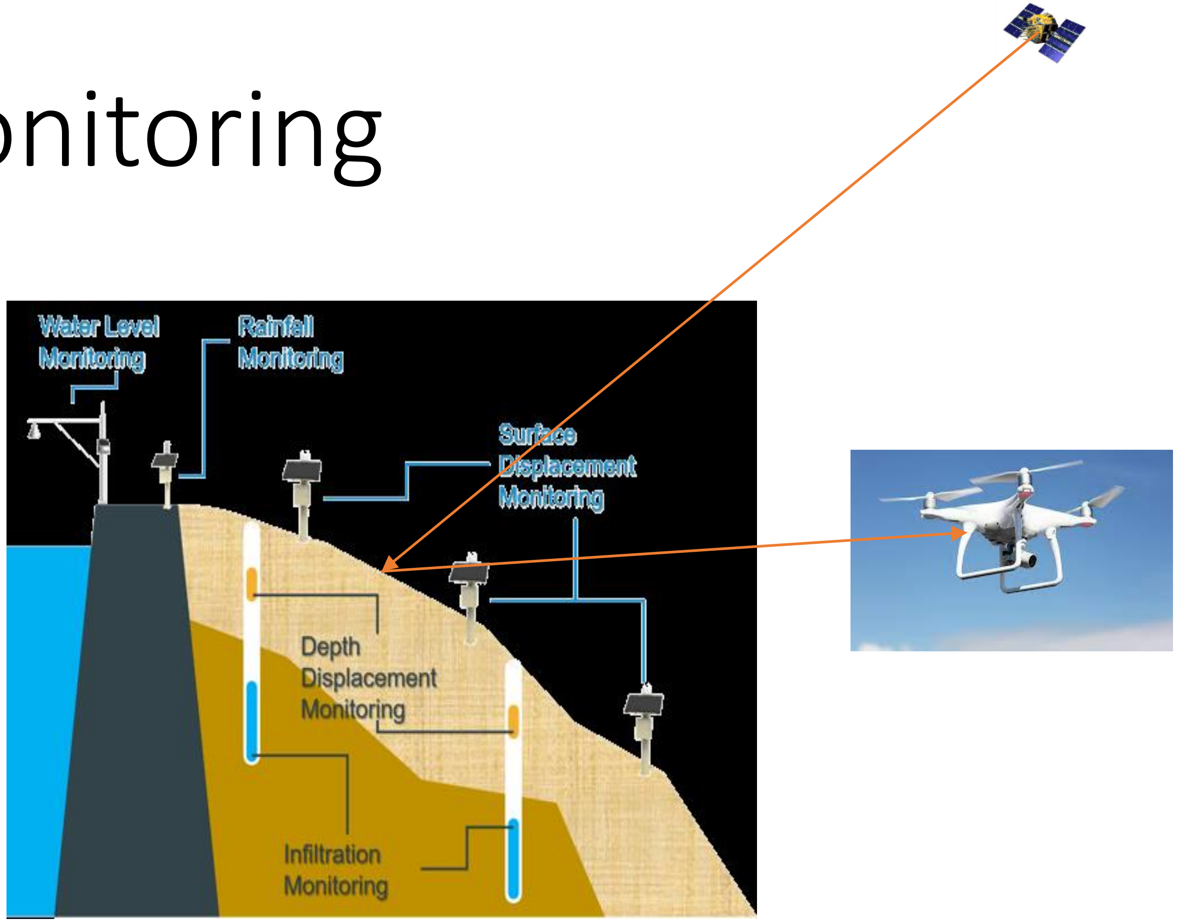

https://en.hi-target.com.cn/automatic-monitoring

Deformation monitoring: based on Carrier

- The synchronized direct and reflected signal are acquired and tracked, and output the track results such as carrier phase, code phase and Doppler frequency for each channel, then the difference between the track results can be monitored.
- The carrier phase difference is crucial in this application, which not only influenced by the movement of the reflected surface, but also the movement of the satellite.

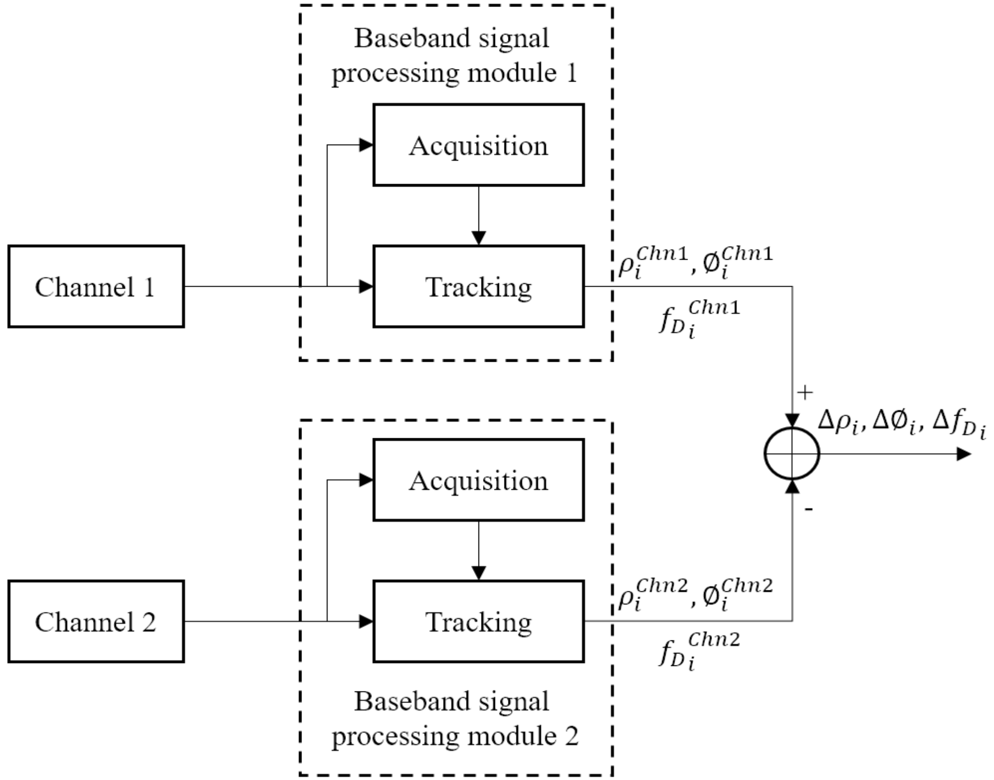

Deformation monitoring of single target

- Geometry model
- A geometry model which reveals the relationship between the propagation path difference(Δd) and the geometry parameters

$$\begin{cases} \Delta d = 2 * d * \cos(\beta) \\ \sin(\beta) = \sin(\beta') * \cos(\alpha') \\ \beta' = \pi - \theta' - \gamma \\ \tan(\alpha') = \tan(\alpha) * \cos(\theta') \\ \tan(\theta) = \tan(\theta')\cos(\alpha) \\ \alpha = \alpha_s - \alpha_r \end{cases}$$

- satellite elevation angle (θ), azimuth angle (α_s), the reflect surface tilt angle (γ), azimuth angle (α_r) and the distance between the antenna and the reflect surface (d)

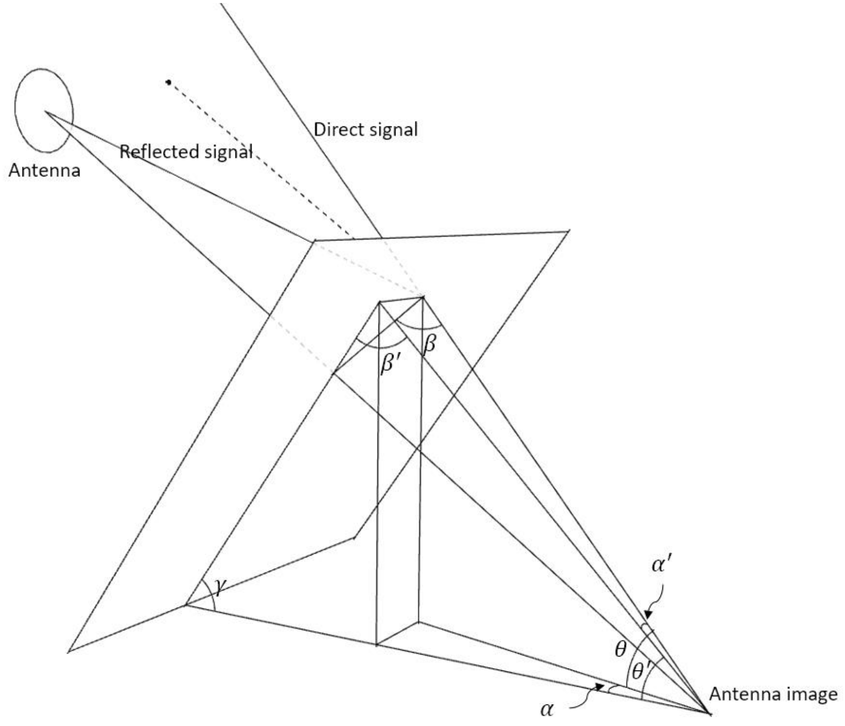

Experiment Test

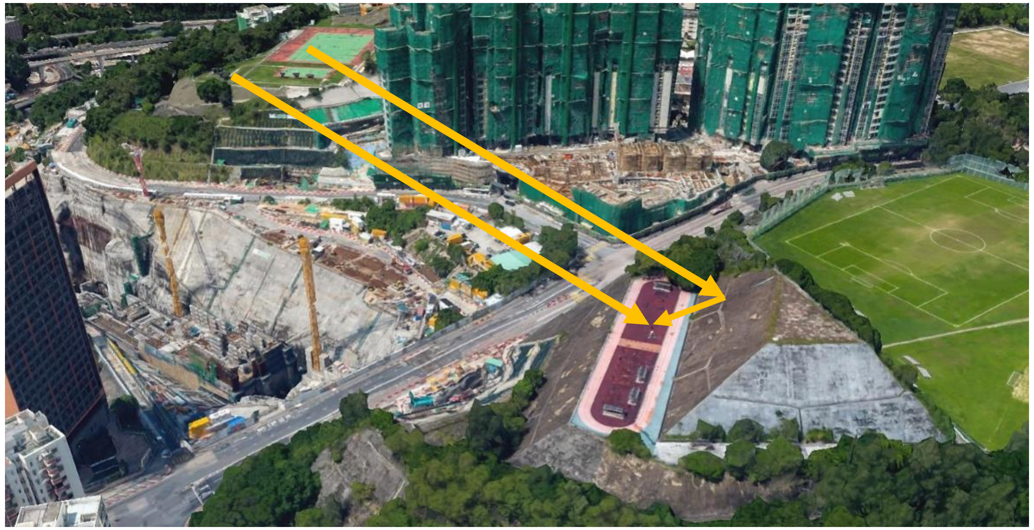

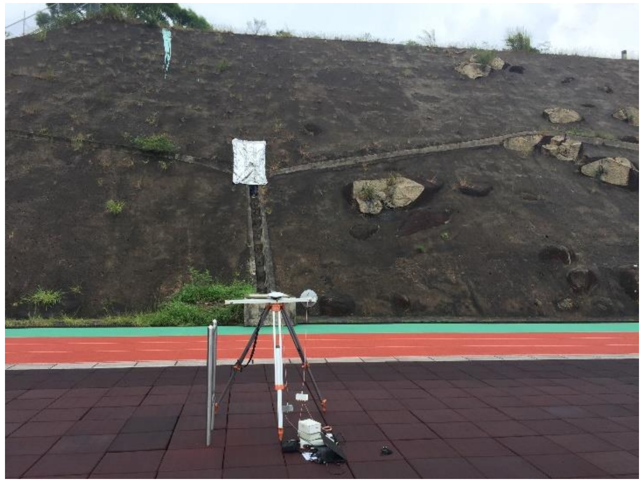

Deformation monitoring using GNSS-R

- Software define radio (SDR) receiver approaches: **carrier phase monitoring for kinematic deformation**

Slope monitoring with distance of 300m
Moving antenna for 2cm (1.81 cm at normal direction) to simulate deformation of slope.

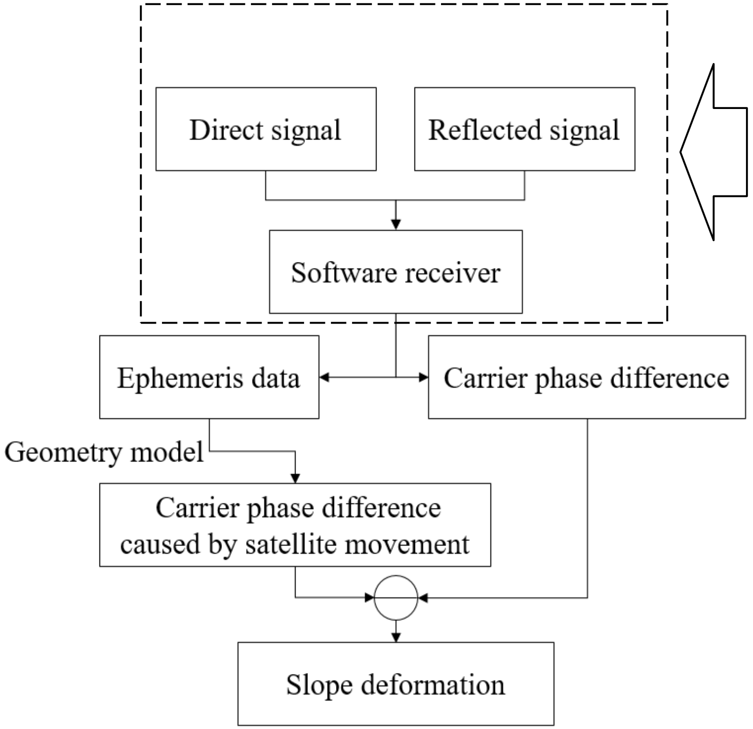

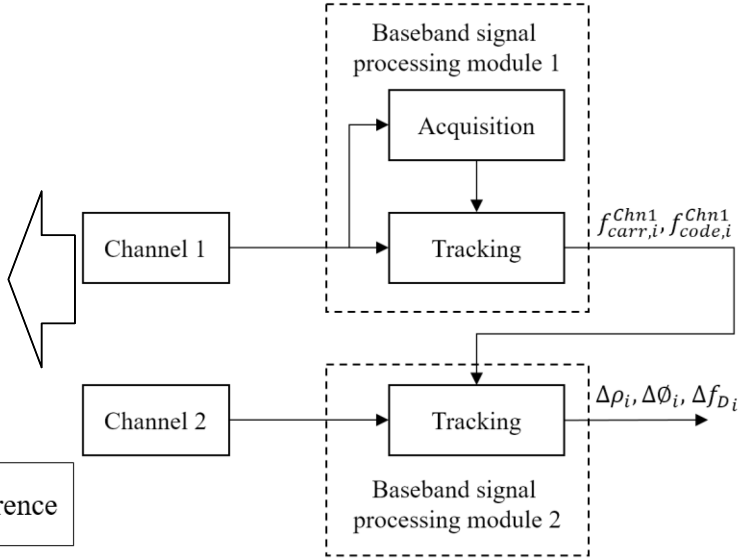

Interference signal tracking loop

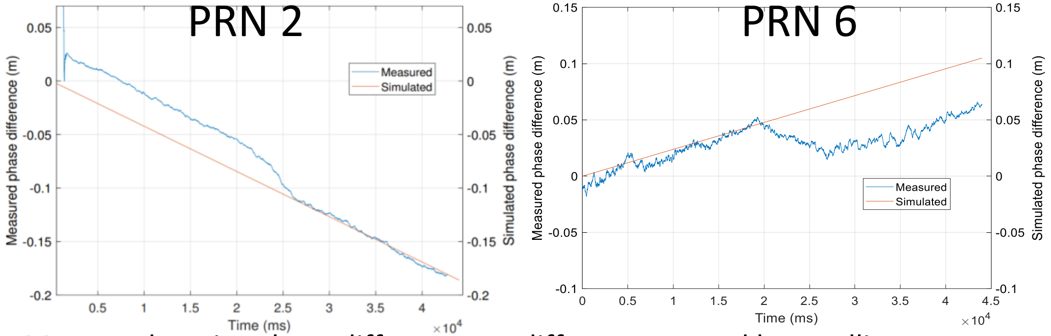

Measured carrier phase difference vs. difference caused by satellite movement

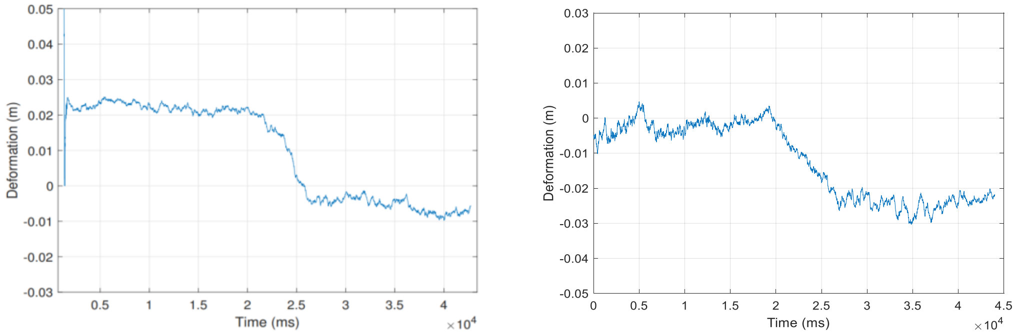

Slope deformation after eliminate influence of satellite movement

Mean error = 0.39cm
RMSE = 0.52cm

	Mean before movement (cm)	Mean after movement (cm)	Deformation (cm)	Error (cm)
Dataset 1 PRN 2	2.22	-0.53	-2.75	0.94
Dataset 1 PRN 6	0.22	2.42	-2.2	0.39
Dataset 2 PRN 2	0.03	1.83	1.80	-0.01
Dataset 2 PRN 6	0.15	2.19	2.04	0.23

Deformation monitoring of multiple targets?

- Due to the uneven reflect surface, sometimes there are more than one areas that can reflect signal with significant power, which can be considered as interesting points that represent this reflect surface for the use of deformation monitoring.
- In this case, multiple reflected signals are received by the LHCP antenna, the previous deformation monitoring algorithm of calculating the carrier phase between the direct and reflected signal will not be correct.

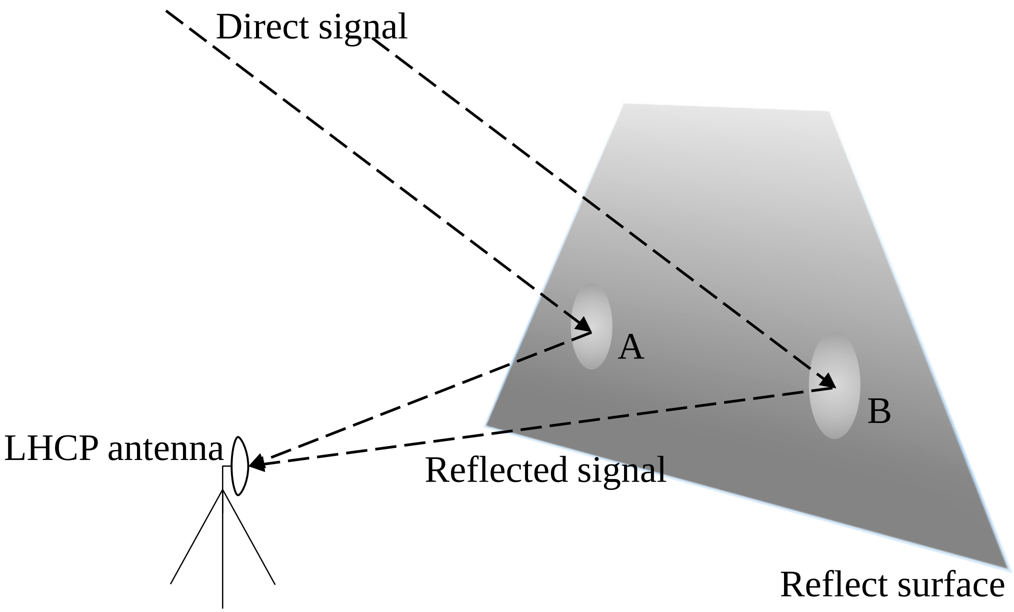

Deformation monitoring of multiple targets

- Based on the special properties of the PRN code, the code phase of sub-signals can be distinguished by using correlation function. And the correlation function of the received signal is also the superposition of the correlation function of sub-signals, as shown in figure below.
- the correlation amplitude of $Peak_A$ and $Peak_B$ are given by

$$\begin{cases} P_A = A_1 cos\varphi_1 + \Delta c \cdot A_2 cos\varphi_2 \\ P_B = A_2 cos\varphi_2 + \Delta c \cdot A_1 cos\varphi_1 \end{cases}$$

$$A_1^{\perp} = A_1 cos\varphi_1$$

$$A_2^{\perp} = A_2 cos\varphi_2$$

Where $A_1^{\perp}$ and $A_2^{\perp}$ is projected amplitude of sub-signal S_1 and S_2, respectively. $\Delta c = \left(1 - \frac{\Delta d}{N}\right)$, Δd is the code phase difference in sample, and N is the number of samples per code chip.

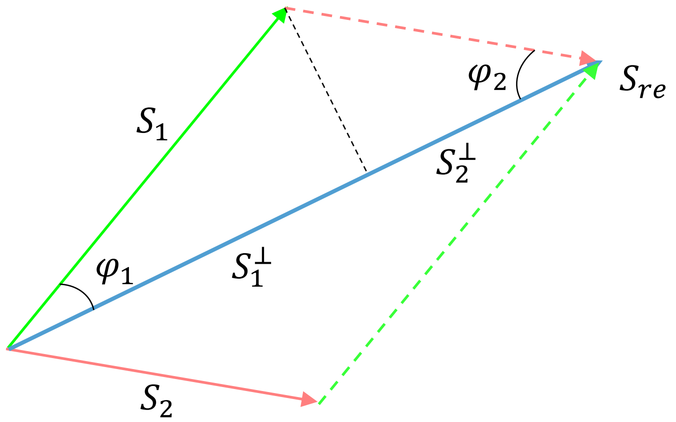

Figure, Signal superposition with different carrier phases.

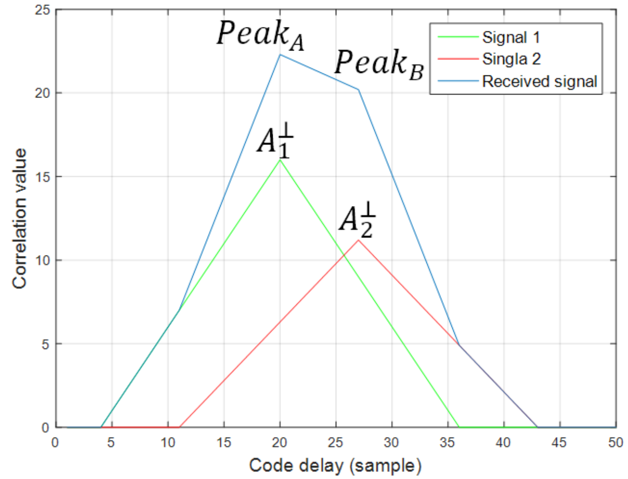

Figure, Correlation function for received signal and estimated sub-signals.

Deformation monitoring of multiple targets

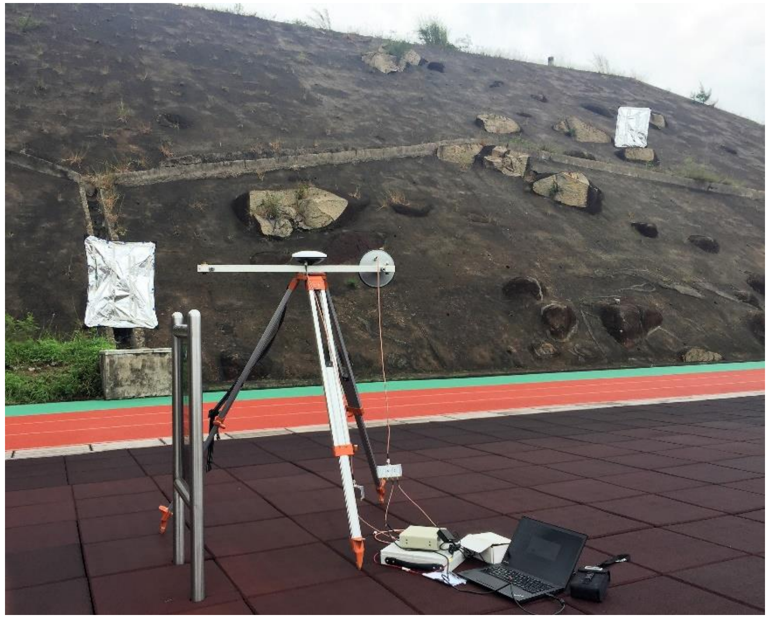

Test Site

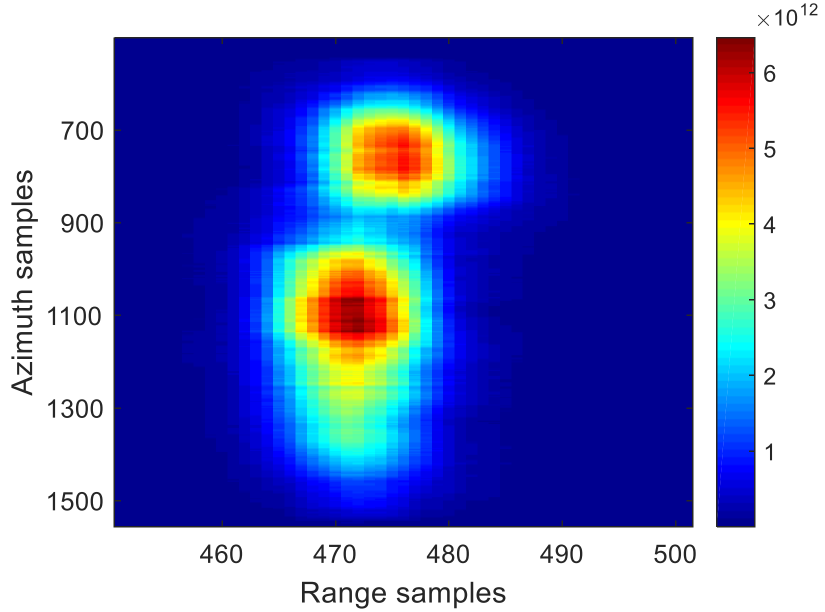

Deformation monitoring using GNSS-R

- Software define radio (SDR) receiver approaches: **Relative deformation monitoring**

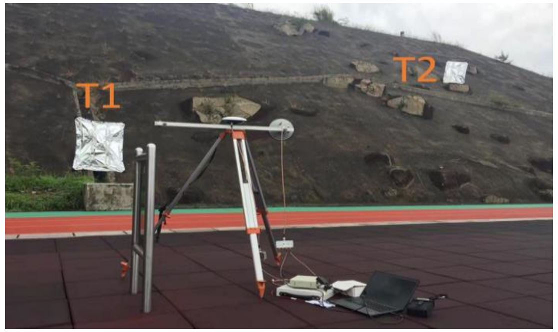

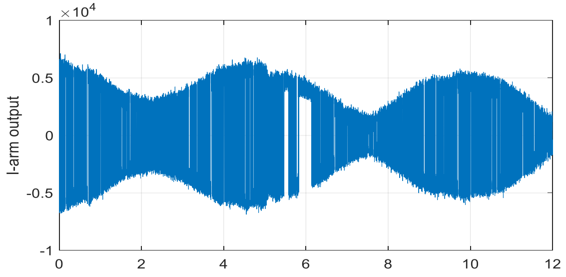

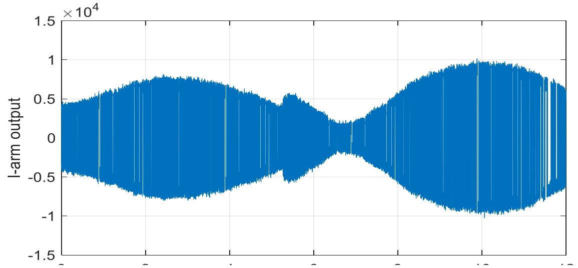

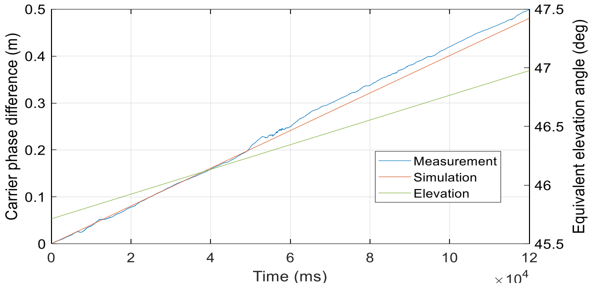

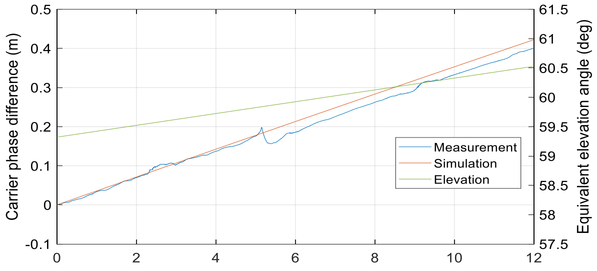

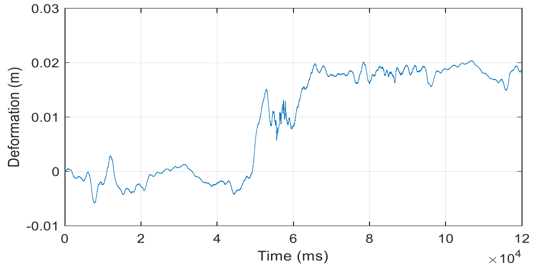

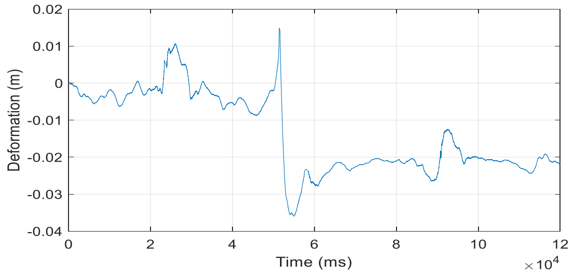

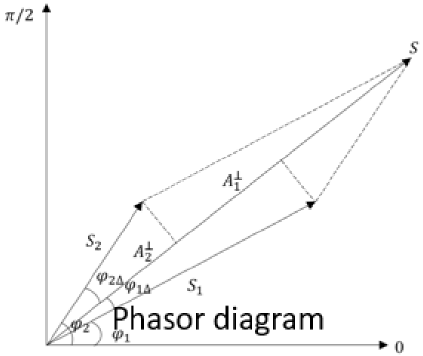

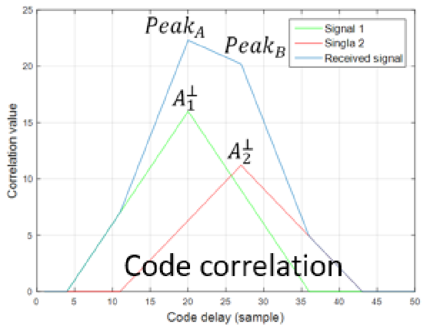

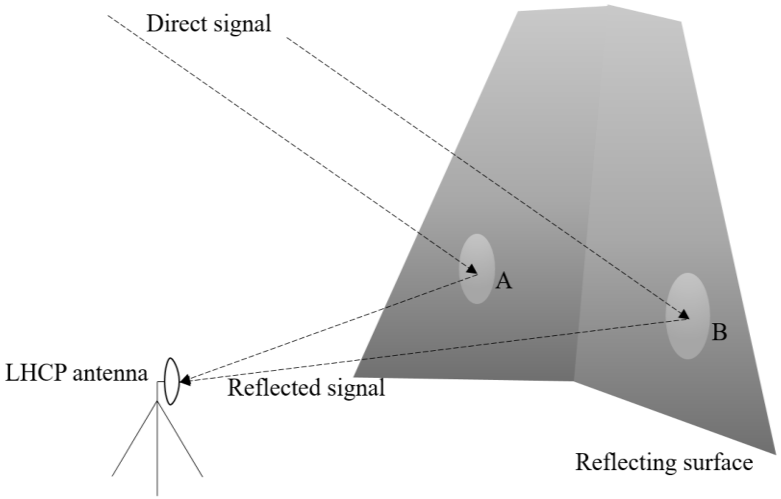

Dataset 1	Mean (cm)	Std. (cm)	Deformation (cm)
Before deformation	-0.15	0.17	1.98
After deformation	1.83	0.11	
Dataset 2	Mean (cm)	Std. (cm)	Deformation (cm)
Before deformation	-0.23	0.4	-1.92
After deformation	-2.15	0.27	

Deformation monitoring using GNSS-R

- Software define radio (SDR) receiver approaches: **SNR monitoring for quasi-static deformation**

Deformation monitoring simulation:

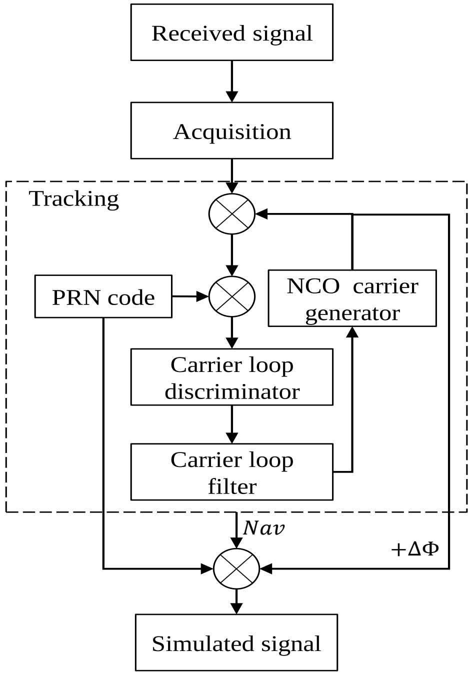

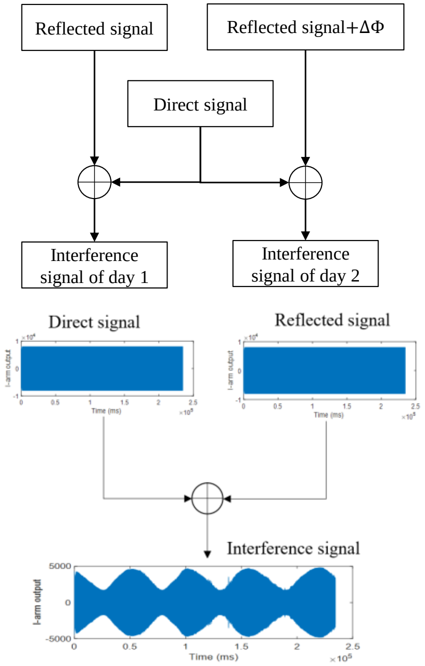

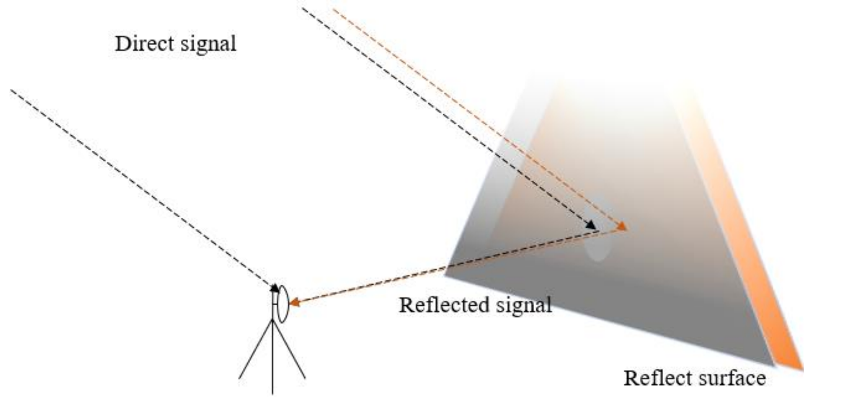

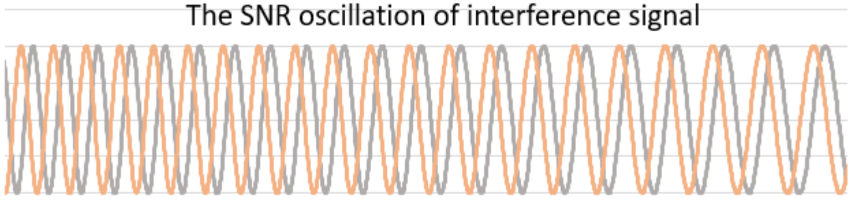

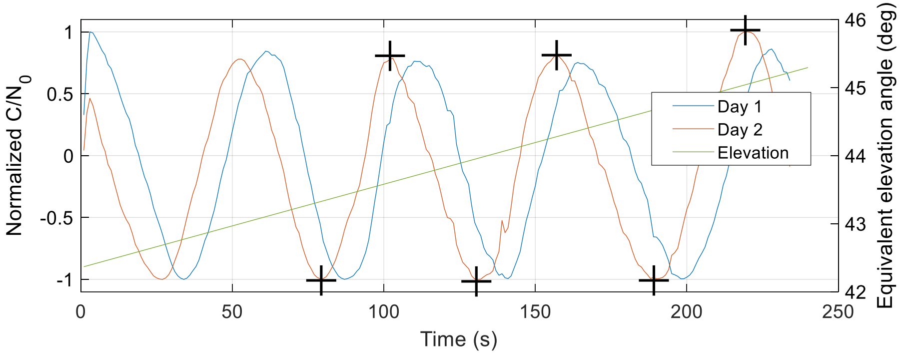

	Delay lags (s)	Waveform length (s)	Phase shift (rad)	Deformation (cm)
Waveform1 trough	-8	53	-0.95	-2.10
Waveform2 crest	-7	49	-0.90	-1.97
Waveform2 trough	-10	54	-1.16	-2.54
Waveform3 crest	-7	54	-0.81	-1.77
Waveform3 trough	-8	57	-0.88	-1.90
Waveform4 crest	-9	64	-0.88	-1.89

Mean error =0. 03cm RMSE=0.25cm

Deformation monitoring using GNSS-R

- Software define radio (SDR) receiver approaches: SNR monitoring for quasi-static deformation

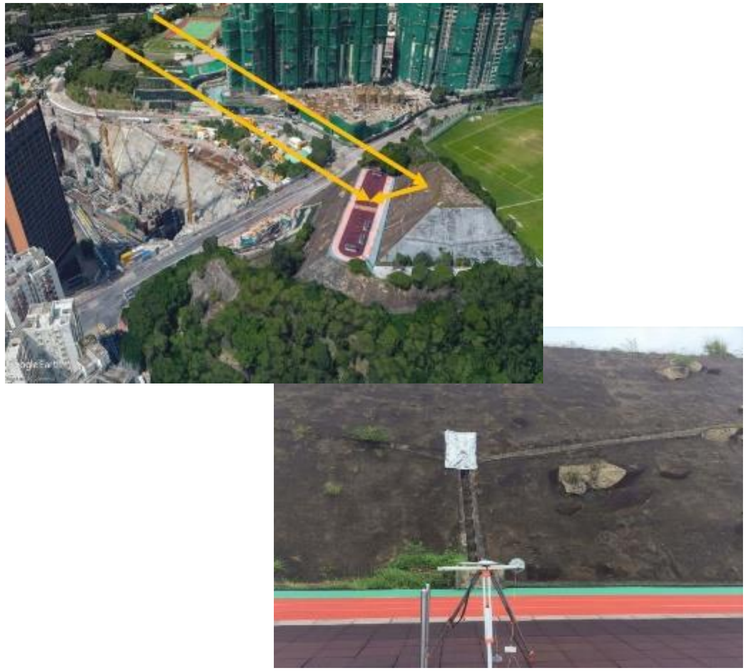

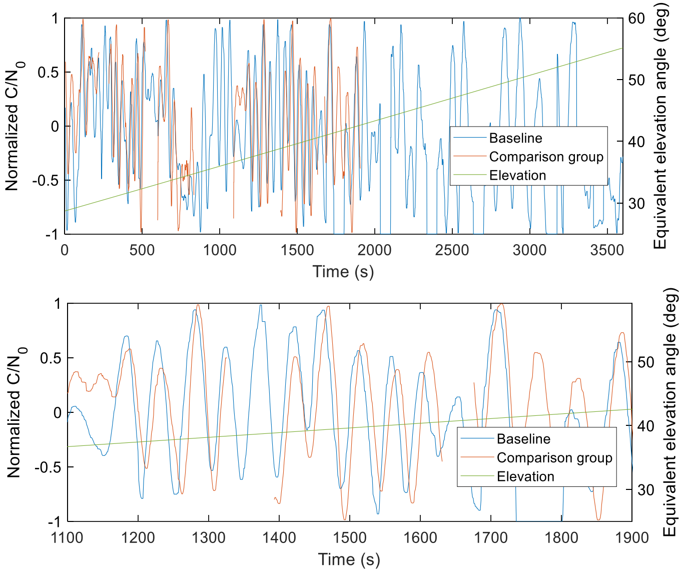

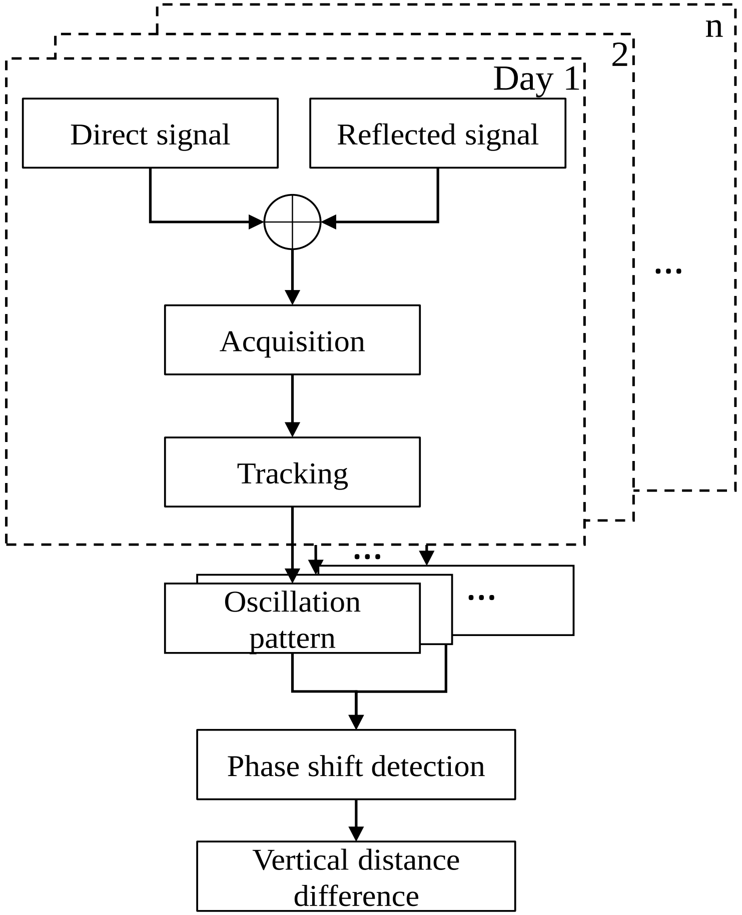

	Results of each waveform (cm)	Mean of each data set (cm)
Collection 1	2.56 0.58 1.26 2.88	1.82
Collection 2	1.23 1.39 3.00 1.77 1.28 1.04 3.41 2.99 2.72	2.09
Collection 3	2.26 3.75	3.00
Collection 4	4.16 2.18 2.60 1.44 2.67 0.68	2.29
Collection 5	0.38 0.96 1.98 1.63 2.03 2.22 2.41	1.80
Collection 6	2.12 2.22 1.33	1.89

Mean = 2.15 cm; RMSE =0.91 cm

- No need for continuous observation
- Data volume is small when using SNR as observation
- More robust for SNR observation, compared with carrier phase

Deformation monitoring using GNSS-R

- **Commercial receiver approaches**: SNR monitoring for quasi-static deformation

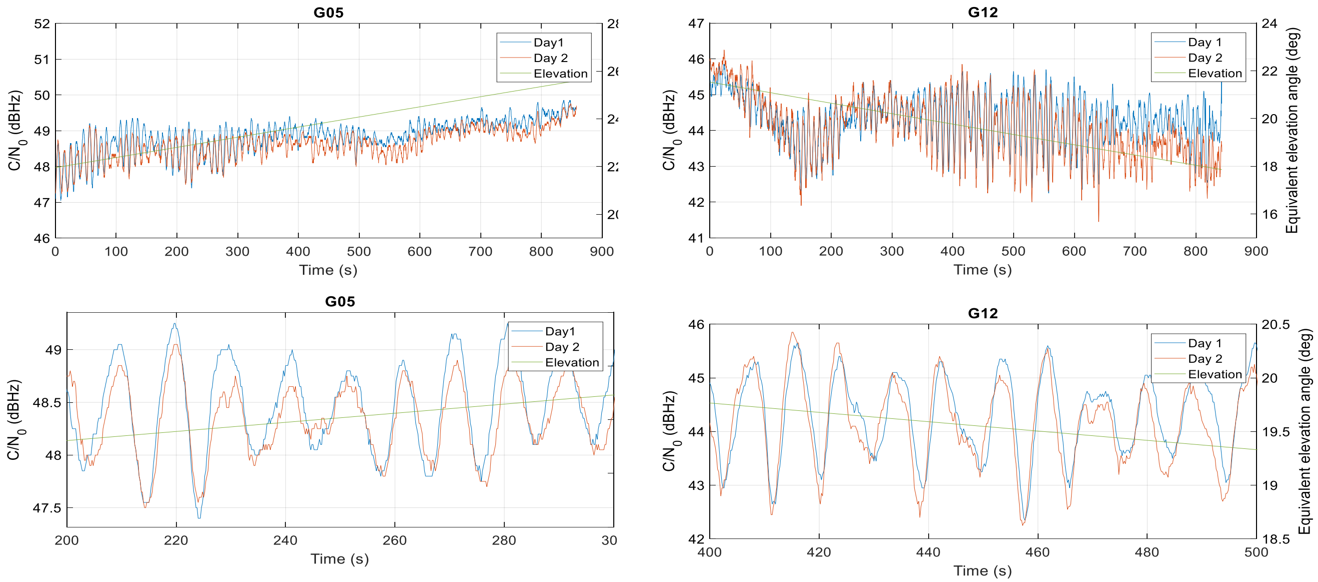

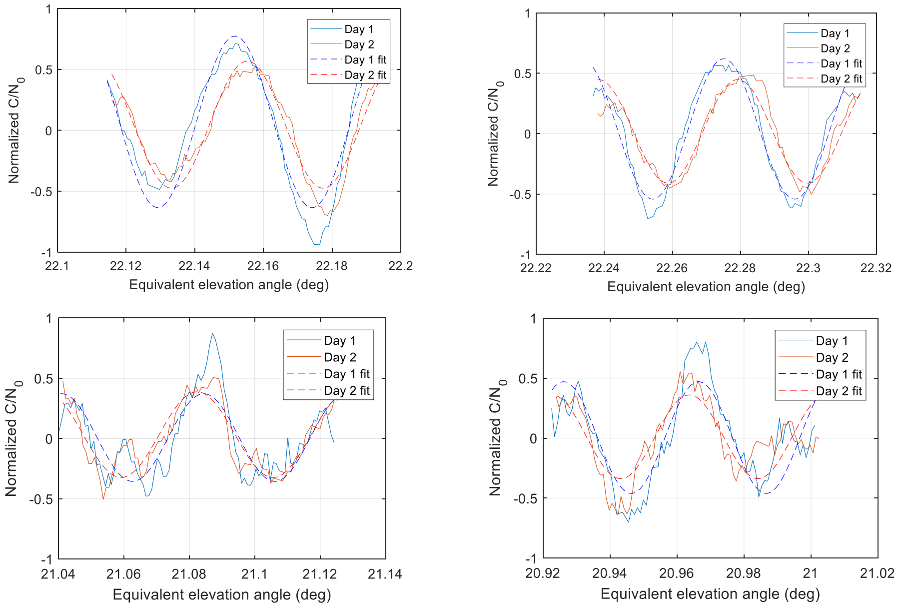

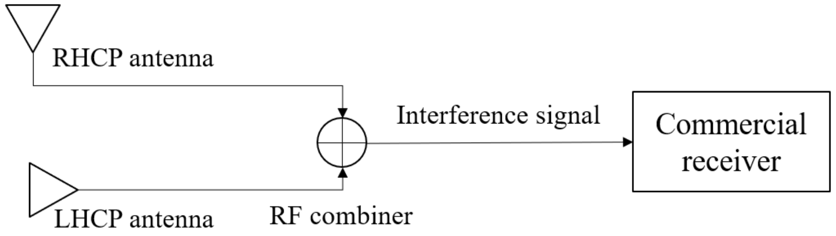

PRN05: Mean = 1.27cm; RMSE = 1.43cm

PRN12: Mean = 2.04cm; RMSE = 2.1cm

	Phase angle (rad)	Phase diff (rad)	Deformation (abs.) (cm)
PRN 5, subsection 1, day 1	0.47	-0.34	1.38
PRN 5, subsection 1, day 2	0.12		
PRN 5, subsection 2, day 1	0.09	-0.44	1.75
PRN 5, subsection 2, day 2	-0.34		
PRN 12, subsection 1, day 1	-0.06	0.45	1.90
PRN 12, subsection 1, day 2	0.38		
PRN 12, subsection 2, day 1	0.16	0.63	2.69
PRN 12, subsection 2, day 2	0.79		

Deformation monitoring using GNSS-R

- **Commercial receiver approaches**: double difference carrier phase approach
  - Using **two commercial GNSS receivers** without synchronization of receiver clock.
  - Introducing satellite from zenith (sat. B) to correct receiver clock error.

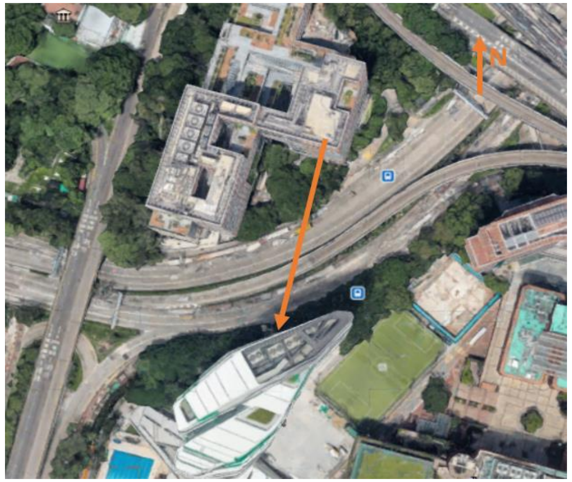

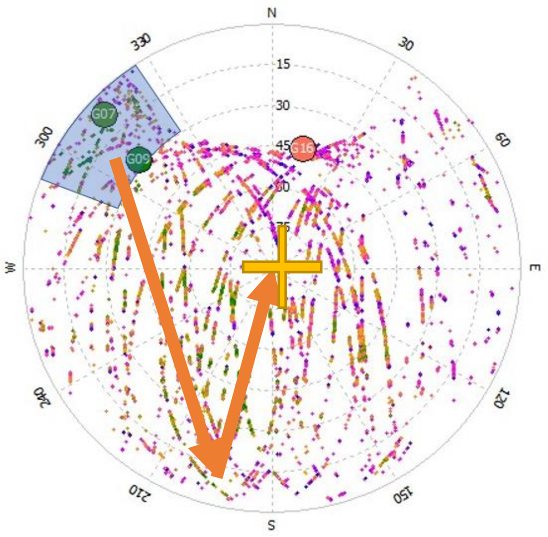

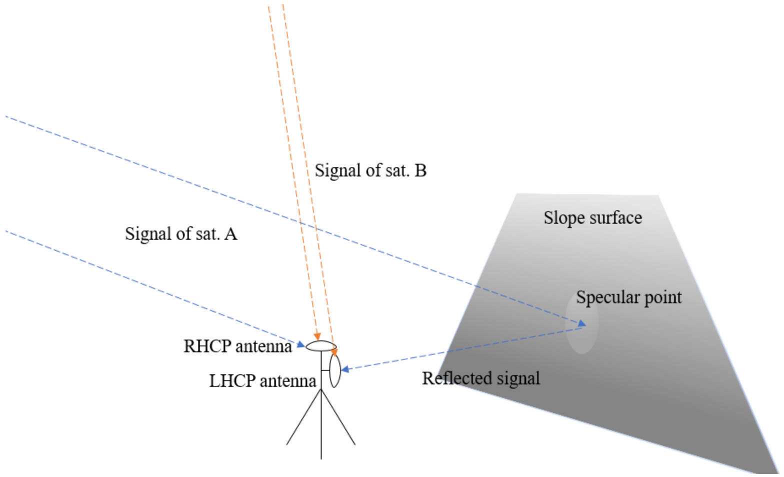

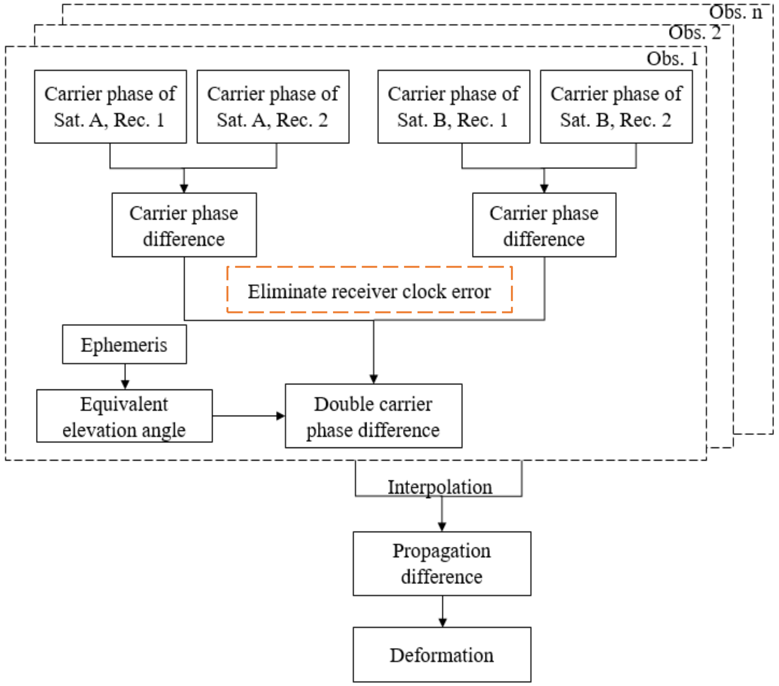

Waiting for satellite revisiting for same geometry

High resistance to carrier phase noise by averaging

Low update rate (24h for GPS)

G07	Mean(cm)	Std.(cm)	Average (cm)
D98	0.03	0.43	0.15
D99	0.34	0.40	
D100	-1.88	0.36	-1.81
D101	-1.60	0.32	
D102	-1.96	0.41	
		Deformation	-1.96

G09	Mean(cm)	Std.(cm)	Average (cm)
D98	-0.02	0.28	0.06
D99	0.12	0.30	
D100	-2.07	0.30	-1.91
D101	-1.78	0.27	
D102	-1.93	0.29	
		Deformation	-1.97

PRN07

PRN09

Carrier phase double difference

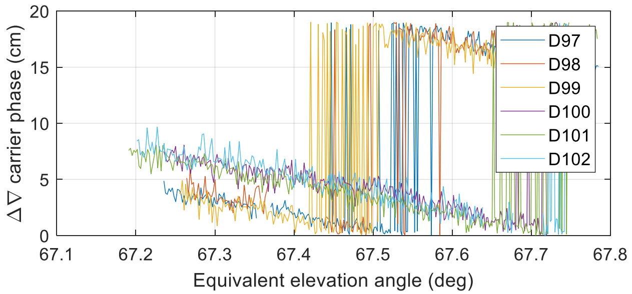

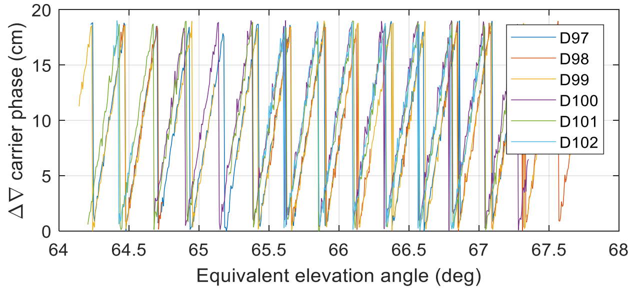

Propagation path difference

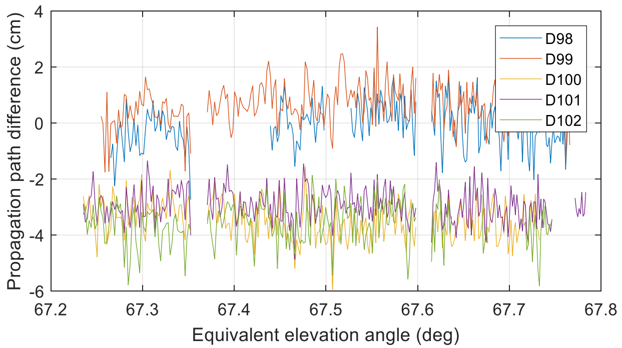

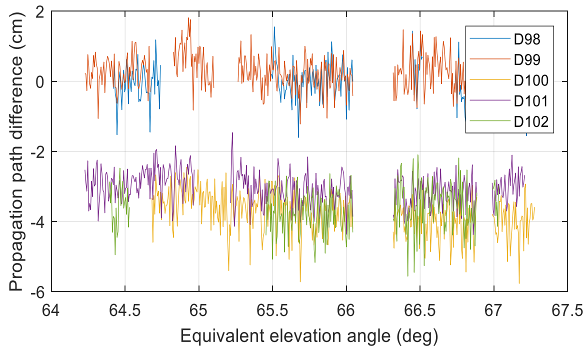

Deformation

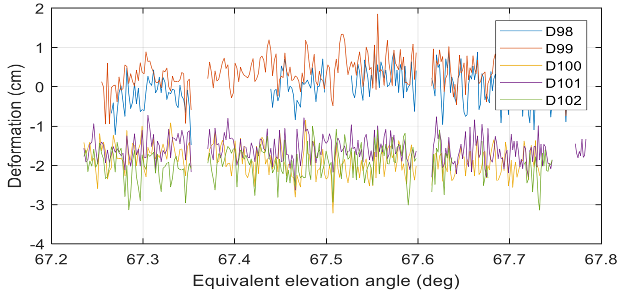

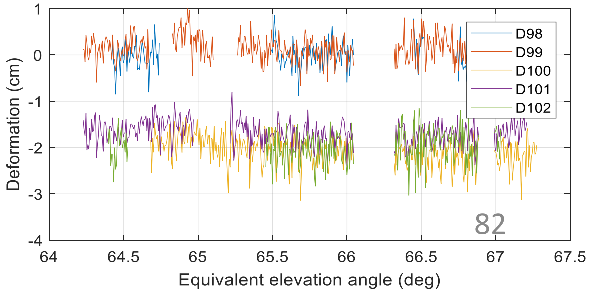

Use cross orbit of different satellites for same geometry

High noise level, cannot be suppressed by averaging

High update rate:

min: 1 min 10 sec;

max: 4 h 45 min 9 sec;

Average: 38 min 5 sec

	Mean (cm)	Std. (cm)	Average (cm)
D97	-0.17	0.55	0.06
D98	0.39	0.60	
D99	-0.03	0.58	
D100	-1.16	0.67	-1.47
D101	-1.55	0.51	
D102	-1.71	0.45	
Deformation			-1.54

Theoretically visible satellites' tracks on D97

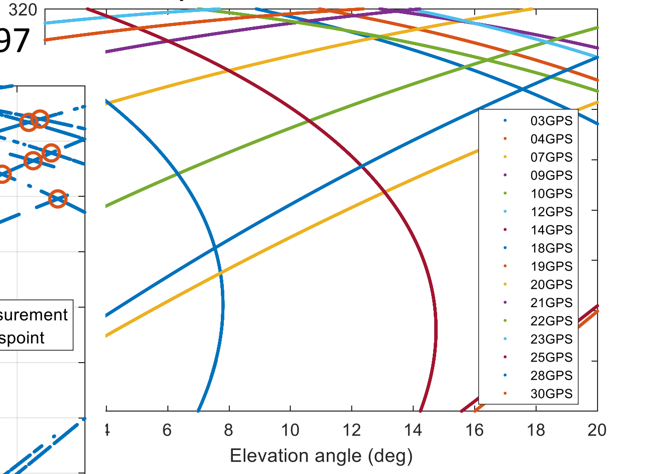

Available observations and the cross points on D97

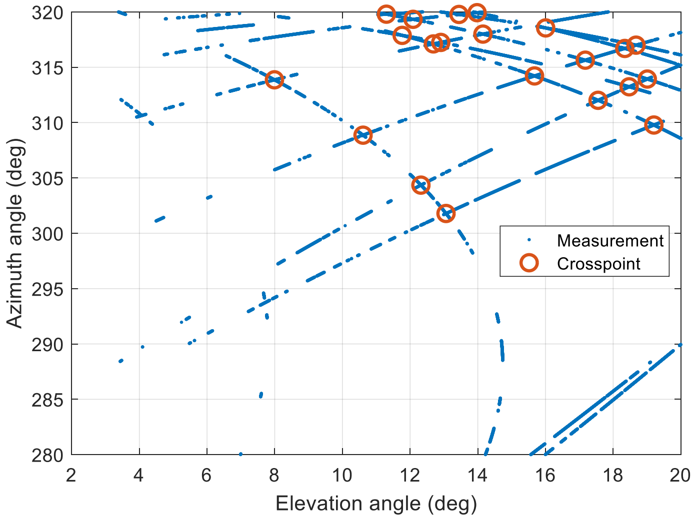

Propagation path difference

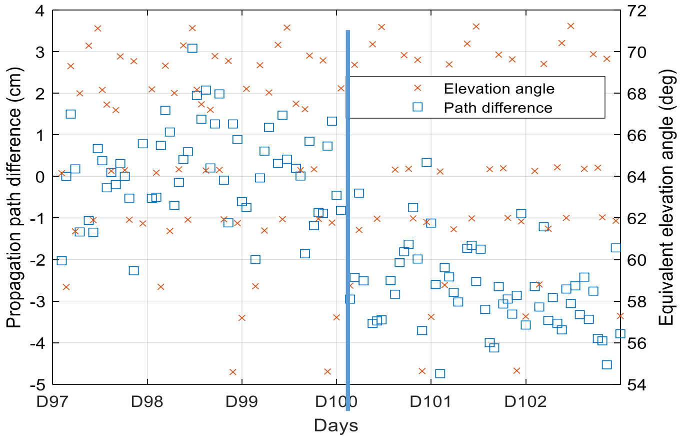

Deformation

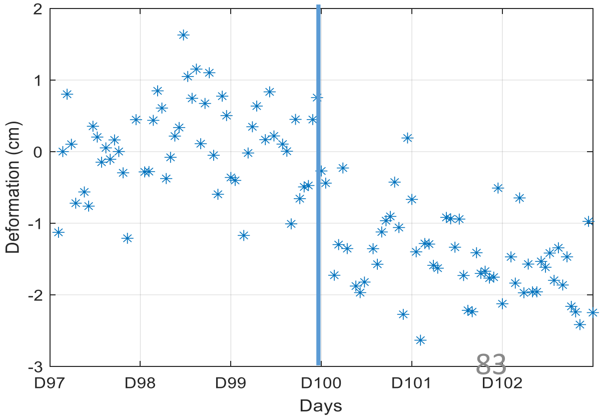

Frequency Bands for satellite missions

- P band (225 and 390 MHz)
  - Remote sensing for vegetation
- L-band (1–2 GHz)
  - **Global Positioning System (GPS)** carriers and also satellite mobile phones, such as Iridium; Inmarsat providing communications at sea, land and air; WorldSpace satellite radio.
- S-band (2–4 GHz)
  - Weather radar, surface ship radar, and some communications satellites, especially those of NASA for communication with ISS and Space Shuttle. In May 2009, Inmarsat and Solaris mobile (a joint venture between Eutelsat and Astra) were awarded each a 2×15 MHz portion of the S-band by the European Commission.
- C-band (4–8 GHz)
  - Primarily used for satellite communications, for full-time satellite TV networks or raw satellite feeds. Commonly used in areas that are subject to tropical rainfall, since it is less susceptible to rainfade than Ku band (the original Telstar satellite had a transponder operating in this band, used to relay the first live transatlantic TV signal in 1962).
- X-band (8–12 GHz)
  - Primarily used by the military. Used in radar applications including continuous-wave, pulsed, single-polarisation, dual- polarisation, synthetic aperture radar and phased arrays. X-band radar frequency sub-bands are used in civil, military and government institutions for weather monitoring, air traffic control, maritime vessel traffic control, defence tracking and vehicle speed detection for law enforcement.
- Ku-band (12–18 GHz)
  - Used for satellite communications. In Europe, Ku-band downlink is used from 10.7 GHz to 12.75 GHz for direct broadcast satellite services, such as Astra.
- Ka-band (26–40 GHz)
  - Communications satellites, uplink in either the 27.5 GHz and 31 GHz bands, and high-resolution, close-range targeting radars on military aircraft.

Possible Use of Signal of Opportunities

- Using existing signals
  - Multiple frequency band signals
- One designed signal source, multiple receivers

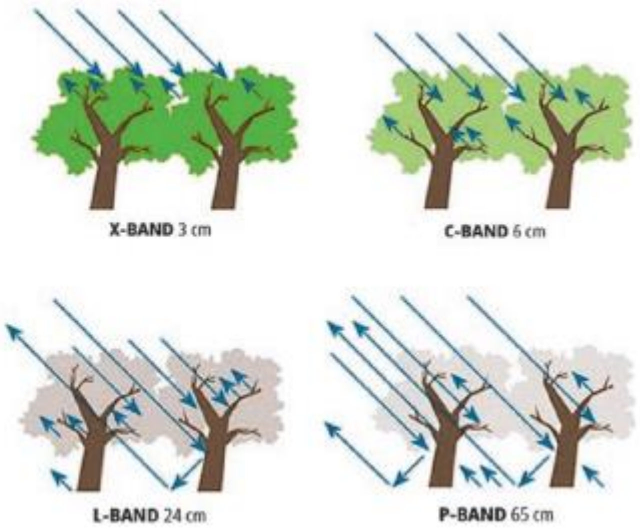

http://www.ciche.org.tw/wordpress/wp-content/uploads/2022/05/DB4901-P021-GNSS-R-%E9%81%99%E6%B8%AC%E6%8A%80%E8%A1%93.pdf

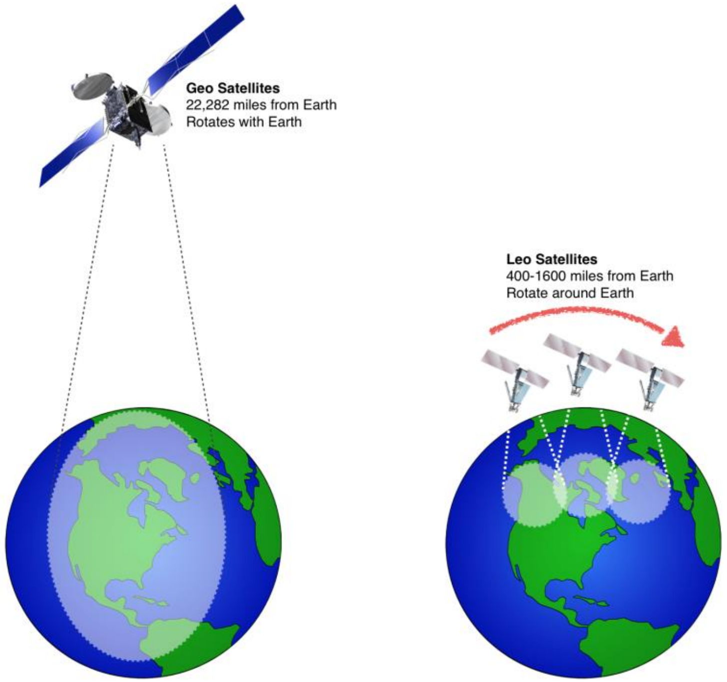

Thank You